Threshold and Dynamics in Semiconductor Quantum Well Lasers

Thesis by

Bin Zhao

In Partial Fulfillment of the Requirements

for the Degree of

Doctor of Philosophy

California Institute of Technology

Pasadena, California

1994

(Defended November 24, 1993)

To My Parents and Hua

Acknowledgments

I am very grateful to my advisor Professor Amnon Yariv who led me into this fascinating field of optoelectronics by not just providing the invaluable guidance to my research but also having me as a teaching assistant in his courses throughout my entire years at Caltech. His dynamic vision and keen physical insight provided me invaluable supervision in my research. His encouragement and trust in my abilities have been inspiring me over the years and will always be remembered and appreciated. In his group I found the atmosphere and resources necessary for exciting research and for my growth as an independent scientist. It truly has been both a privilege and a rewarding experience to work in the creative atmosphere of his research group.

Special thanks to Professor T. R. Chen and Y. H. Zhuang who taught me the liquid phase epitaxy, device fabrication and processing and collaborated with me on many projects. I enjoyed the collaboration and the friendship.

I would like to express my appreciation to Yoshiro Yamada, John Iannelli, Ali Shakouri, John Kitching, Nao Kuze, Dr. Shuwu Wu and Jing Feng who closely worked with me on different research projects over the years. I thank Dr. Steve Sanders, Randy Salvatore, Thomas Schrans, Dr. Lars Eng, Richard Boyd, Yuanjian Xu, Gilad Almogy, John O'Brien, Bill Marshall, Dr. Ya'akov Shevy and Dr. Amir Sa'ar for laboratory assistance and fruitful discussions. I would like to thank Markus Kajanto who first taught me the liquid phase epitaxy and Dr. Michael Mittelstein who first introduced me to the quantum well lasers when I joined the Yariv group.

Special thanks to Dr. Moti Segev, Songo Yagi, and Gert Cauwenberghs for their friendship, many discussions and suggestions beyond the research. Thanks are also extended to Dr. Giora Griffel and Dr. Sidney Kan. I would like to express my appreciation to Jana Mercado, Ali Gaffari, Kevin Cooper, and Desmond Armstrong for the help I received during my stay with the group. Thanks are also extended to many other current and former members of the group.

I have also received invaluable help from many other faculty, students and staff at Caltech throughout the years. Especially I would like to thank Professor Kerry Vahala for his encouragement and advise. Thanks are extended to Dr. Mike Newkirk, Dr. Peter Sercel, Charles Tsai, Jianhui Zhou, Namkyoo Park and David Geraghty for their laboratory assistance and/or fruitful discussions. Special thanks to Yixin Liu and Dr. Frank Shi for many fruitful and stimulating discussions. I thank Professor Noel Corngold for his kindly help and support of my attending an international conference in Japan. The help and kindness of Paula Samazan and Larry Begay are truly appreciated.

I would like to thank Professors Keqian Zhang, Bingkun Zhou and Yanbiao Liao of Tsinghua University, China for their very important help and support when I was trying to get permission from the university to study abroad then.

This thesis is dedicated to my mother, father and Hua, whose love, expectation, and faith in me have always inspired me for achievement of excellence.

Publication List

This publication list shows the work done at Caltech. Some subjects are not covered in the content of this thesis.

I. Books

[1] B. Zhao, and A. Yariv, "Quantum Well Semiconductor Lasers," a chapter in the book *Semiconductor Lasers*, Academic Press, 1994, in process.

[2] H. Wu, F. Barnes, A. Yariv, B. Zhao, W. Wu, and R. Hoffmeister, "Solution Manual for Optical Electronics, 4ed.," Saunders College Publishing, 1991.

II. Journals

[3] B. Zhao, T. R. Chen, A. Shakouri, and A. Yariv, "Performance Improvement in Quantum Well Lasers by Optimizing the Band Gap Offset at Quantum Well Heterojunctions," *Appl. Phys. Lett.*, vol.63, p.432, 1993.

[4] B. Zhao, T. R. Chen, S. Wu, Y. H. Zhuang, Y. Yamada, and A. Yariv, "Direct Measurement of Linewidth Enhancement Factors in Quantum Well Lasers of Different Quantum Well Barrier Heights," *Appl. Phys. Lett.*, vol.62, p.1591, 1993.

[5] B. Zhao, T. R. Chen, J. Iannelli, Y. H. Zhuang, Y. Yamada, and A. Yariv, "State Filling Effect on Spectral Linewidth of Quantum Well Lasers," *Appl. Phys. Lett.*, vol.62, p.1200, 1993.

[6] B. Zhao, T. R. Chen, and A. Yariv, "A Comparison of Amplitude-Phase Coupling and Linewidth Enhancement in Semiconductor Quantum Well and Bulk Lasers," *IEEE J. Quantum Electron.*, vol.QE-29, p.1027, 1993.

[7] T. R. Chen, B. Zhao, L. E. Eng, Y. H. Zhuang, J. O'Brien, and A. Yariv, "Very High Modulation Efficiency of Ultralow Threshold Single Quantum Well InGaAs Lasers," *Electron. Lett.*, vol.29, p.1525, 1993.

[8] T. R. Chen, L. E. Eng, B. Zhao, Y. H. Zhuang, and A. Yariv, "Strained Single Quantum Well InGaAs Lasers with a Threshold Current of 0.25 mA," *Appl. Phys. Lett.*, vol.63, p.2621, 1993.

[9] B. Zhao, T. R. Chen, Y. Yamada, Y. H. Zhuang, N. Kuze, and A. Yariv, "Evidence for State Filling Effect on High Speed Modulation Dynamics of Quantum Well Lasers," *Appl. Phys. Lett.*, vol.61, p.1907, 1992.

[10] B. Zhao, T. R. Chen, and A. Yariv, "The Gain and Carrier Density in Semiconductor Lasers Under Steady-State and Transient Conditions," *IEEE J. Quantum Electron.*, vol.QE-28, p.1479, 1992.

[11] B. Zhao, T. R. Chen, and A. Yariv, "Effect of State Filling on the Modulation Response and the Threshold Current of Quantum Well Lasers," *Appl. Phys. Lett.*, vol.60, p.1930, 1992.

[12] B. Zhao, T. R. Chen, Y. Yamada, Y. H. Zhuang, and A. Yariv, "Modulation and Spectral Dynamics in Semiconductor Quantum Well Lasers," *Lasers and Optoelectronics*, Proc. SPIE, vol.1979, p.334, 1992.

[13] B. Zhao, T. R. Chen, Y. H. Zhuang, A. Yariv, J. E. Ungar, and S. Oh, "High-Speed Operation of Very Low Threshold Strained InGaAs/GaAs Double Quantum Well Lasers," *Appl. Phys. Lett.*, vol.60, p.1295, 1992.

[14] B. Zhao, T. R. Chen, and A. Yariv, "The Extra Differential Gain Enhancement

in Multiple Quantum Well Lasers," *IEEE Photon. Tech. Lett.*, vol.4, p.124, 1992.

[15] T. R. Chen, B. Zhao, L. Eng, Y. H. Zhuang, and A. Yariv, "New Achievement in Ultralow Threshold Lasers," *Lasers and Optoelectronics*, Proc. SPIE, vol.1979, p.325, 1992.

[16] T. R. Chen, B. Zhao, Y. Yamada, Y. H. Zhuang, and A. Yariv, "Modulation Bandwidth Enhancement in Single Quantum Well GaAs/AlGaAs Lasers," *Electron. Lett.*, vol.28, p.1989, 1992.

[17] B. Zhao, T. R. Chen, and A. Yariv, "On the High Speed Modulation Bandwidth of Quantum Well Lasers," *Appl. Phys. Lett.*, vol.60, p.313, 1992.

[18] T. R. Chen, B. Zhao, Y. H. Zhuang, A. Yariv, J. E. Ungar, and S. Oh, "Ultralow Threshold Strained Layer InGaAs Multi-Quantum Well Lasers," *Appl. Phys. Lett.*, vol.60, p.1782, 1992.

[19] T. R. Chen, Y. H. Zhuang, Y. J. Xu, B. Zhao, A. Yariv, J. E. Ungar, and S. Oh, "Second Quantized State Oscillation and Wavelength Switching in Strained-Layer Multiquantum-Well Lasers," *Appl. Phys. Lett.*, vol.60, p.2954, 1992.

[20] B. Zhao, T. R. Chen, and A. Yariv, "Comparison of Differential Gain in Single Quantum Well and Bulk Double Heterostructure Lasers," *Electron. Lett.*, vol.27, p.2343, 1991.

[21] T. R. Chen, L. Eng, B. Zhao, Y. H. Zhuang, S. Sanders, H. Morkoç, and A.Yariv, "Submilliamp Threshold Current Strained Layer InGaAs/GaAs Quantum Well Lasers," *IEEE J. Quantum Electron.*, vol.QE-26, p.1183, 1990.

[22] T. R. Chen, B. Zhao, Y. H. Zhuang, A. Yariv, H. Blauvelt, and N. Bar-Chaim,

"High-Power and High-Frequency Operation of InGaAsP/InP Lasers at 1.3 μm," *Fiber and Integrated Optics*, vol.9, p.347, 1990.

[23] L. Eng, T. R. Chen, S. Sanders, Y. H. Zhuang, B. Zhao, A. Yariv, and H. Morkoç, "Submilliamp Threshold Current Pseudomorphic InGaAs/AlGaAs Buried-Heterostructure Quantum Well Lasers Grown by Molecular Beam Epitaxy," *Appl. Phys. Lett.*, vol.55, p.1378, 1989.

III. Conferences

[24] B. Zhao, T. R. Chen, A. Shakouri, and A. Yariv, "Optimization of Bandgap Offset at Quantum Well Heterojunction for Better Performance in Quantum Well Lasers," *The Conference on Lasers and Electro-Optics*, Baltimore, 1993.

[25] T. R. Chen, B. Zhao, L. E. Eng, Y. H. Zhuang, and A. Yariv, "5 GHz/mA$^{1/2}$ Modulation Bandwidth in Ultralow Threshold Semiconductor Quantum Well Lasers," *The Conference on Lasers and Electro-Optics*, Baltimore, 1993.

[26] B. Zhao, T. R. Chen, S. Wu, Y. H. Zhuang, Y. Yamada, and A. Yariv, "Observation of Large Variation in Linewidth Enhancement Factor of Quantum Well Lasers," *The Optical Fiber Communication Conference and International Conference on Integrated Optics and Optical Fiber Communication*, San Jose, 1993.

[27] B. Zhao, T. R. Chen, Y. Yamada, Y. H. Zhuang, J. Iannelli, and A. Yariv, "State Filling and Dynamics in Semiconductor Quantum Well Lasers," *The DARPA Optoelectronics Material Center Review*, Pasadena, 1993.

[28] B. Zhao, T. R. Chen, J. Iannelli, Y. H. Zhuang, Y. Yamada, and A. Yariv, "Influence of Quantum Well Barrier Height on the Amplitude-Phase Coupling and the

Spectral Linewidth in Quantum Well Lasers," *The Annual Meeting of IEEE Lasers and Electro-Optics Society*, Boston, 1992.

[29] T. R. Chen, B. Zhao, Y. Yamada, Y. H. Zhuang, and A. Yariv, "Modulation Bandwidth Enhancement in Single Quantum Well GaAs Lasers Through a Novel Design of Graded Index Separate Confinement Heterostructure," *The Annual Meeting of IEEE Lasers and Electro-Optics Society*, Boston, 1992.

[30] B. Zhao, T. R. Chen, Y. Yamada, Y. H. Zhuang, N. Kuze, and A. Yariv, "Theoretical and Experimental Investigation of the Effect of State Filling on High Speed Modulation Dynamics of Quantum Well Lasers," *The 13th IEEE International Semiconductor Laser Conference*, Takamatsu, Japan, 1992.

[31] B. Zhao, T. R. Chen, Y. H. Zhuang, and A. Yariv, "Dynamics in Semiconductor Quantum Well Lasers," *The International Conference on Lasers and Optoelectronics*, Beijing, China, 1992.

[32] T. R. Chen, B. Zhao, L. Eng, Y. H. Zhuang, and A. Yariv, "Very Low Threshold and Very High Speed Single Quantum Well InGaAs/AlGaAs Lasers," *The 13th IEEE International Semiconductor Laser Conference*, Takamatsu, Japan, 1992.

[33] B. Zhao, T. R. Chen, Y. Yamada, Y. H. Zhuang, N. Kuze, and A. Yariv, "Investigating the State Filling Effect in Quantum Well Lasers," *The Annual Meeting of Optical Society of America*, Albuquerque, 1992.

[34] T. R. Chen, B. Zhao, L. Eng, Y. H. Zhuang, and A. Yariv, "Recent Development in Ultralow Threshold Semiconductor Lasers," *The International Conference on Lasers and Optoelectronics*, Beijing, China, 1992.

[35] T. R. Chen, B. Zhao, Y. H. Zhuang, Y. J. Xu, A. Yariv, J. E. Ungar, and S. Oh, "Wavelength Switching Between First and Second Quantized States in Multiquantum Well Lasers," *The 8th Interdisciplinary Laser Science Conference*, Albuquerque, 1992.

[36] B. Zhao, T. R. Chen, and A. Yariv, "Fundamental Examination of Gain, Differential Gain and Modulation Dynamics in Bulk and Quantum Well Lasers," *The Conference on Lasers and Electro-Optics*, Anaheim, 1992.

[37] B. Zhao, T. R. Chen, and A. Yariv, "State Filling and Modulation Dynamics in Quantum Well Lasers," *The 9th IEEE/LEOS Semiconductor Laser Device Physics Workshop*, Anaheim, 1992.

[38] B. Zhao, T. R. Chen, Y. H. Zhuang, A. Yariv, J. E. Ungar, and S. Oh, "High Speed Operation of InGaAs/GaAs Strained Dual Quantum Well Buried Heterostructure Lasers," *The Annual Meeting of IEEE Lasers and Electro-Optics Society*, San Jose, 1991.

[39] T. R. Chen, B. Zhao, Y. H. Zhuang, A. Yariv, J. E. Ungar, and S. Oh, "Very Low Threshold Strained Layer InGaAs Double Quantum Well Lasers," *The Annual Meeting of IEEE Lasers and Electro-Optics Society*, San Jose, 1991.

[40] B. Zhao, T. R. Chen, and A. Yariv, "Ultimate Modulation Bandwidth in Semiconductor Quantum Well Lasers," *The Annual Meeting of Optical Society of America*, San Jose, 1991.

[41] T. R. Chen, L. Eng, Y. H. Zhuang, B. Zhao, S. Sanders, H. Morkoç, and A. Yariv, "Submilliamp Threshold Current Strained Layer InGaAs Quantum Well Lasers, *International Conference on Lasers '89*, New Orleans, 1989.

Abstract

The application of semiconductor lasers to optical communications and interconnects requires low threshold current, high-frequency modulation, and low-noise characteristics. Quantum well (QW) lasers have received considerable attention due to the demonstrated low threshold current, predicted superior modulation and spectral dynamics due to the reduction of active layer thickness and corresponding modification of density of states for the injected carriers in the extremely thin active region. However, in comparison with their bulk counterparts - double heterostructure (DH) lasers, quantum well lasers have not experimentally demonstrated significant improvement in the modulation bandwidth especially in the case of single quantum well (SQW) lasers.

In a practical quantum well structure, the separate confinement heterostructure (SCH) is usually used to confine the optical field in the waveguide and the injected carriers in the quantum well region. The fundamental Fermi-Dirac statistics results in that, in addition to the carrier population in the quantum well region, there is also a significant carrier population in the optical confining region. In the previous differential gain evaluations, the carrier population in the energy states in the optical confining region of the separate confinement heterostructure (referred as the state/band filling effects in QW lasers) was omitted.

The state filling effects are, in principle, inherent in any QW structure due to the Fermi distribution of the injected carriers. A re-evaluation of differential gain

for typical GaAs/AlGaAs QW and DH bulk lasers with consideration of state filling shows that (i) there is no differential gain enhancement in SQW lasers in comparison to the bulk lasers; (ii) there is an additional differential gain enhancement in multiple quantum well (MQW) lasers stemming from the reduction of state filling. These conclusions are consistent with the experimental results of high speed modulation bandwidth in semiconductor lasers.

These theoretical and experimental investigations provide useful guides in design of QW lasers of ultra-high performance. Using these design criteria, strained InGaAs MQW buried heterostructure (DH) lasers have been fabricated. These lasers have demonstrated record low lasing threshold currents (0.25 mA) and high speed at low operation current (3dB bandwidth of 5 GHz at 2.1 mA). These lasers are potentially important for optical interconnects and local area network communication systems.

Contents

List of Figures

List of Tables

Chapter 1

Introduction

1.1 Semiconductor Lasers

Since their invention in the early 1960s [4,5,21,30], semiconductor lasers have found many applications such as cable TV signal transmission, telephone and image transmission, computer interconnects and networks, compact disk (CD) player, code reading in supermarkets and libraries, laser printers, two-dimensional display panels, erasable optical data and image storage, and medical, welding and spectroscopic applications. Semiconductor lasers have assumed an important technological role and become the most important class of lasers. The main reasons behind this major surge in the role played by semiconductor lasers are major improvements in their performance specially in threshold current, direct current modulation speed, spectral linewidth, optical output power and so on.

As shown in Figure 1.1, a semiconductor laser is basically a p-i-n diode. When it

is forward-biased, electrons in the conduction band and holes in the valence band are injected into the intrinsic region (also called the active region) from the n-type doped and the p-type doped regions, respectively. The electrons and the holes accumulate in the active region and are induced to recombine by the lasing mode optical field present in the same region. The energy released by this process (a photon for each electron-hole recombination) is added coherently to the optical field (laser action). In conventional bulk semiconductor lasers, as shown in Figure 1.1 and Figure 1.2(a) a double heterostructure (DH) is used to confine the injected carriers and the optical field to the same spatial region thus enhancing the interaction of the charge carriers with the optical field.

It was showed that in order for optical radiation at frequency ν to experience gain (amplification) rather than loss in a semiconductor medium, the Fermi energy separation for electrons and holes in the medium must exceed the photon energy $\hbar\nu$ [4,5]. To achieve this state of affairs for lasing, a certain minimum value of injected carrier density N_{tr} (transparency carrier density) is required. This transparency carrier density is maintained by a (transparency) current to a semiconductor laser, which is usually the major component of the threshold current of a semiconductor laser and can be written as

$$I_{tr} = J_{tr}\ w\ L \tag{1.1}$$

where w is the laser diode width and L is the laser cavity length as shown in Figure 1.1.

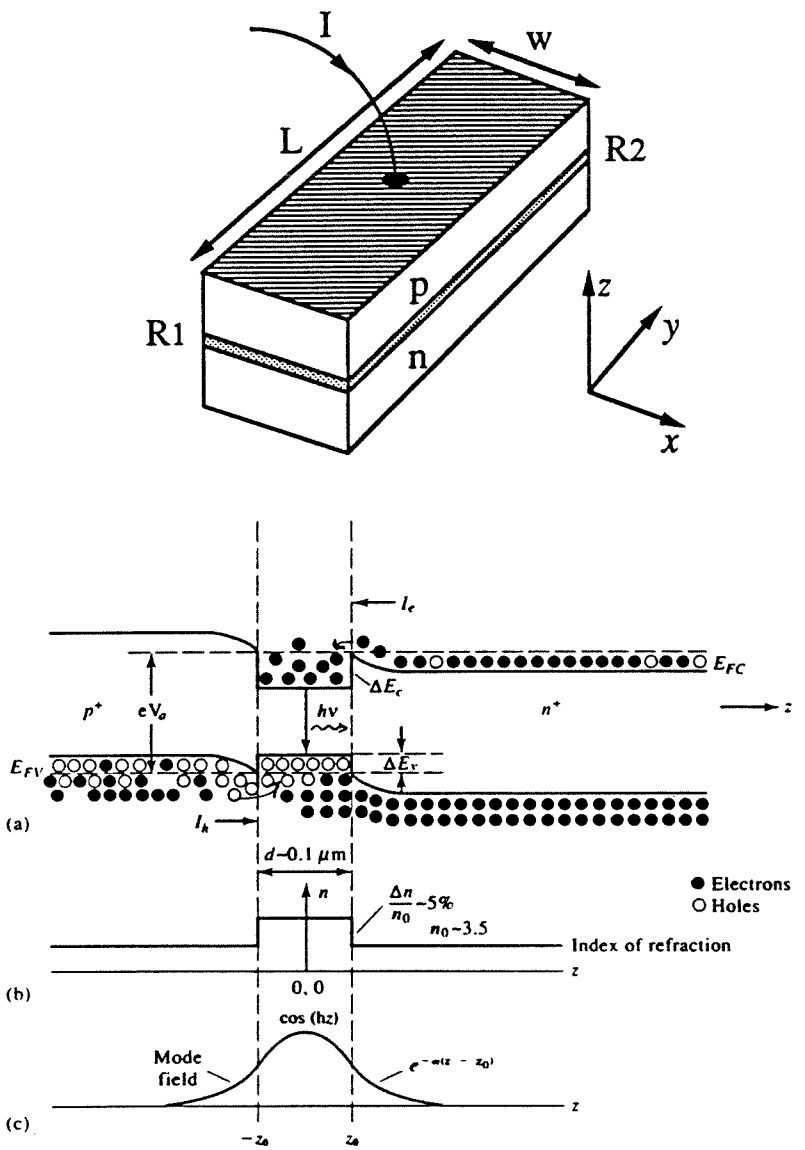

Figure 1.1: A schematic description of a semiconductor laser diode (a) the energy band structure of a forward-biased double heterostructure laser diode; (b) the spatial profile of the refractive index which is responsible for the dielectric waveguiding of the optical field; (c) the intensity profile of the fundamental optical mode.

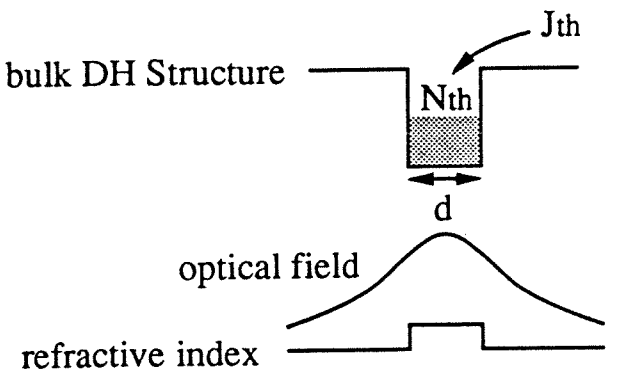

(a)

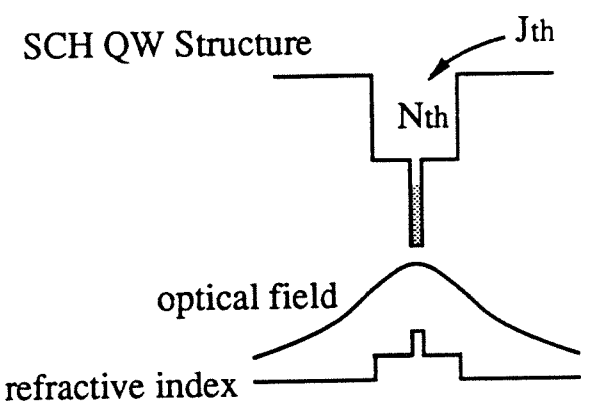

(b)

Figure 1.2: Schematic structures for (a) bulk double heterostructure semiconductor lasers; (b) separate confinement heterostructure quantum well lasers.

J_{tr} is the transparency current density which can written as

$$J_{tr} = \frac{e\ N_{tr}\ d}{\tau_{sp}} \tag{1.2}$$

where e is the fundamental electron charge, d is the active layer thickness, and τ_{sp} is the spontaneous lifetime for electron-hole recombination at N_{tr}. (1.1) and (1.2) indicate the major strategies to reduce the threshold current of a semiconductor laser: (i) reduction in the dimensions of the laser active region (w, L, d); (ii) reduction in the necessary carrier density inversion N_{tr} for the required Fermi level separation; (iii) reduction of the carriers' spontaneous decay rate (increase in τ_{sp}). Each of these strategies has stimulated research and technical efforts in semiconductor lasers. For example, pursuing (i) has resulted in the generation of quantum well, quantum wire, quantum dot, and micro cavity semiconductor lasers; pursuing (ii) has resulted in electronic band structure engineering for the active region of semiconductor lasers, such as the valence band effective mass reduction and large sub-band separation due to the addition of strain and different substrate orientation; pursuing (iii) has led to the research in squeezing and control of the spontaneous emission in micro cavity semiconductor lasers.

1.2 Quantum Well Semiconductor Lasers

In conventional bulk semiconductor lasers, as shown in Figure 1.1 and Figure 1.2(a), a double heterostructure (DH) is used to confine the injected carriers and the optical field to the same spatial region thus enhancing the interaction of the charge carriers

with the optical field.

As shown in (1.2) a reduction in the active layer thickness d will lead to a reduction in the transparency current density which is the major component of the threshold current density. As the active layer thickness d is reduced from $\sim$ 1000 Å in conventional DH lasers by an order of magnitude to, say, below 100 Å, the threshold current density, hence the threshold current, should be reduced by roughly the same order of magnitude. However, as d approached the 100 Å region, the structure shown in Figure 1.2(a) cannot confine the optical field any more. To effectively confine a photon or an electron, the feature size of the confinement structure needs to be comparable to their wavelengths. Thus, a separate confinement heterostructure as shown in Figure 1.2(b) is needed. The injected carriers are confined in the active region of quantum size in the direction perpendicular to the active layer while the optical field is confined in a region with size comparable to its wavelength. The active layer is a, so called, quantum well and the lasers are called quantum well (QW) lasers.

In addition to low threshold current, there are other performance characteristics which are important. In Figure 1.3, are shown the schematic structures for bulk, quantum well, quantum wire and quantum dot and their corresponding carrier density of states. The optical properties of these structures strongly depend on the carrier density of states. Since the carrier density of states is strongly structure dependent, use of these different structures in semiconductor lasers thus results in different performance characteristics.

The electrons and the holes in the QW display quantum effects evidenced mostly

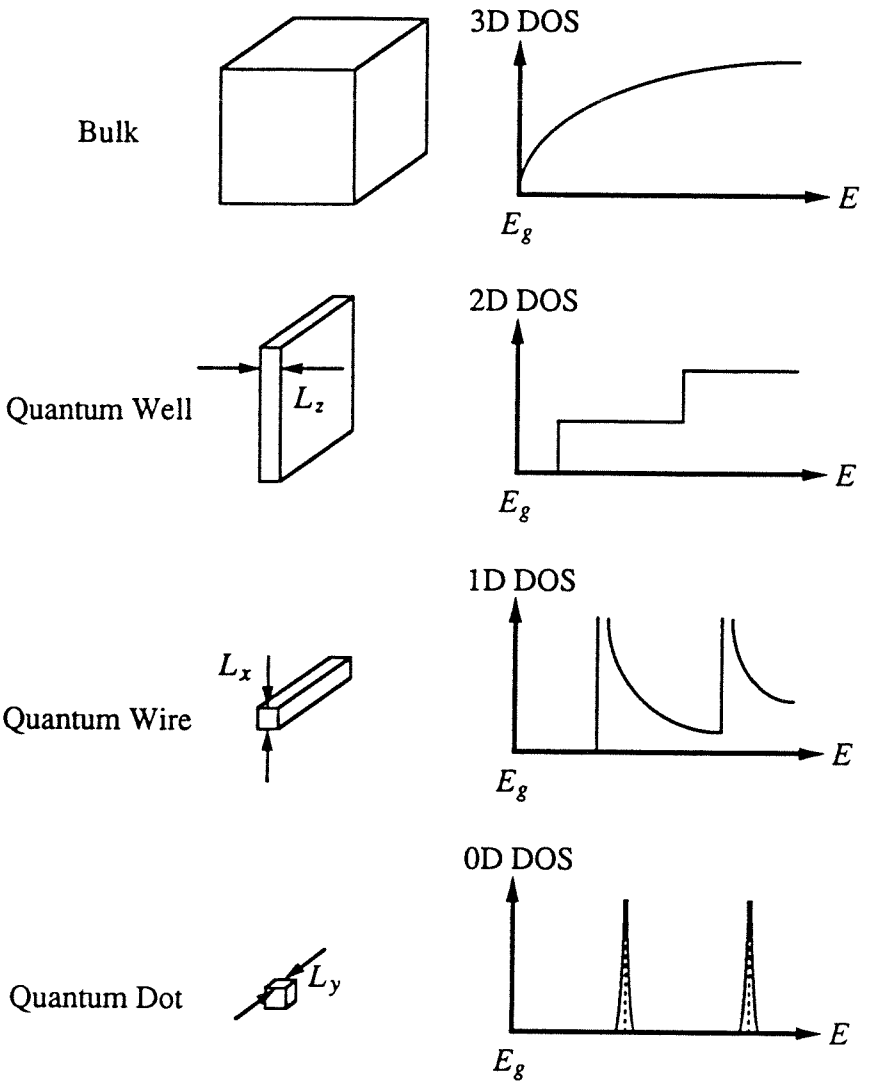

Figure 1.3: Schematic structures and corresponding carrier density of states (DOS) for three-dimensional (3D) bulk, two-dimensional (2D) quantum well, one-dimensional (1D) quantum wire and zero-dimensional (0D) quantum dot.

by the modification in the carrier density of states. In addition to the threshold current reduction due to the scaling down of the active region in QW lasers, these quantum effects greatly modify other device performance features. These include modulation and spectral dynamics, radiation polarization, ultra short optical pulse generation, as well as lasing wavelength tuning and switching.

Many of these technical achievements are based on joint progress in material growth technologies and theoretical understanding of the quantum well lasers. The pioneering work using the techniques of molecular beam epitaxy (MBE) [11,12,35,36, 52] and metal organic chemical vapor deposition (MOCVD) [15,16,17,18] to grow ultra thin layers, on the order of ten atomic layers, for quantum well laser structures has paved the way for the development of this new type of semiconductor lasers. In the meantime, the improved theoretical understanding and corresponding experimental investigations [43,22,9,18,6,1,5,56,15] in the properties of quantum well lasers have speeded up the development.

Very low threshold current density and threshold current have been demonstrated in QW lasers [52,11,17,9,19,7,16,2,58,63,11,4]. It has been theoretically predicted that the differential gain should be enhanced by a factor of at least 2~4 in the QW lasers and this differential gain enhancement would be independent on the number of quantum wells [9,1,5]. The consequence of the differential gain enhancement is the improvement of the high speed modulation bandwidth. However, high speed modulation experiments to date indicate no significant improvement in QW laser modulation bandwidth compared to DH lasers. In Figure 1.4, it is shown the highest modula-

tion bandwidth demonstrated in the semiconductor lasers of different materials and different structures [26,17,59,40,41,32,33,29,36,30,13]. There exist two definite trends in these lasers. First, in comparison to the bulk counterpart, the unstrained SQW lasers do not show significant improvement in the modulation bandwidth. Secondly, the use of MQW as active region leads to improvement in the modulation bandwidth over the SQW counterparts. These two facts are contrary to the previous theoretical predictions on modulation bandwidth in the QW lasers, and this motivated part of the work in this thesis.

1.3 Outline of the Thesis

In Chapter 2, we discuss the fundamental issues essential to understand the behavior of injected carriers in a semiconductor medium and how these injected carriers interact with an optical field. We first state some elementary results about the electronic band structures, *i.e.*, the electronic states available for the injected carriers to occupy in a semiconductor medium. Then, we discuss how these electronic states are occupied by the injected carriers, *i.e.*, the carrier distribution functions under the presence of a optical field. Finally, we describe the optical transitions due to the interaction between the injected carriers and an optical field. The discussions in this chapter are very general so that they are applicable to various semiconductor laser structures, *i.e.*, bulk, quantum well, quantum wire structures.

In Chapter 3, the basics necessary to understanding the properties of QW lasers

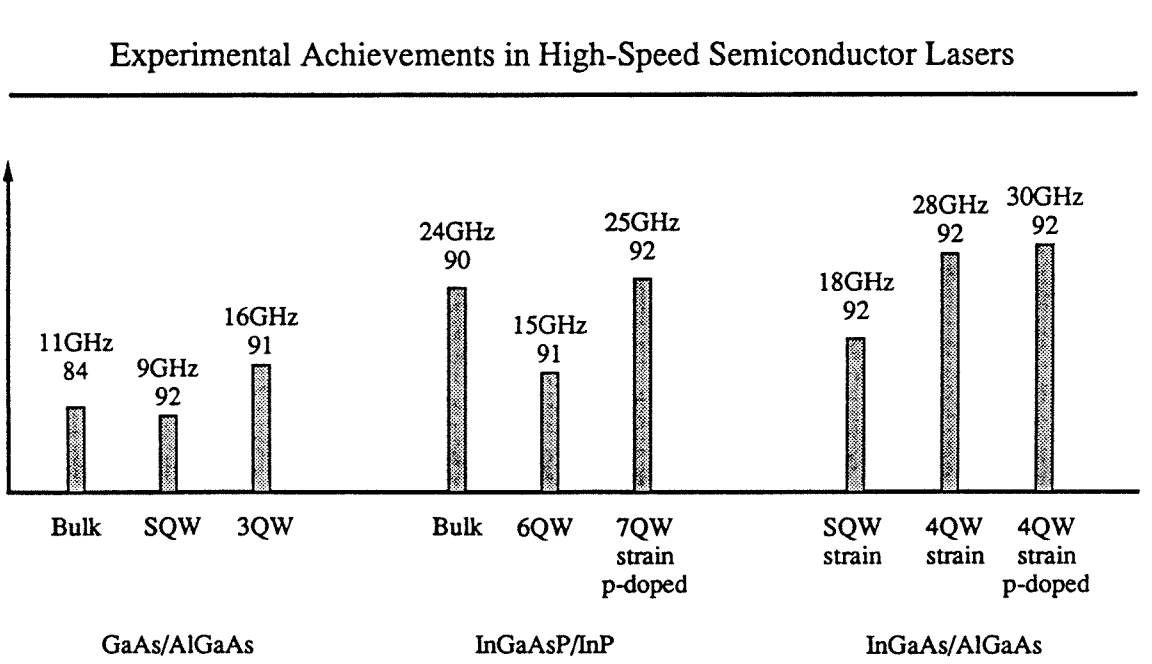

1. Why no significant improvement in QW lasers?
2. Why MQW is superior to SQW?

Figure 1.4: The highest modulation bandwidth demonstrated in the semiconductor lasers of different materials and different structures.

are discussed. The modifications of transition matrix elements and density of states in QW structures due to the quantized effects of injected carriers are discussed.

The physics specific to the threshold current and modulation bandwidth of QW lasers is addressed in Chapter 4. It is found both theoretically and experimentally that the state/band filling (the carrier population on the energy states in the optical confining region of the separate confinement heterostructure) has significant influence on the modulation dynamics. These conclusions are very consistent with the experimental results of the high modulation bandwidth in semiconductor lasers and provide very useful guides in design of QW lasers of ultra-high performance.

Using design criteria inspired by the arguments in Chapter 4, strained InGaAs MQW buried heterostructure (BH) lasers have been fabricated for high performance. The results are presented in Chapter 5. The lasers have demonstrated record low lasing threshold current (0.25 mA) and high speed at low operation current (3dB bandwidth of 5 GHz at 2.1 mA). These lasers are potentially important for optical interconnects and local area network communication systems.

Bibliography

[1] Y. Arakawa and A. Yariv, "Theory of gain, modulation response, and spectral linewidth in AlGaAs quantum well lasers," *IEEE J. Quantum Electron.*, vol.QE-21, p.1666, 1985

[2] Y. Arakawa and A. Yariv, "Quantum well lasers — gain, spectra, dynamics," *IEEE J. Quantum Electron.*, vol.QE-22, p.1887, 1986

[3] M. Asada, A. Kameyama, and Y. Suematsu, "Gain and intervalence band absorption in quantum-well lasers," *IEEE J. Quantum Electron.*, vol.QE-20, p.745, 1984

[4] N. G. Basov, O. N. Krokhin, and Y. M. Popov, "Production of negative-temperature states in p-n junctions of degenerate semiconductors," *Soviet Physics - JETP*, vol.13, p.1320, 1961

[5] M. G. Bernard and G. Duraffourg, "Laser conditions in semiconductors," *Phys. Status Solidi*, vol.1, p.699, 1961

[6] M. G. Burt, "Gain spectra of quantum-well lasers," *Electron. Lett.*, vol.19, p.210,

1983

[7] N. Chand, E. E. Becker, J. P. van der Ziel, S. N. G. Chu, and N. K. Dutta, "Excellent uniformity and very low (< 50 A/cm^2) threshold current density strained InGaAs quantum well diode lasers on GaAs substrate," *Appl. Phys. Lett.*, vol.58, p.1704, 1991

[8] H. Z. Chen, A. Ghaffari, H. Morkoç, and A. Yariv, "Very low threshold current densities (under 100 A/cm^2) in AlGaAs/GaAs single-quantum-well GRINSCH lasers grown by molecular beam epitaxy," *Electron. Lett.*, vol.23, p.1334, 1987

[9] T. R. Chen, B. Zhao, Y. H. Zhuang, A. Yariv, J. E. Ungar, and S. Oh, "Ultralow threshold strained layer InGaAs multi-quantum well lasers," *Appl. Phys. Lett.*, vol.60, p.1782, 1992

[10] S. R. Chinn, P. S. Zory, and A. R. Reisinger "A model for GRIN-SCH-SQW diode lasers," *IEEE J. Quantum Electron.*, vol.QE-24, p.2191, 1988

[11] A. Y. Cho, "Film deposition by molecular beam techniques," *J. Vac. Sci.*, vol.8, p.S31, 1971

[12] A. Y. Cho, R. W. Dixon, H. C. Casey, Jr, and R. L. Hartman, "Continuous room-temperature operation of GaAs-$Al_xGa_{1-x}As$ double-heterostructure lasers prepared by molecular-beam epitaxy," *Appl. Phys. Lett.*, vol.28, p.501, 1976

[13] H. K. Choi and C. A. Wang, "InGaAs/AlGaAs strained single quantum well diode lasers with extremely low threshold current density and high efficiency,"

Appl. Phys. Lett., vol.57, p.321, 1990

[14] P. L. Derry, T. R. Chen, Y. H. Zhuang, J. Paslaski, M. Mittelstein, K. Vahala, A. Yariv, K. Lau, and N. Bar-Chaim, "Properties of ultra low threshold single quantum well (Al,Ga)As lasers for computer interconnects," *Optoelectronics – Devices and Technologies*, vol.3, p.117, 1988

[15] R. D. Dupuis and P. D. Dapkus, "Room temperature operation of $Ga_{1-x}Al_xAs$/GaAs double-heterostructure lasers grown by metalorganic chemical vapor deposition," *Appl. Phys. Lett.*, vol.31, p.466, 1977

[16] R. D. Dupuis, P. D. Dapkus, N. Holonyak Jr., E. A. Rezek, and R. Chin, "Room temperature operation of quantum-well $Ga_{1-x}Al_x$-GaAs laser diodes grown by metalorganic chemical vapor deposition," *Appl. Phys. Lett.*, vol.32, p.295, 1978

[17] R. D. Dupuis, P. D. Dapkus, R. Chin, N. Holonyak Jr., and S. Kirchoefer, "Continuous 300 K operation of single-quantum-well Al_xGa_{1-x}-GaAs heterostructure diodes grown by metalorganic chemical vapor deposition," *Appl. Phys. Lett.*, vol.34, p.265, 1979

[18] R. D. Dupuis, P. D. Dapkus, N. Holonyak Jr., and R. M. Kolbas, "Continuous room-temperature multiple-quantum-well Al_xGa_{1-x}-GaAs injection lasers grown by metalorganic chemical vapor deposition," *Appl. Phys. Lett.*, vol.35, p.487, 1979

[19] N. K. Dutta, "Calculated threshold current of GaAs quantum well lasers," *J.*

Appl. Phys., vol.53, p.7211, 1982

[20] L. E. Eng, T. R. Chen, S. Sanders, Y. H. Zhuang, B. Zhao, A. Yariv, and H. Morkoç, "Submilliamp threshold current pseudomorphic InGaAs/AlGaAs buried-heterostructure quantum well lasers grown by molecular beam epitaxy," *Appl. Phys. Lett.*, vol.55, p.1378, 1989

[21] R. N. Hall, G. E. Fenner, J. D. Kingsley, T. J. Soltys, and R. O. Carlson, "Coherent light emission from GaAs junctions," *Phys. Rev. Lett.*, vol.9, p.366, 1962

[22] N. Holonyak Jr., R. M. Kolbas, R. D. Dupuis, P. D. Dapkus, "Quantum-well heterostructure lasers," *IEEE J. Quantum Electron.*, vol.QE-16, p.170, 1980

[23] E. Kapon, S. Simhony, J. P. Harbison, and L. T. Florez, "Threshold current reduction in patterned quantum well semiconductor lasers grown by molecular beam epitaxy," *Appl. Phys. Lett.*, vol.56, p.1825, 1990

[24] K. Y. Lau, N. Bar-Chaim, I. Ury, and A. Yariv, "11-GHz direct modulation bandwidth GaAlAs window laser on semi-insulating substrate operating at room temperature," *Appl. Phys. Lett.*, vol.45, p.316, 1984

[25] K. Y. Lau, P. L. Derry, and A. Yariv, "Ultimate limit in low threshold quantum well GaAlAs semiconductor lasers," *Appl. Phys. Lett.*, vol.52, p.88, 1988

[26] I. F. Lealman, M. Bagley, D. M. Cooper, N. Fletcher, M. Harlow, S. D. Perrin, R. H. Walling, and L. D. Westbrook, "Wide bandwidth multiple quantum well 1.55 μm lasers," *Electro. Lett.*, vol.27, p.1191, 1991

[27] L. F. Lester, S. S. O'Keefe, W. J. Schaff, and L. F. Eastman, "Multiquantum well strained-layer lasers with improved low frequency response and very low damping," *Electro. Lett.*, vol.28, p.383, 1992

[28] E. Meland, R. Holmstrom, J. Schlafer, R. B. Lauer, and W. Powazinik, "Extremely high-frequency (24 GHz) InGaAsP diode lasers with excellent modulation efficiency," *Electro. Lett.*, vol.26, p.1827, 1990

[29] P. A. Morton, R. A. Logan, T. Tanbun-Ek, P. F. Sciortino Jr., A. M. Sergent, R. K. Montgomery, and B. T. Lee, "25 GHz bandwidth 1.55 μm GaInAsP p-doped strained multiquantum-well lasers," *Electro. Lett.*, vol.28, p.2156, 1992

[30] M. I. Nathan, W. P. Dumke, G. Burns, F. H. Dills, and G. Lasher, "Stimulated emission of radiation from GaAs p-n junctions," *Appl. Phys. Lett.*, vol.1, p.62, 1962

[31] R. Nagarajan, T. Fukushima, J. E. Bowers, R. S. Geels, and L. A. Coldren, "Single quantum well strained InGaAs/GaAs lasers with large modulation bandwidth and low damping," *Electro. Lett.*, vol.27, p.1058, 1991

[32] J. D. Ralston, D. F. G. Gallagher, P. J. Tasker, H. P. Zappe, I. Esquivias, and J. Fleissner, "Vertical compact 15 GHz GaAs/AlGaAs multiple quantum well laser grown by molecular beam epitaxy," *Electro. Lett.*, vol.27, p.1720, 1991

[33] J. D. Ralston, I. Esquivias, S. Weisser, D. F. G. Gallagher, P. J. Tasker, E. C. Larkins, J. Rosenzweig, H. P. Zappe, J. Fleissner, and D. J. As, "16 GHz

GaAs/AlGaAs multiple quantum well laser with vertical compact structure," *High-Speed Electronics and Optoelectronics*, Proc. SPIE vol.1680, p.127, 1992

[34] P. J. A. Thijs, J. J. M. Binsma, L. F. Tiemeijer, R. W. M. Slootweg, R. van Roijen, and T. van Dongen, "Sub-mA threshold operation of $\lambda = 1.5\mu$m strained InGaAs multiple quantum well lasers grown on (311)B InP substrates," *Appl. Phys. Lett.*, vol.60, p.3217, 1992

[35] W. T. Tsang, "Low-current-threshold and high-lasing uniformity GaAs-$Al_xGa_{1-x}As$ double heterostructure lasers grown by molecular beam epitaxy," *Appl. Phys. Lett.*, vol.34, p.473, 1978

[36] W. T. Tsang, C. Weisbuch, R. C. Miller, and R. Dingle, "Current injection GaAs-$Al_xGa_{1-x}As$ multi-quantum-well heterostructure lasers prepared by molecular beam epitaxy," *Appl. Phys. Lett.*, vol.35, p.673, 1979

[37] W. T. Tsang, "Extremely low threshold (AlGa)As graded-index waveguide separate-confinement heterostructure lasers grown by molecular-beam epitaxy," *Appl. Phys. Lett.*, vol.40, p.217, 1982

[38] C. Weibbuch and J. Nagle "The physics of the quantum well laser," *Physica Scripta*, vol.T19, p.209,1987

[39] S. Weisser, J. D. Ralston, E. C. Larkins, I. Esquivias, P. J. Tasker, J. Fleissner, and J. Rosenzweig, "Efficient high-speed direct modulation in p-doped

$In_{0.35}Ga_{0.65}As/GaAs$ multiquantum well lasers," *Electro. Lett.*, vol.28, p.2141, 1992

[40] R. L. Williams, M. Dion, F. Chatenoud, and K. Dzurko, "Extremely low threshold current strained InGaAs/AlGaAs lasers by molecular beam epitaxy," *Appl. Phys. Lett.*, vol.58, p.1816, 1991

[41] H. D. Wolf, H. Lang and L. Korte, "High-speed AlGaAs/GaAs multiple quantum well ridge waveguide lasers," *Electro. Lett.*, vol.25, pp.1249, 1989

[42] C. E. Zah, R. Bhat, B. Pathak, C. Caneau, F. J. Favire, N. C. Andreadakis, D. M. Hwang, M. A. Koza, C. Y. Chen, and T. P. Lee, "Low threshold 1.5 μm tensile-strained single quantum well lasers," *Electron. Lett.*, vol.27, p.1414, 1991

[43] J. P. Van Der Ziel, R. Dingle, R. Miller, W. Wiegmann, and W. A. Nordland, Jr., "Laser oscillations from quantum states in very thin GaAs-$Al_{0.2}Ga_{0.8}As$ multilayer structures," *Appl. Phys. Lett.*, vol.26, p.463, 1975

Chapter 2

Fundamentals in Semiconductor Laser Structures

Before dealing with the optical properties of a semiconductor medium or a semiconductor laser structure, it is essential to understand the behavior of injected carriers in a semiconductor medium and how these injected carriers interact with an optical field. In this chapter, we first state some elementary results about the electronic band structures, *i.e.*, the electronic states available for the injected carriers to occupy in a semiconductor medium. Detailed treatment of this topic can be found in numerous references dealing with the wave mechanics of solids. Then, we discuss how these electronic states are occupied by the injected carriers, *i.e.*, the carrier distribution functions under the presence of a optical field. Finally, we describe the optical transitions due to the interaction between the injected carriers and an optical field. We will make the discussions in this chapter as general as possible so that they are applicable

to various semiconductor laser structures, *i.e.*, bulk, quantum well, quantum wire and quantum dot structures.

2.1 Electronic States in a Semiconductor Structure

In a semiconductor medium, the wavefunction of an electron in a given band is a solution of the Schrödinger equation

$$H_{crystal}\ \Psi_n(\mathbf{r}) = [\frac{\mathbf{p}^2}{2m_0} + U_p(\mathbf{r}) + U(\mathbf{r})]\ \Psi_n(\mathbf{r}) = E_n\ \Psi_n(\mathbf{r}) \tag{2.1}$$

where $\mathbf{p} = -i\hbar\nabla$ is the momentum operator, m_0 is the free electron mass, $U_p(\mathbf{r})$ is the periodic potential of the bulk semiconductor crystal $U(\mathbf{r})$ is the additional potential (*e.g.*, the potential due to the quantum well), and n designates the corresponding band. If $U(\mathbf{r}) = 0$, the solution to Eq.(2.1) is the Bloch function:

$$\Psi_{n,\mathbf{k}}(\mathbf{r}) = u_{n,\mathbf{k}}(\mathbf{r})\ \frac{1}{\sqrt{V}} e^{i\mathbf{k}\cdot\mathbf{r}} \tag{2.2}$$

where $u_{n,\mathbf{k}}(\mathbf{r})$ has the periodicity of the crystalline lattice, $\mathbf{k} = k_x\hat{\mathbf{x}} + k_y\hat{\mathbf{y}} + k_z\hat{\mathbf{z}}$ is the wavevector of the electron, k_q is quantized as

$$k_q = j\ \frac{2\pi}{L_q}\ , \tag{2.3}$$

j is an integer, L_q is the length of the crystal in the q direction ($q = x, y, z$) and $V = L_x \cdot L_y \cdot L_z$. The functions $\Psi_{n,\mathbf{k}}(\mathbf{r})$ form a complete set. For $U(\mathbf{r}) \neq 0$, the

solution of (2.1) can be written as an expansion in the basis set $\Psi_{n,\mathbf{k}}(\mathbf{r})$

$$\Psi_n(\mathbf{r}) = \sum_{m,\mathbf{k}} F_m(\mathbf{k})\ u_{m,\mathbf{k}}(\mathbf{r})\ \frac{1}{\sqrt{V}} e^{i\mathbf{k}\cdot\mathbf{r}}\ . \tag{2.4}$$

Note any periodic function can be expanded by the Bloch functions at the band edge ($\mathbf{k} = 0$) which are complete with respect to periodic functions:

$$u_{m,\mathbf{k}}(\mathbf{r}) = \sum_{l} c_{ml}(\mathbf{k})\ u_{l,0}(\mathbf{r})\ . \tag{2.5}$$

Therefore

$$\Psi_n(\mathbf{r}) = \sum_{l} \Phi_l(\mathbf{r})\ u_{l,0}(\mathbf{r})\ \equiv \sum_{l} \Phi_l(\mathbf{r})\ u_l(\mathbf{r}) \tag{2.6}$$

where

$$\Phi_l(\mathbf{r}) = \sum_{m,\mathbf{k}} F_m(\mathbf{k})\ c_{ml}(\mathbf{k})\ \frac{1}{\sqrt{V}} e^{i\mathbf{k}\cdot\mathbf{r}} \tag{2.7}$$

is called as the envelope functions. $u_{l,0}(\mathbf{r}) \equiv u_l(\mathbf{r})$ satisfies

$$< u_l(\mathbf{r}) \,|\, u_{l'}(\mathbf{r}) >= \frac{1}{\Omega} \int_{\text{cell}} u_l^*(\mathbf{r})\ u_{l'}(\mathbf{r})\ d\mathbf{r} = \delta_{ll'}\ , \tag{2.8}$$

where Ω is the volume of the unit cell. In the envelope function approximation, which has assumed that $\Phi_l(\mathbf{r})$ varies slowly within one unit cell of the crystal, a $\mathbf{k}\cdot\mathbf{p}$ approximation up to the second order of the wave vector shows that the $\Phi_l(\mathbf{r})$ are governed by a set of coupled Schrödinger equations [7,8,5,6]

$$\sum_{l'} \{ \sum_{\alpha\alpha'} [D_{ll'}^{\alpha\alpha'}(-i\partial_\alpha)(-i\partial_{\alpha'})] + \delta_{ll'} U(\mathbf{r}) \} \Phi_{l'}(\mathbf{r}) = [E_n - E_{l0}] \Phi_l(\mathbf{r})\ , \tag{2.9}$$

where $\partial_\alpha = \frac{\partial}{\partial \alpha}$, ($\{\alpha\} = \{x, y, z\}$), E_{l0} is the energy of a free electron in the semiconductor medium at the band edge (*i.e.*, for $U(\mathbf{r}) = 0$ and $\mathbf{k} = 0$). $D_{ll'}^{\alpha\alpha'}$ are a set of constants depending on the crystal symmetry, the choice of the coordinate system

and the basis functions $\{u_l\}$. The symmetry of the crystal, proper choices of the coordinate system and $\{u_l\}$ will significantly simplify (2.1) since many of the $D_{ll'}^{\alpha\alpha'}$ vanish.

If $\partial U/\partial q = 0$ but $\partial U/\partial s \neq 0$ where $\{q, s\} = \{x, y, z\}$, the envelope functions can be written as

$$\Phi_l(\mathbf{r}) = \Phi_{l_s,k_q}(s)\ \frac{1}{\sqrt{L_q}} e^{ik_q q}\ . \tag{2.10}$$

$\Phi_{l_s,k_q}(s)$ satisfy

$$\sum_{l'}\{\sum_{\alpha\alpha'}[D_{ll'}^{\alpha\alpha'}(-i\partial_\alpha)(-i\partial_{\alpha'})] + \delta_{ll'}U(\mathbf{r})\}\Phi_{l'_s,k_q}(s) = [E_n(k_q) - E_{l0}]\Phi_{l_s,k_q}(s) \tag{2.11}$$

with $-i\partial_q$ is replaced by k_q.

The above argument is general in the sense that it applies to various semiconductor structures, such as bulk, quantum well, quantum wire and quantum dot structures. In Table I, we show how to choose the coordinates in the analysis for these different structures. $E_n(k_q)$ can be obtained by solving (2.11). Essentially, knowledge of the dependence of $E_n(k_q)$ gives the description of the electronic states in a given band of a semiconductor structure.

If the band-to-band coupling is very weak and negligible, as is the case for electrons in the conduction band, the wavefunction can be written as a single term

$$\Psi_n(\mathbf{r}) = u_n(\mathbf{r})\ \Phi_{n_s,k_q}(s)\ \frac{1}{\sqrt{L_q}} e^{ik_q q} \tag{2.12}$$

where $\Phi_{n_s,k_q}(s)$ satisfies the Schrödinger equation

$$[-\frac{\hbar^2}{2m_n}\frac{\partial^2}{\partial s^2} + \frac{\hbar^2}{2m_n}k_q^2 + U(s)]\ \Phi_{n_s,k_q}(s) = [E_n(k_q) - E_{n0}]\ \Phi_{n_s,k_q}(s) \tag{2.13}$$

Structure	q	$\frac{1}{\sqrt{L_q}} e^{ik_q q}$	s	$\frac{\partial^2}{\partial^2 s}$
Bulk	$x\ y\ z$	$\frac{1}{\sqrt{L_x L_y L_z}} e^{i(k_x x+k_y y+k_z z)}$	/	/
Quantum Well	$x\ y$	$\frac{1}{\sqrt{L_x L_y}} e^{i(k_x x+k_y y)}$	z	$\frac{\partial^2}{\partial^2 z}$
Quantum Wire	y	$\frac{1}{\sqrt{L_y}} e^{ik_y y}$	$x\ z$	$\frac{\partial^2}{\partial^2 x}+\frac{\partial^2}{\partial^2 z}$
Quantum Dot	/	/	$x\ y\ z$	$\frac{\partial^2}{\partial^2 x}+\frac{\partial^2}{\partial^2 y}+\frac{\partial^2}{\partial^2 z}$

Table 2.1: The coordinates choice in analysis of energy band structures in bulk, quantum well, quantum wire and quantum dot semiconductor structures.

or

$$[-\frac{\hbar^2}{2m_n}\frac{\partial^2}{\partial s^2} + U(s)]\ \Phi_{n_s,k_q}(s) = E_{n_s}\ \Phi_{n_s,k_q}(s)\ , \tag{2.14}$$

where the electron energy is

$$E_n(k_q) = E_{n_s} + E_{n0} + \frac{\hbar^2}{2m_n}k_q^2 \tag{2.15}$$

so that E_{n_s} is the quantized energy due to the potential $U(s)$. (2.15) shows that $E_n(k_q)$ is parabolic in k_q. The constant m_n is the effective mass of the electron (or hole) in the n band. The electronic band structure [$E_n(k_q)$ relation] is characterized by the constant of effective mass m_n and $E_{n0} + E_{n_s}$. This is the well known parabolic band approximation.

If the band-to-band coupling (such as that in the degenerate valence bands) is taken into account, The $E_n(k_q)$ relation in these bands can be obtained by solving the coupled Schrödinger equations (2.9) or (2.11). The $E_n(k_q)$ is no longer parabolic and the band structures are more complicated.

2.2 Carrier Distribution Functions and the Induced Polarization

In the previous section, we discussed the electronic states in a semiconductor structure. In the following we will discuss the interaction between an optical field and the carriers occupying these electronic states.

In the presence of an optical field in a semiconductor medium, the Hamiltonian

of the Schrödinger equation (2.1) $H_{crystal}$ changes to

$$H = \frac{[\mathbf{p} + e\mathbf{A}(\mathbf{r},t)]^2}{2m_0} + U_p(\mathbf{r}) + U(\mathbf{r}) = H_{crystal} + H' \tag{2.16}$$

where $\mathbf{A}(\mathbf{r},t)$ is the vector potential of the optical field ($\nabla \cdot \mathbf{A}(\mathbf{r},t) = 0$, Coulomb gauge), and the interaction Hamiltonian is

$$H' = \frac{e}{m_0}\mathbf{A}(\mathbf{r},t) \cdot \mathbf{p} + \frac{e^2}{2m_0} \mid \mathbf{A}(\mathbf{r},t) \mid^2 = \frac{e}{m_0}\mathbf{A}(\mathbf{r},t) \cdot \mathbf{p} \ . \tag{2.17}$$

The $\mid \mathbf{A}(\mathbf{r},t) \mid^2$ term yields zero matrix elements for interband transitions due to the fact that $< u_l \mid u_{l'} >= 0 (l \neq l'$ and that $\mathbf{A}(\mathbf{r},t)$ varies slowly within one unit cell of the crystal.

It can be shown that the interaction Hamiltonian H' can also be written as [9,12]

$$H' = - \ (-e\mathbf{r}) \cdot \mathbf{E}(\mathbf{r},t) = \hat{\mu} \cdot \mathbf{E}(\mathbf{r},t) \tag{2.18}$$

where $\mathbf{E}(\mathbf{r},t) = -\partial\mathbf{A}(\mathbf{r},t)/\partial t = \mathcal{E}(\mathbf{r},t)\hat{\mathbf{a}}$ is the optical field and $\hat{\mathbf{a}}$ is the unit vector along the direction of the optical field polarization.

The semiclassical theory is used here to treat the interaction between the semiconductor medium and the optical field. The carriers in the semiconductor medium are described quantum mechanically by the Schrödinger equation. The optical field is described classically by the Maxwell equations. The transition matrix element for the optical field induced transition of an electron from the conduction to the valence band, or in reverse, is

$$H'_{vc} \ = \ < \Psi_v \mid \hat{\mu} \mid \Psi_c > \cdot \mathbf{E}(\mathbf{r},t) \tag{2.19}$$

$$= e \int u_v^*(\mathbf{r}) \Phi_{n_{sv},k_{qv}}^*(s) \frac{1}{\sqrt{L_q}} e^{-ik_{qv}q} \, (\hat{\mathbf{a}} \cdot \mathbf{r}) \, u_c(\mathbf{r}) \Phi_{n_{sc},k_{qc}}(s) \frac{1}{\sqrt{L_q}} e^{ik_{qc}q} \, d\mathbf{r}$$
$$\times \mathcal{E}(\mathbf{r},t) \, .$$

Notice that $\Phi_{n_{sl},k_{ql}}(s)$ and $e^{ik_{ql}q}$ $(l = c, v)$ vary slowly within one unit cell of the crystal and $< u_v(\mathbf{r}) \,|\, u_c(\mathbf{r}) > = 0$, so that

$$H'_{vc} = e < u_v(\mathbf{r}) \,|\, \hat{\mathbf{a}} \cdot \mathbf{r} \,|\, u_c(\mathbf{r}) > \tag{2.20}$$
$$\times \int \Phi_{n_{sv},k_{qv}}^*(s) \frac{1}{\sqrt{L_q}} e^{-ik_{qv}q} \, \Phi_{n_{sc},k_{qc}}(s) \frac{1}{\sqrt{L_q}} e^{ik_{qc}q} \, d\mathbf{r} \;\; \mathcal{E}(\mathbf{r},t)$$

where

$$< u_v(\mathbf{r}) \,|\, \hat{\mathbf{a}} \cdot \mathbf{r} \,|\, u_c(\mathbf{r}) > = \frac{1}{\Omega} \int_{\text{cell}} u_v^*(\mathbf{r}) \, \hat{\mathbf{a}} \cdot \mathbf{r} \, u_c(\mathbf{r}) \, d\mathbf{r} \, . \tag{2.21}$$

(2.20) indicates that $H'_{vc} = 0$ unless

$$k_{qv} = k_{qc} = k_q \, . \tag{2.22}$$

(2.22) is a necessary condition for band-to-band optical transition in a semiconductor structure and is called "k-selection rule." The transition matrix element becomes

$$H'_{vc} = \tilde{\mu}(\tilde{\alpha}) \, \mathcal{E}(\mathbf{r},t) \tag{2.23}$$

where

$$\tilde{\mu}(\tilde{\alpha}) = e < u_v(\mathbf{r}) \,|\, \hat{\mathbf{a}} \cdot \mathbf{r} \,|\, u_c(\mathbf{r}) > \int \Phi_{n_{sv},k_q}^*(s) \, \Phi_{n_{sc},k_q}(s) \, ds \tag{2.24}$$

and $\tilde{\alpha}$ represents the quantum numbers $\{k_q, n_{sv}, n_{sc}\}$, n_{sv} and n_{sc} are the quantum numbers associated with the wavefunctions $\Phi_{n_{sv},k_q}(s)$ and $\Phi_{n_{sc},k_q}(s)$ in the s direction(s), respectively, which are determined by the potential $U(s)$.

We assume a single mode monochromatic optical field propagates along the y direction, in which direction there is no spatial variation in the potential $U(\mathbf{r})$, *i.e.*, $\partial U/\partial y = 0$,

$$\mathcal{E}(\mathbf{r},t) = \frac{1}{2}\,\mathcal{E}_0\,\mathrm{e}^{i(\beta y-\omega t)} + c.c. \tag{2.25}$$

then

$$H'_{vc} = \frac{1}{2}\,\tilde{\mu}(\tilde{\alpha})\,[\mathcal{E}_0\,\mathrm{e}^{i(\beta y-\omega t)} + c.c.] \tag{2.26}$$

where β is the propagation constant and ω is the optical frequency.

The density-matrix formalism is used to obtain the carrier distribution functions – the probabilities that carriers occupy these states in a semiconductor medium in the presence of an optical field. We use the density-matrix formalism for two-level systems [9,12] and treat the semiconductor active medium as an ensemble of two-level systems [13] with quantum number n_{sc} and n_{sv} and a rigorous k-selection rule applied to the recombining electron-hole pairs, *i.e.*, $k_{qc} = k_{qv} = k_q$. We rewrite the density-matrix equations in terms of the distribution (occupation) functions for electrons $\rho_{ee}(\tilde{\alpha})$, and holes $\rho_{hh}(\tilde{\alpha})$, in the presence of an optical field

$$\frac{d}{dt}[\rho_{ee}(\tilde{\alpha})] = \frac{i}{\hbar}[H'_{vc}\,\rho_{eh}(\tilde{\alpha}) - c.c.] - \frac{\rho_{ee}(\tilde{\alpha}) - f_e}{\tau_e} \tag{2.27}$$

$$\frac{d}{dt}[\rho_{hh}(\tilde{\alpha})] = \frac{i}{\hbar}[H'_{vc}\,\rho_{eh}(\tilde{\alpha}) - c.c.] - \frac{\rho_{hh}(\tilde{\alpha}) - f_h}{\tau_h} \tag{2.28}$$

$$\frac{d}{dt}[\rho_{eh}(\tilde{\alpha})] = \frac{i}{\hbar}H'^{*}_{vc}\,[\rho_{ee}(\tilde{\alpha}) + \rho_{hh}(\tilde{\alpha}) - 1] - \frac{i}{\hbar}E_{\tilde{\alpha}}\,\rho_{eh}(\tilde{\alpha}) - \frac{\rho_{eh}(\tilde{\alpha})}{T_2} \tag{2.29}$$

where

$$f_e = f_e(k_q, n_{sc}, F_e) = \frac{1}{\exp(\frac{E_e(k_q,n_{sc})-F_e}{k_BT}) + 1} \tag{2.30}$$

and

$$f_h = f_h(k_q, n_{sv}, F_h) = \frac{1}{\exp(\frac{E_h(k_q,n_{sv})-F_h}{k_BT}) + 1} \tag{2.31}$$

are the quasi-Fermi distributions that the electrons and the holes tend to relax to in the absence of the optical field perturbation, $E_e(k_q, n_{sc})$ and $E_h(k_q, n_{sv})$ are the energy of an electron and a hole with wavevector k_q and quantum numbers n_{sc} and n_{sv} respectively, F_e and F_h are the quasi-Fermi energy levels for electrons and holes respectively, $\rho_{eh}(\tilde{\alpha})$ is the off-diagonal (electron-hole) density matrix element, $E_{\tilde{\alpha}}$ is the transition energy of a electron-hole pair with wavevector k_q and quantum numbers n_{sc} and n_{sv}, τ_e and τ_h are the intraband relaxation times for electrons in the conduction band and holes in the valence band respectively, T_2 is the interband dephasing time.

$\rho_{ee}(\tilde{\alpha})$ and $\rho_{hh}(\tilde{\alpha})$ can be obtained from Eq.(2.27)-(2.29) as [13]

$$\rho_{ee}(\tilde{\alpha}) = f_e - \frac{\tau_e}{\tau_e + \tau_h}[f_e + f_h - 1]\frac{\mathcal{L}(E - E_{\tilde{\alpha}})\frac{P}{\tilde{P}_s}}{1 + \mathcal{L}(E - E_{\tilde{\alpha}})\frac{P}{\tilde{P}_s}} \tag{2.32}$$

$$\rho_{hh}(\tilde{\alpha}) = f_h - \frac{\tau_h}{\tau_e + \tau_h}[f_e + f_h - 1]\frac{\mathcal{L}(E - E_{\tilde{\alpha}})\frac{P}{\tilde{P}_s}}{1 + \mathcal{L}(E - E_{\tilde{\alpha}})\frac{P}{\tilde{P}_s}} \tag{2.33}$$

where

$$\mathcal{L}(E - E_{\tilde{\alpha}}) = E_{T_2}^2/[E_{T_2}^2 + (E - E_{\tilde{\alpha}})^2] \,, \tag{2.34}$$

$E_{T_2} = \hbar/T_2$, $E = \hbar\omega$ is the photon energy of the optical field, $P = \frac{1}{2}\epsilon_o n_r^2 |\mathcal{E}_0|^2/E$ is the photon density, $\tilde{P}_s = \hbar^2\epsilon_o n_r^2/[|\tilde{\mu}(\tilde{\alpha})|^2 E(\tau_e + \tau_h)T_2]$, and n_r is the refractive index.

Eqs.(2.32) and (2.33) show that the presence of optical field causes spectral "holes" in the Fermi-like distributions. The spectral "holes" are the terms involving P.

The solution for $\rho_{eh}(\tilde{\alpha})$ is

$$\rho_{eh}(\tilde{\alpha}) = -\frac{1}{2}\tilde{\mu}^*(\tilde{\alpha})[\rho_{ee}(\tilde{\alpha}) + \rho_{hh}(\tilde{\alpha}) - 1]\frac{1}{(E - E_{\tilde{\alpha}}) + iE_{T_2}}\mathcal{E}_0 e^{i(\beta y - \omega t)} . \tag{2.35}$$

The induced polarization can be written as

$$\begin{aligned}
\mathcal{P}_{in}(\mathbf{r},t) &= \frac{1}{2}\,\mathcal{P}_{in,0}\, e^{i(\beta y-\omega t)} + c.c. \qquad (2.36)\\
&= \mathrm{Tr}[\,\hat{\rho}(-\hat{\mu}/V)\,] = -\sum_{\tilde{\alpha}}\frac{\zeta(\mathbf{r},\tilde{\alpha})}{V(\tilde{\alpha})}[\rho_{eh}(\tilde{\alpha})\;\tilde{\mu}(\tilde{\alpha}) + c.c.]\\
&= \frac{1}{2}\sum_{\tilde{\alpha}}\frac{\zeta(\mathbf{r},\tilde{\alpha})}{V(\tilde{\alpha})}\,|\tilde{\mu}(\tilde{\alpha})|^2\,[\rho_{ee}(\tilde{\alpha}) + \rho_{hh}(\tilde{\alpha}) - 1]\\
&\quad \times\frac{1}{(E - E_{\tilde{\alpha}}) + iE_{T_2}}\mathcal{E}_0 e^{i(\beta y-\omega t)}\\
&\quad + \quad c.c.\\
&= \frac{1}{2}\,\epsilon_o(\chi_r + i\chi_i)\mathcal{E}_0 e^{i(\beta y-\omega t)} + c.c.
\end{aligned}$$

where $V(\tilde{\alpha})$ is the confinement volume of electrons and holes and

$$\zeta(\mathbf{r},\tilde{\alpha}) = \begin{cases} 1 & [\,\mathbf{r}\ \text{inside}\ V(\tilde{\alpha})\,] \\ 0 & [\,\mathbf{r}\ \text{outside}\ V(\tilde{\alpha})\,] \end{cases} . \tag{2.37}$$

Thus the susceptibility $\chi = \chi_r + i\chi_i$ can be obtained. The real part (χ_r) and imaginary part (χ_i) of the susceptibility can be written as

$$\chi_r = -\sum_{\tilde{\alpha}}\frac{\zeta(\mathbf{r},\tilde{\alpha})}{\epsilon_o V(\tilde{\alpha})}\,|\tilde{\mu}(\tilde{\alpha})|^2\,[\rho_{ee}(\tilde{\alpha}) + \rho_{hh}(\tilde{\alpha}) - 1]\;\mathcal{L}_r(E_{\tilde{\alpha}} - E) \tag{2.38}$$

$$\chi_i = -\sum_{\tilde{\alpha}}\frac{\zeta(\mathbf{r},\tilde{\alpha})}{\epsilon_o V(\tilde{\alpha})}\,|\tilde{\mu}(\tilde{\alpha})|^2\,[\rho_{ee}(\tilde{\alpha}) + \rho_{hh}(\tilde{\alpha}) - 1]\;\mathcal{L}_i(E_{\tilde{\alpha}} - E) \tag{2.39}$$

where

$$\mathcal{L}_r(E_{\tilde{\alpha}} - E) = \frac{E_{\tilde{\alpha}} - E}{E_{T_2}^2 + (E_{\tilde{\alpha}} - E)^2} \tag{2.40}$$

$$\mathcal{L}_i(E_{\tilde{\alpha}} - E) = \frac{E_{T_2}}{E_{T_2}^2 + (E_{\tilde{\alpha}} - E)^2} \cdot \tag{2.41}$$

2.3 Optical Transitions and Gain Coefficients

In section 2.2 we have obtained the polarization $\mathcal{P}_{in}$ due to an optical field induced transitions in the active region. (2.36) and (2.37) indicate that the active region is the region where electron wavefunctions and hole wavefunctions co-exist. In the active region the electron density and hole density can be related by a quasi-neutrality condition

$$\frac{1}{V_{MD}} \sum_{k_q, n_{cs}} f_e(k_q, n_{cs}, F_e) = \frac{1}{V_{MD}} \sum_{k_q, n_{vs}} f_h(k_q, n_{vs}, F_h) = N_{MD} \cdot \tag{2.42}$$

In (2.42) V_{MD} represents the "dimensional volume" of a semiconductor laser structure in which the injected carriers are regarded as M-dimensional, *e.g.*,

$$V_{MD} = \begin{cases} V = L_x \cdot L_y \cdot L_z & \text{(M = 3, bulk)} \\ S = L_x \cdot L_y & \text{(M = 2, quantum well)} \\ L = L_y & \text{(M = 1, quantum wire)} \end{cases} \cdot \tag{2.43}$$

and N_{MD} is the M-dimensional carrier density. Using the unperturbed quasi-Fermi distributions [(2.30) and (2.31)] to calculate the carrier density is very good approximation. The relative error due to the spectral hole burning is less than 1% [13] for the values of carrier density and photon density of interest.

Next we analyze how the optical field induced transitions will in turn contribute to the optical field. We start with the Maxwell wave equation in the form

$$\nabla^2 \mathcal{E}(\mathbf{r},t) - \mu_o \epsilon(\mathbf{r}) \frac{\partial^2}{\partial t^2} \mathcal{E}(\mathbf{r},t) = \mu_o \frac{\partial^2}{\partial t^2} \mathcal{P}_{in}(\mathbf{r},t) \tag{2.44}$$

where μ_o and $\epsilon(\mathbf{r})$ are the magnetic and electric permeabilities, respectively. The variation in $\epsilon(\mathbf{r}) = \epsilon(s')$ (where $s' = \{x, z\}$) manifests the lateral and transverse optical confinement of the laser structures. Assume that the optical field $\mathcal{E}_0$ in (2.25) can be written as

$$\mathcal{E}_0 = A_0(t)\ E_0(s') \tag{2.45}$$

where A_0 is a complex number including both the amplitude and the phase of the optical field and $E_0(s')$ is the eigenmode of the optical confinement structures with

$$(\frac{\partial^2}{\partial s'^2} - \beta^2) E_0(s') + \omega^2 \mu_o \epsilon(s') E_0(s') = 0\ . \tag{2.46}$$

In most semiconductor lasers, the lasing action occurs in the fundamental eigenmode. Substitution of (2.25),(2.36),(2.45) and (2.46) in (2.44) leads to

$$\begin{aligned} 2i\ \epsilon(s')\ E_0(s')\ \frac{dA_0}{dy} \ &= \ -\omega \sum_{\tilde{\alpha}} \frac{\zeta(\mathbf{r},\tilde{\alpha})}{V(\tilde{\alpha})}\ |\tilde{\mu}(\tilde{\alpha})|^2\ [\rho_{ee}(\tilde{\alpha}) + \rho_{hh}(\tilde{\alpha}) - 1] \\ &\quad \times \frac{1}{(E - E_{\tilde{\alpha}}) + iE_{T_2}}\ E_0(s')\ A_0\ , \end{aligned} \tag{2.47}$$

where we assume slow variation so that

$$|\frac{d^2 A_0}{dt^2}| \ \ll \ \omega\ |\frac{dA_0}{dt}|\ . \tag{2.48}$$

We take the product of (2.47) with $E_0^*(s')$ and integrate over $s' = \{x, z\}$ from $-\infty$ to $+\infty$. The result is

$$\frac{dA_0}{dt} \ = \ \frac{i\omega}{2} A_0 \sum_{\tilde{\alpha}} \frac{1}{V(\tilde{\alpha})} \frac{\int \zeta(\mathbf{r},\tilde{\alpha})\ |E_0(s')|^2 ds'}{\int \epsilon(s')\ |E_0(s')|^2 ds'} \tag{2.49}$$

$$\times |\tilde{\mu}(\tilde{\alpha})|^2 [\rho_{ee}(\tilde{\alpha}) + \rho_{hh}(\tilde{\alpha}) - 1] \frac{1}{(E - E_{\tilde{\alpha}}) + iE_{T_2}} .$$

When the summation over k_q has to be made for the evaluation of the carrier density [Eq.(2.42)] and the right term in (2.49), one needs to make an integration over the carrier density of states. For different laser structures (e.g., quantum well, quantum wire), there is no additional potential in the q-dimension(s) for the injected carriers. It is convenient to take the "dimensional volume" V_{MD} [see (2.43)] out of $V(\tilde{\alpha})$ in (2.49) and define

$$v(n_{sc}, n_{sv}) = V(\tilde{\alpha})/V_{MD} . \tag{2.50}$$

$v(n_{sc}, n_{sv})$ can be regarded as the "dimensional volume" associated with the s-dimension(s). Assume that the photons has a normalized distribution $\Theta(s') = \Theta(x, z)$ in a semiconductor laser structure

$$\Theta(s') = \epsilon(s') |E_0(s')|^2 / [\int \epsilon(s') |E_0(s')|^2 ds'] . \tag{2.51}$$

If the carrier localization is much stronger than that of the optical field, $\Theta(s')$ in the active region can be approximated by its value at the center of the active region ($s' = 0$). In this case, (2.48) can be written as

$$\frac{dA_0}{dt} = \frac{i\omega}{2\epsilon_o n_r^2} A_0 \sum_{\tilde{\alpha}} \Gamma_{MD} \frac{1}{V_{MD}} |\tilde{\mu}(\tilde{\alpha})|^2 [\rho_{ee}(\tilde{\alpha}) + \rho_{hh}(\tilde{\alpha}) - 1] \times \frac{1}{(E - E_{\tilde{\alpha}}) + iE_{T_2}} \tag{2.52}$$

where

$$\Gamma_{MD} = \Theta(0) \frac{S_{ac}}{v(n_{cs}, n_{vs})} \tag{2.53}$$

is the coupling factor reflecting how the injected carriers in different semiconductor structures (which might be 3D bulk, 2D quantum well or 1D quantum wire structures) interact with the 3D photons in the active region and S_{ac} is the area of the active region normal to the direction of mode propagation, *i.e.*, in the $x-z$ plane. In Table II, we have listed the corresponding parameters for different semiconductor laser structures. In the case of 3D bulk lasers, the coupling factor is the conventional confinement factor. (2.52) can be re-written as

$$\frac{dA_0}{dt} = \frac{1}{2}v_g(\Gamma_{MD}G - i\Gamma_{MD}N_r)A_0 = \frac{1}{2}v_g(g - i\vartheta)A_0 \tag{2.54}$$

where $v_g = c/n_r$, $g = \Gamma_{MD}G(E)$ is the so called modal (exponential) gain coefficient,

$$\begin{aligned} G(E) &= \frac{1}{V_{MD}}\sum_{\tilde{\alpha}} \frac{|\tilde{\mu}(\tilde{\alpha})|^2}{\hbar c\epsilon_o n_r} E\,[\rho_{ee}(\tilde{\alpha}) + \rho_{hh}(\tilde{\alpha}) - 1]\,\mathcal{L}_i(E_{\tilde{\alpha}} - E) \qquad (2.55)\\ &= \frac{1}{V_{MD}}\sum_{\tilde{\alpha}} \frac{|\tilde{\mu}(\tilde{\alpha})|^2}{\hbar c\epsilon_o n_r}\frac{E}{E_{T_2}}[\rho_{ee}(\tilde{\alpha}) + \rho_{hh}(\tilde{\alpha}) - 1]\,\mathcal{L}(E - E_{\tilde{\alpha}})\\ N_r(E) &= \frac{1}{V_{MD}}\sum_{\tilde{\alpha}} \frac{|\tilde{\mu}(\tilde{\alpha})|^2}{\hbar c\epsilon_o n_r} E\,[\rho_{ee}(\tilde{\alpha}) + \rho_{hh}(\tilde{\alpha}) - 1]\,\mathcal{L}_r(E_{\tilde{\alpha}} - E)\,, \qquad (2.56) \end{aligned}$$

and $\vartheta = \Gamma_{MD}N_r(E)$. If the photon density inside the active region is denoted by P

$$P = \frac{1}{2}\epsilon_o n_r^2\,|\mathcal{E}_0(t, s' = 0)|^2/E = \frac{1}{2}\epsilon_o n_r^2\,|A_0E_0(0)|^2/E, \tag{2.57}$$

we get from (2.54)

$$\frac{dP}{dt}|_{stim.} = v_g\ g\ P\ =\ v_g\ \Gamma_{MD}\ G\ P \tag{2.58}$$

which is the photon density increase rate due to the stimulated optical transitions in the active region.

The total optical power generated due to the stimulated optical transitions in the

	S_{ac}	V_{MD}	$\nu(n_{sc},n_{sv})$	$\Theta(0)$	Γ_{MD}
Bulk	$w\ d_z$	V	1	$1/(w\ t_z)$	d_z/t_z
Quantum Well	$w\ d_z$	S	d_z	$1/(w\ t_z)$	$1/t_z$
Quantum Wire	$d_x\ d_z$	L	$d_x\ d_z$	$1/(t_x\ t_z)$	$1/(t_x\ t_z)$

Table 2.2: The coupling factors and associated parameters in semiconductor bulk, quantum well, and quantum wire structures.

active region is

$$-\int < \mathcal{E}(\mathbf{r},t)\frac{d\mathcal{P}_{in}(\mathbf{r},t)}{dt} >_t d\mathbf{r} = -\int \frac{1}{2}\mathrm{Re}[\mathcal{E}_0(-i\omega\mathcal{P}_{in,0})^*]d\mathbf{r} \qquad (2.59)$$
$$= -\hbar\omega\, V_{MD}\, \frac{dN_{MD}}{dt}\,|_{stim.}$$

where $< >_t$ denotes to an average over the time. (2.59) and (2.36) lead to

$$\frac{dN_{MD}}{dt}\,|_{stim.} = -v_g G(E) P \ . \qquad (2.60)$$

$-V_{MD}(dN_{MD}/dt)\,|_{stim.}$ is the total injected carrier transition number at the active region due to the stimulated emissions which is equal to the total number of photons coherently added to the optical mode. N_{MD} and V_{MD} are defined in (2.42) and (2.43), respectively.

(2.58) and (2.60) are two very important relations to describe the interaction between the injected carriers and the photons in various semiconductor laser structures. Based on (2.58) and (2.60), rate equations for photon density and carrier density can be obtained to describe the static and dynamic characteristics of a semiconductor laser.

Using (2.55), (2.32), (2.33) and assuming $P/\tilde{P}_s < 1$, the "dimensional gain coefficient" $G(E)$ can be approximately written as

$$G(E) = G_0(E) - G_1(E)\frac{P}{\tilde{P}} \qquad (2.61)$$

where

$$G_0(E) = \frac{1}{V_{MD}}\sum_{\tilde{\alpha}} \frac{|\tilde{\mu}(\tilde{\alpha})|^2}{\hbar c\epsilon_o n_r}\frac{E}{E_{T_2}}[f_e(\tilde{\alpha}) + f_h(\tilde{\alpha}) - 1]\ \mathcal{L}(E - E_{\tilde{\alpha}}) \qquad (2.62)$$

$$G_1(E) = \frac{1}{V_{MD}}\sum_{\tilde{\alpha}} \frac{|\tilde{\mu}(\tilde{\alpha})|^2}{\hbar c\epsilon_o n_r}\frac{E}{E_{T_2}}[f_e(\tilde{\alpha}) + f_h(\tilde{\alpha}) - 1]\ \mathcal{L}^2(E - E_{\tilde{\alpha}})\ . \qquad (2.63)$$

G_0 is the linear gain coefficient and G_1 is the nonlinear gain coefficient. $G_1 \neq 0$ describes the gain decrease at photon energy E due to the presence of the optical field, *i.e.*, the spectral hole burning [3,10,11,2,4,1].

The definition for the "dimensional gain coefficients" G_0 and G_1 seems to be superfluous. However, since the "dimensional differential gain" dG/dN has a universal unit in all different structures where N is the "dimensional carrier density," this facilitates the comparison between different laser structures. As we will show later, many dynamic properties of a semiconductor laser are determined by the differential gain values.

Bibliography

[1] G. P. Agrawal, "Spectral hole-burning and gain saturation in semiconductor lasers: strong-signal theory," *J. Appl. Phys.*, vol.63, p.1232, 1988

[2] M. Asada and Y. Suematsu, "Density-matrix theory of semiconductor lasers with relaxation broadening model – gain and gain-suppression in semiconductor lasers," *IEEE J. Quantum Electron.*, vol.QE-21, p.434, 1985

[3] D. P. Channin, "Effect of gain saturation on injection laser switching," *J. Appl. Phys.*, vol.50, p.3858, 1979

[4] W. W. Chow, G. C. Dente and D. Depatie, "Saturation effect in semiconductor lasers," *IEEE J. Quantum Electron.*, vol.QE-23, p.1314, 1987

[5] G. Dresselhaus, "Spin-orbit coupling effects in zinc blende structures," *Phys. Rev.*, vol.100, p.580, 1955

[6] E. O. Kane, "Band structure of indium antimonide," *J. Phys. Chem. Solids*, vol.100, p.580, 1957

[7] J. M. Luttinger and W. Kohn, "Motion of electrons and holes in perturbed periodic fields," *Phys. Rev.*, vol.97, p.869, 1955

[8] J. M. Luttinger, "Quantum theory of cyclotron resonance in semiconductors: general theory," *Phys. Rev.*, vol.102, p.1030, 1956

[9] M. Sargent III, M. O. Scully, and W. E. Lamb, Jr., *Laser Physics*, Addison-Wesley, 1974

[10] M. Yamada and Y. Suematsu, "Analysis of gain suppression in undoped injection lasers," *J. Appl. Phys.*, vol.52, p.2653, 1981

[11] M. Yamada, "Transverse and longitudinal mode control in semiconductor injection lasers," *IEEE J. Quantum Electron.*, vol.QE-19, p.1365, 1983

[12] A. Yariv, *Quantum Electronics*, 3rd Ed., John Wiley & Sons, 1989

[13] B. Zhao, T. R. Chen, and A. Yariv, "The gain and carrier density in semiconductor lasers under steady-state and transient conditions," *IEEE J. Quantum Electron.*, vol.QE-28, p.1479, 1992

Chapter 3

Basics in Semiconductor Quantum Well Lasers and Their Performance

In Chapter 2, we have presented a general analysis of the optical transitions, carrier distribution functions, and gain coefficients in semiconductor lasers of various structures. In order to obtain the description of optical properties in various semiconductor laser structures, one needs first to obtain the transition matrix elements $|\tilde{\mu}(\tilde{\alpha})|^2$. In addition, one needs to know how to calculate $\frac{1}{V_{MD}}\sum_{\tilde{\alpha}}$ for these laser structures. As we will show next, the calculation of $\frac{1}{V_{MD}}\sum_{\tilde{\alpha}}$ can be done by obtaining the density of states for the carriers and then integrating over those electronic states. Both transition matrix elements and the density of states are dependent on the electronic band structures of the semiconductor active media. From now on, we

concentrate our analysis on the QW laser structure.

3.1 Transition Matrix Elements and Density of States

The expressions for $G_0(E)$, $G_1(E)$ and $\tilde{P}_s$ depend on the transition matrix element $|\tilde{\mu}(\tilde{\alpha})|^2$. $\tilde{\mu}(\tilde{\alpha})$ is given in (2.24) for a single band model. The transition matrix elements are quite different for different semiconductor laser structures due to the different spatial symmetry. We will first study the transition matrix elements in a bulk semiconductor structure and then the ones in quantum well semiconductor structures.

As we discussed in Section 2.1, to obtain the solutions for the electronic states one needs to solve the Schrödinger equation or coupled Schrödinger equations. Usually, the coordinate system is chosen such that the x, y and z axes are along the crystalline axes. So the matrix elements in the coupled Schrödinger equation can be significantly simplified because of the symmetry of the crystal. This will also facilitate the treatment of the interaction between the optical field and the semiconductor medium since the polarization of the optical field is usually also along one of the crystalline axes.

In a zinc blende crystal with large direct band gap, the conduction band structure is well described by the single band model [(2.12) - (2.15)]. The Bloch functions at

the conduction band edge are written as

$$u_c(\mathbf{r}) = \begin{cases} |S> \cdot |\uparrow> \\ |S> \cdot |\downarrow> \end{cases} \tag{3.1}$$

where $|S>$ is the S-like isotropic spatial function, $|\uparrow>$ and $|\downarrow>$ are the spin functions with the spin along the $\mathbf{z}$ and $-\mathbf{z}$ directions, respectively. The envelope function for the electrons in the conduction band and the conduction band structure $E_e(\mathbf{k})$ can be obtained by solving

$$\frac{\hbar^2}{2m_e}[\hat{k_x}^2 + \hat{k_y}^2 + \hat{k_z}^2 + U_c(\mathbf{r})]\ \Phi_e(\mathbf{r}) = E_e\ \Phi_e(\mathbf{r}) \tag{3.2}$$

where m_e is the effective mass of the electrons in the conduction bands, $\hat{k_r} = -i\partial_r = -i\partial/\partial_r$ $(r = x, y, z)$, and the electron energy is measured from the bottom of the conduction band (*i.e.*, assuming $E_{c0} = 0$).

For the zinc blende direct band gap semiconductor with large spin-orbit energy separation, the valence bands have a four-fold degeneracy (including the two-fold spin degeneracy) at the band edge. The Bloch functions at the valence band edge can be written as [8]

$$u_v(\mathbf{r}) = |j> = \begin{cases} |\frac{3}{2}> &= \frac{1}{\sqrt{2}}(|X> + i\,|Y>)\cdot|\uparrow> \\ |\frac{1}{2}> &= \frac{i}{\sqrt{6}}[(|X> + i\,|Y>)\cdot|\uparrow> - 2\,|Z>\cdot|\downarrow>] \\ |-\frac{1}{2}> &= \frac{1}{\sqrt{6}}[(|X> - i\,|Y>)\cdot|\downarrow> + 2\,|Z>\cdot|\uparrow>] \\ |-\frac{3}{2}> &= \frac{i}{\sqrt{2}}(|X> - i\,|Y>)\cdot|\downarrow> \end{cases} \tag{3.3}$$

where $|X>$, $|Y>$, $|Z>$ are the P-like spatial functions. $|\frac{3}{2}>$ and $|-\frac{3}{2}>$ correspond to the heavy hole valence bands; $|\frac{1}{2}>$ and $|-\frac{1}{2}>$ correspond to the light hole

valence bands. The valence band structure can be obtained by solving the coupled Schrödinger equations [(2.9) and (2.11)] which can be written explicitly as [8,9]

$$\begin{bmatrix} P+Q & L & M & 0 \\ L^* & P-Q & 0 & M \\ M^* & 0 & P-Q & -L \\ 0 & M^* & -L^* & P+Q \end{bmatrix} \begin{bmatrix} \Phi_{h,\frac{3}{2}}(\mathbf{r}) \\ \Phi_{h,\frac{1}{2}}(\mathbf{r}) \\ \Phi_{h,-\frac{1}{2}}(\mathbf{r}) \\ \Phi_{h,-\frac{3}{2}}(\mathbf{r}) \end{bmatrix} = E_h \begin{bmatrix} \Phi_{h,\frac{3}{2}}(\mathbf{r}) \\ \Phi_{h,\frac{1}{2}}(\mathbf{r}) \\ \Phi_{h,-\frac{1}{2}}(\mathbf{r}) \\ \Phi_{h,-\frac{3}{2}}(\mathbf{r}) \end{bmatrix} \tag{3.4}$$

where

$$P = \frac{\hbar^2}{2m_0}\gamma_1 [\hat{k_x}^2 + \hat{k_y}^2 + \hat{k_z}^2 + U_v(\mathbf{r})] \tag{3.5}$$

$$Q = \frac{\hbar^2}{2m_0}\gamma_2 [\hat{k_x}^2 + \hat{k_y}^2 - 2\hat{k_z}^2] \tag{3.6}$$

$$L = -i\sqrt{12}\frac{\hbar^2}{2m_0}\gamma_3 [\hat{k_x} - i\hat{k_y}]\hat{k_z} \tag{3.7}$$

$$M = \sqrt{3}\frac{\hbar^2}{2m_0}\{\gamma_2[\hat{k_x}^2 - \hat{k_y}^2] - i2\gamma_3\hat{k_x}\hat{k_y}\} \tag{3.8}$$

γ_1, γ_2 and γ_3 are the so called Luttinger parameters, and the valence band energy is measured downward from the top of the valence band edge, *i.e.*, assuming $E_{v0} = 0$ and $E_h = -E_v \geq 0$. The wavefunction of a hole in the valence band is written as

$$\Psi_h(\mathbf{r}) = \sum_j |j> \Phi_{h,j}(\mathbf{r}) \qquad (j = \frac{3}{2}, \frac{1}{2}, -\frac{1}{2}, -\frac{3}{2}) \,. \tag{3.9}$$

(3.4)-(3.8) were obtained by a $\mathbf{k}\cdot\mathbf{p}$ approximation up to the second order in the wave vector (k^2). There should be some linear k terms in (3.4)-(3.8) due to the lack of inversion symmetry in zinc blende structure in comparison with that for the diamond structure (such as Si and Ge) [8,6,7]. However, these linear k terms are negligible for the zinc blende crystals with large spin-orbit energy separation [6,7,5].

For bulk semiconductor structure $U_c(\mathbf{r}) = 0$ and $U_v(\mathbf{r}) = 0$, the conduction band structure $E_e(\mathbf{k})$ and the valence band structure $E_h(\mathbf{k})$ can be obtained by taking the envelope functions $\Phi_l(\mathbf{r}) \propto \exp(i\mathbf{k}\cdot\mathbf{r})/\sqrt{V}$ in (2.9). (3.2) results in a parabolic relation $E_e(\mathbf{k}) = \hbar^2 k^2/(2m_e)$ where $k = \mid \mathbf{k} \mid$. Under spherical approximation [4] $\gamma_2 = \gamma_3 = \bar{\gamma} \equiv (2\gamma_2 + 3\gamma_3)/5$ in (3.5)-(3.8), (3.3) can be diagonalized under a unitary transformation [9,7]. The new Bloch functions at the band edge under the unitary transformation are

$$
u_v(\mathbf{r}) = \mid j' > = \left\{ \begin{array}{rcl}
\mid \frac{3}{2}' > & = & \frac{1}{\sqrt{2}}[(\cos\phi\cos\theta - i\sin\phi)\mid X> \\
 & & +(\sin\phi\cos\theta + i\cos\phi)\mid Y> - \sin\theta\mid Z>]\cdot\mid\uparrow'> \\
\mid \frac{1}{2}' > & = & \frac{i}{\sqrt{6}}\{[(\cos\phi\cos\theta - i\sin\phi)\mid X> \\
 & & +(\sin\phi\cos\theta + i\cos\phi)\mid Y> - \sin\theta\mid Z>]\cdot\mid\uparrow'> \\
 & & -2[\cos\phi\sin\theta\mid X> + \sin\phi\sin\theta\mid Y> \\
 & & +\cos\theta\mid Z>]\cdot\mid\downarrow'>\} \\
\mid -\frac{1}{2}' > & = & \frac{1}{\sqrt{6}}\{[(\cos\phi\cos\theta + i\sin\phi)\mid X> \\
 & & +(\sin\phi\cos\theta - i\cos\phi)\mid Y> - \sin\theta\mid Z>]\cdot\mid\downarrow'> \\
 & & +2[\cos\phi\sin\theta\mid X> + \sin\phi\sin\theta\mid Y> \\
 & & +\cos\theta\mid Z>]\cdot\mid\uparrow'>\} \\
\mid -\frac{3}{2}' > & = & \frac{i}{\sqrt{2}}[(\cos\phi\cos\theta + i\sin\phi)\mid X> \\
 & & +(\sin\phi\cos\theta - i\cos\phi)\mid Y> - \sin\theta\mid Z>]\cdot\mid\downarrow'>
\end{array} \right. \tag{3.10}
$$

where ϕ and θ are the angles specifying the wave vector $\mathbf{k}$ in a bulk semiconductor

structure as shown in Figure 3.1, $|\uparrow'>$ and $|\downarrow'>$ are the spin functions with the spin along the $\mathbf{k}$ and $-\mathbf{k}$ directions, respectively. $|\frac{3}{2}'>$ and $|-\frac{3}{2}'>$ correspond to the heavy hole valence bands; $|\frac{1}{2}'>$ and $|-\frac{1}{2}'>$ correspond to the light hole valence bands. For the new Bloch functions, the heavy hole valence bands and light hole valence bands are completely decoupled with effective masses of $m_{hh} = m_0/(\gamma_1 - 2\bar{\gamma})$ for the heavy holes and $m_{hl} = m_0/(\gamma_1 + 2\bar{\gamma})$ for the light holes, respectively. Thus, the valence bands can also be treated by the single band model and the valence band structures are described by the parabolic relations with the corresponding effective masses, *i.e.*, $E_{hh}(\mathbf{k}) = \hbar^2 k^2/(2m_{hh})$ and $E_{hl}(\mathbf{k}) = \hbar^2 k^2/(2m_{hl})$. The corresponding Bloch functions for the conduction band under the unitary transformation are

$$u_c(\mathbf{r}) = \begin{cases} |S> \cdot |\uparrow'> \\ \\ |S> \cdot |\downarrow'> \end{cases} . \tag{3.11}$$

Assuming the optical wave propagates along the y direction, the corresponding transition matrix elements $|\tilde{\mu}(k)|^2$ and their average over ϕ and θ are shown in Table 3.1 for the TE mode ($\hat{\mathbf{a}} \parallel \hat{\mathbf{x}}$) and the TM mode ($\hat{\mathbf{a}} \parallel \hat{\mathbf{z}}$). The transition matrix elements shown in Table 3.1 are in unit of μ^2 with

$$\mu^2 \equiv \frac{e^2}{3} |<S|x|X>|^2 = \frac{e^2}{3} |<S|y|Y>|^2 = \frac{e^2}{3} |<S|z|Z>|^2 \tag{3.12}$$

and $< >_{\phi,\theta}$ represents the average over ϕ and θ. Table 3.1 can be summarized as that the conduction band to heavy hole band transitions and conduction band to light hole band transitions have the same transition matrix elements (μ^2) for TE and TM modes in bulk semiconductor structure.

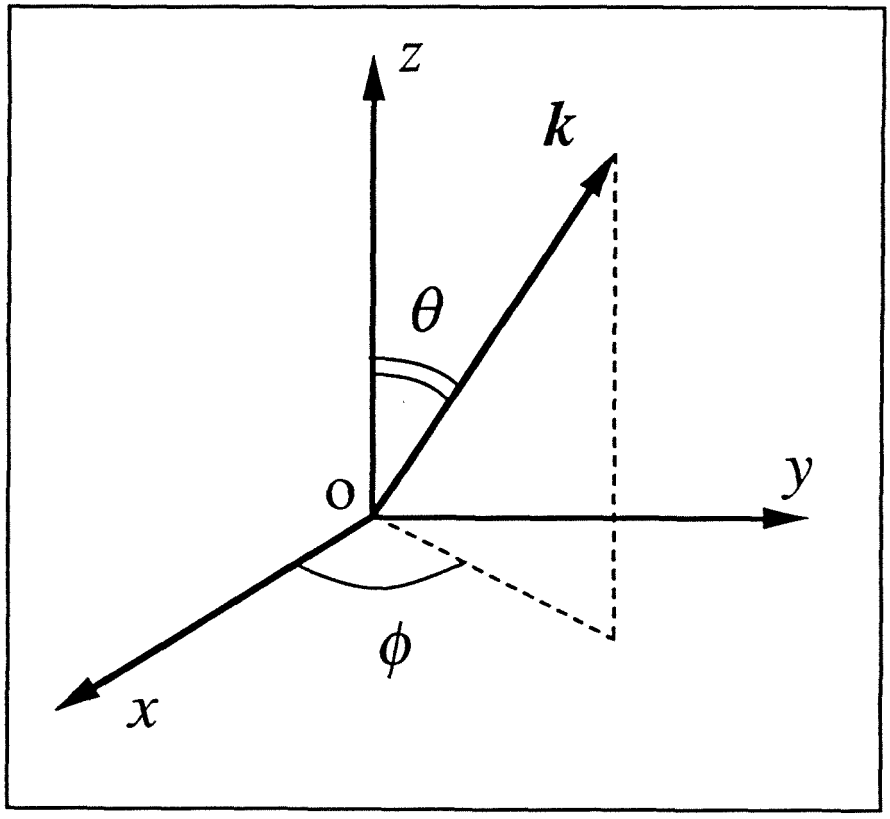

Figure 3.1: The representation of the wave vector for an electron or a hole in the crystalline coordinate system.

TE		
	$\|S>\cdot\|\uparrow'>$	$\|S>\cdot\|\downarrow'>$
$\|\frac{3}{2}'>$	$<\frac{3}{2}(\cos^2\varphi\cos^2\theta+\sin^2\varphi)>_{\varphi,\theta}=1$	0
$\|\frac{1}{2}'>$	$<\frac{1}{2}(\cos^2\varphi\cos^2\theta+\sin^2\varphi)>_{\varphi,\theta}=\frac{1}{3}$	$<2\cos^2\varphi\sin^2\theta>_{\varphi,\theta}=\frac{2}{3}$
$\|-\frac{1}{2}'>$	$<2\cos^2\varphi\sin^2\theta>_{\varphi,\theta}=\frac{2}{3}$	$<\frac{1}{2}(\cos^2\varphi\cos^2\theta+\sin^2\varphi)>_{\varphi,\theta}=\frac{1}{3}$
$\|-\frac{3}{2}'>$	0	$<\frac{3}{2}(\cos^2\varphi\cos^2\theta+\sin^2\varphi)>_{\varphi,\theta}=1$
TM		
	$\|S>\cdot\|\uparrow'>$	$\|S>\cdot\|\downarrow'>$
$\|\frac{3}{2}'>$	$<\frac{3}{2}\sin^2\theta>_{\varphi,\theta}=1$	0
$\|\frac{1}{2}'>$	$<\frac{1}{2}\sin^2\theta>_{\varphi,\theta}=\frac{1}{3}$	$<2\cos^2\theta>_{\varphi,\theta}=\frac{2}{3}$
$\|-\frac{1}{2}'>$	$<2\cos^2\theta>_{\varphi,\theta}=\frac{2}{3}$	$<\frac{1}{2}\sin^2\theta>_{\varphi,\theta}=\frac{1}{3}$
$\|-\frac{3}{2}'>$	0	$<\frac{3}{2}\sin^2\theta>_{\varphi,\theta}=1$

Table 3.1: The transition matrix elements and their angular average for TE and TM modes in bulk semiconductor structure in unit of μ^2. See text for definition of μ^2.

In quantum well semiconductor structure, there exists a thin layer of semiconductor material of smaller energy bandgap E_{g1} bounded on either side by semiconductor materials of bigger energy bandgap E_{g2}, as in Figure 3.2. Correspondingly, this introduces the additional potential $U(\mathbf{r})$ for electrons in conduction band and for holes in valence band. Assume that the z direction is perpendicular to the E_{g1} layer, then $U(\mathbf{r}) = U(z)$, *i.e.*, $s = z$ and $q = x, y$ for the formalism of Chapter 2. The thin E_{g1} region acts as a trap for the electrons in the conduction band and for the holes in the valence band, respectively. If the thickness of the E_{g1} active region approaches the 100 Å region, the confined electrons and holes display quantum effects. The depressed potential region (E_{g1} layer) is called quantum well and the resulting lasers are called quantum well (QW) lasers. The energies and wavefunctions of electrons and holes in the QW are determined by the E_{g1} layer thickness d and the energy depth of the QW. As an example, consider the $Al_xGa_{1-x}As/GaAs/Al_xGa_{1-x}As$ QW structure as depicted in Figure 4.2. The conduction band edge is lower by $\Delta E_c \approx 0.67 \cdot \Delta E_g$ in the GaAs inner region compared to the two side where $\Delta E_g \equiv E_g(Al_xGa_{1-x}As) - E_g(GaAs) = x \cdot 1.27$ eV. Consequently, there exists a discontinuity in the valence band edge $\Delta E_v \approx 0.33 \cdot \Delta E_g$. Correspondingly, $U_c(z)$ and $U_v(z)$ are the conduction band edge and the valance band edge, respectively.

In a QW laser structure, the envelope function of an electron in the conduction

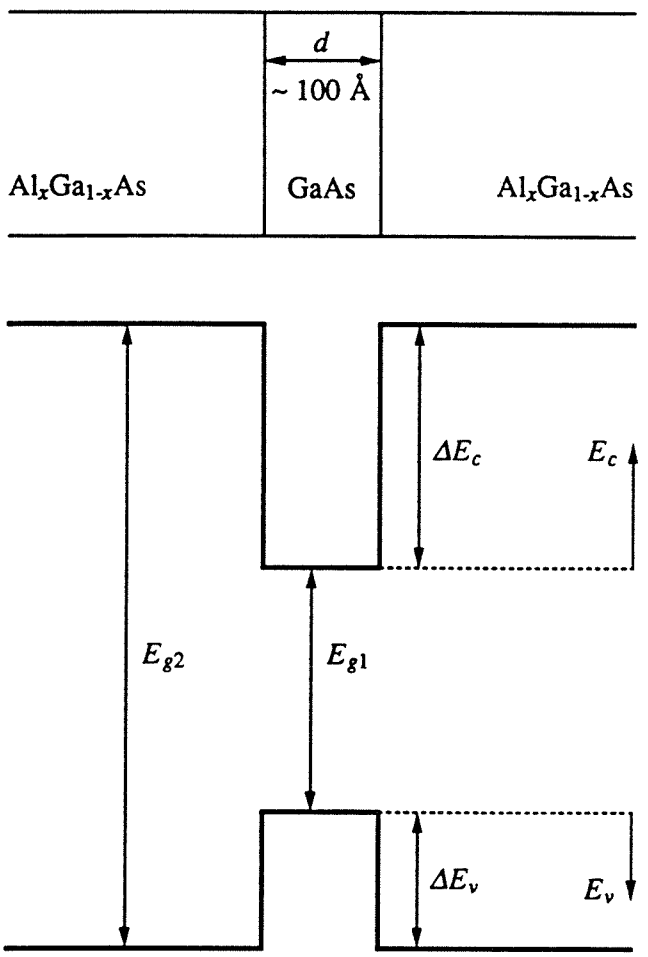

Figure 3.2: The layered structure and the conduction and valence band edges of a AlGaAs/GaAs/AlGaAs quantum well laser structure.

band can be written as

$$\Phi_e(\mathbf{r}) = \Phi_{e,z}(z)\ \frac{1}{\sqrt{S}} e^{i\mathbf{k}_{\|}\cdot\mathbf{r}_{\|}} \tag{3.13}$$

where $\mathbf{r}_{\|}$ and $\mathbf{k}_{\|}$ are the position vector and the wave vector in the plane of the QW plane, respectively, and $S = L_x \cdot L_y$. Substituting (3.13) into (3.2) will result in

$$[-\frac{\hbar^2}{2m_e}\frac{\partial^2}{\partial z^2} + U_c(z)]\ \Phi_{e,z}(z) = E_{e,z}\Phi_{e,z}(z)\ , \tag{3.14}$$

and

$$E_e = \frac{\hbar^2 k^2}{2m_e} + E_{e,z} \tag{3.15}$$

where $k = |\mathbf{k}_{\|}|$, the $E_{e,z}$ are a series of quantized energy levels and the $\Phi_{e,z}(z)$ are the corresponding wavefunctions

$$E_{e,z} = E_{e,z}(n_e)\ ,\quad \Phi_{e,z}(z) = \Phi_{e,z}(z, n_e) \quad (n_e = 1, 2, \cdots)\ . \tag{3.16}$$

The envelope functions for the holes can be written as

$$\Phi_{h,j}(\mathbf{r}) = \Phi_{hj,z}(z)\ \frac{1}{\sqrt{S}} e^{i\mathbf{k}_{\|}\cdot\mathbf{r}_{\|}} \qquad j = \frac{3}{2}, \frac{1}{2}, -\frac{1}{2}, -\frac{3}{2}\ . \tag{3.17}$$

In (3.13) and (3.17), the wave vectors $\mathbf{k}_{\|}$ for the electrons and the holes are not distinguished since for interband transitions the wave vectors must be the same for the electrons and the holes under the k-selection rule. Substitution of (3.17) into (3.4) will result in a set of coupled differential equations similar to (3.4) with $\Phi_{h,j}(\mathbf{r})$ replaced by $\Phi_{hj,z}(z)$, $\hat{k_x}$ and $\hat{k_x}$ replaced by k_x and k_y, respectively. The solutions to this set of coupled Schrödinger equations are a set of energy levels $E_h = E_h(n_h, k_x, k_y)$ and the corresponding envelope functions $\Phi_{hj,z}(z) = \Phi_{hj,z}(z, n_h)$ ($j = \frac{3}{2}, \frac{1}{2}, -\frac{1}{2}, -\frac{3}{2}$ and $n_h = 1, 2, \cdots$).

In a QW semiconductor structure, the transition matrix elements are quite different from that for the bulk semiconductor structure since some of the crystal symmetries are not present due to the addition potential $U(z)$ in the QW structure. The transition matrix elements in QW structures can be generally written as

$$|\tilde{\mu}(\tilde{\alpha})|^2 = |\tilde{\mu}(n_e, n_h, k_x, k_y)|^2 = \mu^2 \delta \tag{3.18}$$

where δ is called as polarization modification factor for the transition matrix elements. In Table 3.2, the polarization modification factors for TE and TM modes are shown for various transitions where

$$< \Phi_{h,j} | \Phi_e > = \int \Phi^*_{hj,z}(z, n_h) \Phi_{e,z}(z, n_e) dz \ . \tag{3.19}$$

The transition matrix elements in the QW structures can be obtained from the electron wave functions $\Phi_{e,z}(z, n_e)$ and the hole wave functions $\Phi_{hj,z}(z, n_h)$. The gain coefficients can be evaluated based on (2.62) and (2.63) by summations over k_x, k_y, n_e and n_h.

In the QW structures, the process of solving coupled Schrödinger equations (3.4) for the holes in the valence band is much more complicated and difficult than that of solving (3.14) for the electrons in the conduction band. There have been several approximation methods used to simplify the process in order to obtain the wave functions for the holes and the transition matrix elements. (3.4) can be block diagonalized into 2×2 blocks under a unitary transformation [5]. Thus, the number of the coupled equations can be reduced from 4 to 2. Further, under the axial approximation, solving the valence band structures can be further simplified [10,1] since the band structures

TE	
$\|\uparrow>$	$\frac{3}{2}\|<\Phi_{h,3/2}\|\Phi_e>\|^2 + \frac{1}{2}\|<\Phi_{h,1/2}\|\Phi_e>\|^2 - i\sqrt{3}\,\mathrm{Im}[<\Phi_{h,3/2}\|\Phi_e><\Phi_e\|\Phi_{h,1/2}>]$
$\|\downarrow>$	$\frac{3}{2}\|<\Phi_{h,-3/2}\|\Phi_e>\|^2 + \frac{1}{2}\|<\Phi_{h,-1/2}\|\Phi_e>\|^2 + i\sqrt{3}\,\mathrm{Im}[<\Phi_{h,-3/2}\|\Phi_e><\Phi_e\|\Phi_{h,-1/2}>]$
TM	
$\|\uparrow>$	$2\|<\Phi_{h,-1/2}\|\Phi_e>\|^2$
$\|\downarrow>$	$2\|<\Phi_{h,1/2}\|\Phi_e>\|^2$

Table 3.2: The polarization modification factors for TE and TM modes in QW structure. The definition of $< \Phi_{h,j} | \Phi_e >$ is given in text.

have a rotation symmetry in the $k_x - k_y$ plane. The axial approximation assumes that $\gamma_2 = \gamma_3 = \bar{\gamma} \equiv (\gamma_2 + \gamma_3)/2$ in the M term of (3.4) [2].

The most simple model used is the decoupled valence band approximation. In this approximation, in order to obtain the transition matrix elements in QW structures it has been assumed that the electrons and the holes have a virtual wave vector k_z along the z direction which is associated with their corresponding quantized energies along the z direction [13,3,11,12]. Then, as the case for the bulk structure, (3.4) can be diagonalized under the spherical approximation and a unitary transformation. The new Bloch functions are the same as given in (3.10). The valence bands are then decoupled and two equations similar to (3.2) can be obtained with corresponding heavy hole effective mass m_{hh} and light hole effective mass m_{lh}, respectively. The polarization modification factors δ for the TE and the TM modes are shown in Table 3.3. δ shown in Table 3.3 have been averaged over φ, *i.e.*, averaged over various k_x and k_y for given value of $k = \sqrt{k_x^2 + k_x^2}$, and

$$\cos^2\theta = \frac{E_{e,z} + E_{h,z}}{E_e + E_h} \tag{3.20}$$

where $E_{i,z}$ and E_i $(i = e, h)$ are the quantized energy associated with the z direction and the total energy for the electrons and the holes, respectively.

The quantized energies $E_{e,z}$ for electrons can be obtained by solving (3.14). The solutions can be found in many books on quantum mechanics. Similar results with $m_e \rightarrow m_{hj}$ $(j = h, l)$ and $U_e \rightarrow U_h$ apply to the holes in the valence bands under the decoupled valence band approximation. The quantized energy levels and correspond-

TE		
	$\|S\rangle \cdot \|\uparrow'\rangle$	$\|S\rangle \cdot \|\downarrow'\rangle$
$\|\frac{3}{2}'\rangle$	$\frac{3}{4}(\cos^2\theta + 1)$	0
$\|\frac{1}{2}'\rangle$	$\frac{1}{4}(\cos^2\theta + 1)$	$1 - \cos^2\theta$
$\|-\frac{1}{2}'\rangle$	$1 - \cos^2\theta$	$\frac{1}{4}(\cos^2\theta + 1)$
$\|-\frac{3}{2}'\rangle$	0	$\frac{3}{4}(\cos^2\theta + 1)$
TM		
	$\|S\rangle \cdot \|\uparrow'\rangle$	$\|S\rangle \cdot \|\downarrow'\rangle$
$\|\frac{3}{2}'\rangle$	$\frac{3}{2}(1 - \cos^2\theta)$	0
$\|\frac{1}{2}'\rangle$	$\frac{1}{2}(1 - \cos^2\theta)$	$2\cos^2\theta$
$\|-\frac{1}{2}'\rangle$	$2\cos^2\theta$	$\frac{1}{2}(1 - \cos^2\theta)$
$\|-\frac{3}{2}'\rangle$	0	$\frac{3}{2}(1 - \cos^2\theta)$

Table 3.3: The polarization modification factors for TE and TM modes in QW structure under the decoupled valance band approximation. $\cos^2\theta$ is defined in text.

ing wavefunctions for the holes in the valence bands are

$$E_{hj,z} = E_{hj,z}(n_{hj}) \ , \quad \Phi_{hj,z}(z) = \Phi_{hj,z}(z, n_{hj}) \quad (j = h, l, \ n_{hj} = 1, 2, \cdots) \ . \tag{3.21}$$

The total energies for the holes in the valence bands are given by

$$E_{hj}(k, n_{hj}) = \frac{\hbar^2 k^2}{2m_{hj}} + E_{hj,z}(n_{hj}) \quad (j = h, l, \ n_h = 1, 2, \cdots) \ . \tag{3.22}$$

It is easy to verify that for deep QW

$$\int \Phi^*_{e,z}(n_e, z)\Phi_{hj,z}(n_{hj}, z)\mathrm{d}z \approx \begin{cases} 1 & n_e = n_{hj} \\ 0 & n_e \neq n_{hj} \end{cases} \ . \tag{3.23}$$

(3.23) gives another selection rule

$$n_e = n_{hj} \ . \tag{3.24}$$

Transitions thus take place between electron and hole states with the same transverse momentum and the same quantized well states.

Since there is no quantum confinement in the x and y directions, the transverse wavevector has the values

$$k_x = m_x \frac{2\pi}{L_x} \quad m_x = 0, \pm 1, \pm 2, \cdots \tag{3.25}$$

$$k_y = m_y \frac{2\pi}{L_y} \quad m_y = 0, \pm 1, \pm 2, \cdots \ . \tag{3.26}$$

Thus every electronic state occupies a "volume" of $4\pi^2/L_xL_y = 4\pi^2/V_{2D}$ in $\mathbf{k}_{||}$ space. The number of electron states with transverse wavevector less than k ($k = |\mathbf{k}_{||}|$) is

$$N(k) = 2\pi k^2/(4\pi^2/S) = \frac{k^2 V_{2D}}{2\pi} \tag{3.27}$$

where a factor of two was included to account for the electron spin degeneracy. The number of states between k and $k + dk$ is

$$\rho(k)dk = \frac{dN}{dk}\, dk = S\, \frac{k}{\pi}\, dk \tag{3.28}$$

so that the number of states with total energy between E_e and $E_e + dE_e$ is

$$D_e(E_e)\, dE_e = \frac{dN}{dE_e}\, dE_e = \frac{dN}{dk}\, \frac{dk}{dE_e}\, dE_e\ . \tag{3.29}$$

From (3.25) and (3.26) with $n_e = 1$

$$k = \sqrt{\frac{2m_e}{\hbar^2}\, [E_e - E_{e,z}(1)]} \tag{3.30}$$

so that the number of states between E_e and $E_e + \mathrm{d}E_e$ per unit area is

$$\rho_e(E_e)\, dE_e = \frac{1}{S}\, D_e(E_e)\, dE_e = \frac{m_e}{\pi\hbar^2}\, dE_e\ . \tag{3.31}$$

In the reasoning leading to (3.31), we consider only one transverse quantum state $n_e = 1$. But once $E > E_{e,z}(2)$, as an example, an electron of a given total energy E_e can be found in either $n_e = 1$ or $n_e = 2$ state so that the density of states doubles. The total density of states increases by $m_e/\pi\hbar^2$ at each of the energies $E_{e,z}(n_e)$, thus

$$\rho_e(E_e) = \sum_{n_e} \frac{m_e}{\pi\hbar^2}\, H[E_e - E_{e,z}(n_e)] \tag{3.32}$$

where $H[x]$ is the Heaviside function which is equal to unity when $x > 0$ and is zero when $x < 0$. Replacing E_e, m_e and $E_{e,z}(n_e)$ in Eq.(3.32) by E_{hj}, m_{hj} and $E_{hj,z}(n_{hj})$, respectively, we can obtain the density of states for the holes in the valence bands $\rho_{hj}(E_{hj})$ $(j = h, l)$. So we have

$$\frac{1}{V_{2D}} \sum_{\mathbf{k}_\parallel} = \frac{1}{S} \sum_{\mathbf{k}_\parallel} \rightarrow \frac{1}{S} \int dk\ D(k)\ = \int dE_{e,hj}\ \rho_{e,hj}(E_{e,hj})\ . \tag{3.33}$$

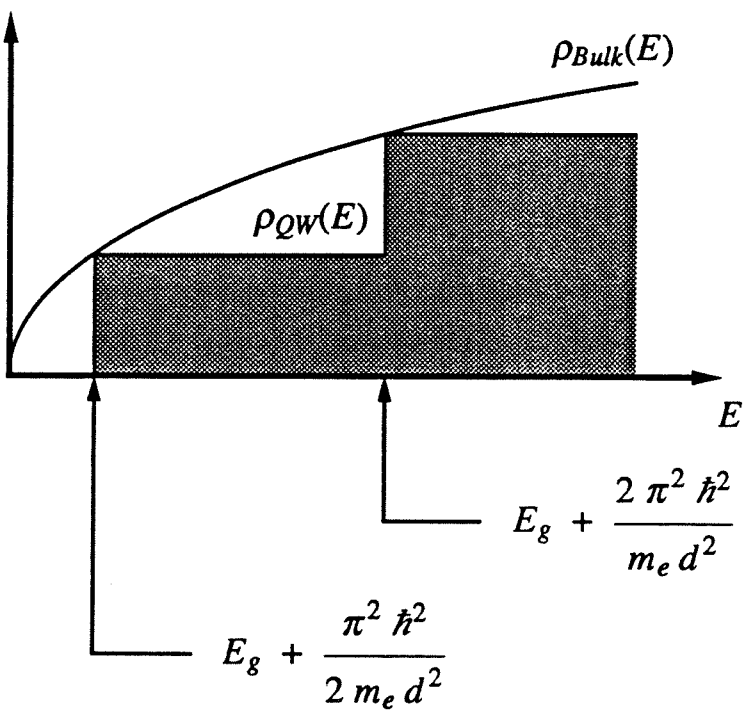

Figure 3.3: The volumetric electron density of states for bulk and infinite deep QW structure. The volumetric density of states for the QW is defined as the 2D density of states divided by the QW thickness.

The first two steps of the staircase density of states are shown in Figure 3.3. In the figure, the volumetric density of states for electrons in an infinite quantum well medium ρ_{2D}/d is plotted so that it can be compared to the density of states for the bulk structures. The QW volumetric density of states equals to the bulk density of states value ρ_{3D} at each of the energy steps as shown in the figure.

(3.33) can be used to calculate the carrier density N_{2D} by an integration of the density of states and the Fermi function over the electron energy or the hole energy

$$N_{2D} = \int \mathrm{d}E_{e,hj}\ \rho_{e,hj}(E_{e,hj})\ f_{e,hj}(E_{e,hj})\ . \tag{3.34}$$

Notice that, in the expression for the susceptibility and the gain coefficients [(2.38), (2.39), (2.62) and (2.63)], $\mathcal{L}_i(E_{\tilde{\alpha}}-E)$, $\mathcal{L}_r(E_{\tilde{\alpha}}-E)$ and $\mathcal{L}(E-E_{\tilde{\alpha}})$ are simple functions of the electron-hole transition energy $E_{\tilde{\alpha}}$, it is convenient to perform the integration over the transition energy $\mathcal{E}$ ($\mathcal{E} \equiv E_{\tilde{\alpha}}$) instead of over the electron energy E_e using

$$\mathcal{E} = E_g + E_e + E_{hj}\ . \tag{3.35}$$

Using (3.15) for the electrons and similar result for the holes we have

$$E_e - E_{e,z}(n_e) = \frac{m_{rj}}{m_e}[\mathcal{E} - E_g - E_{e,z}(n_e) - E_{hj,z}(n_{hj})] \tag{3.36}$$

where the reduced mass is defined as $m_{rj}^{-1} = m_{hj}^{-1} + m_e^{-1}$.

From the transition selection rule $n_e = n_{hj} \equiv n$ we have

$$E_e = E_{e,z}(n) + \frac{m_{rj}}{m_e}[\mathcal{E} - E_g - E_{e,z}(n) - E_{hj,z}(n)]\ . \tag{3.37}$$

And similarly, for the holes

$$E_{hj} = E_{hj,z}(n) + \frac{m_{rj}}{m_{hj}}[\mathcal{E} - E_g - E_{e,z}(n) - E_{hj,z}(n)]\ . \tag{3.38}$$

Thus

$$\int dE_e\ \rho_e(E_e) = \int dE_e\ \sum_n \frac{m_e}{\pi\hbar^2} H[E_e - E_{e,z}(n)] \tag{3.39}$$
$$= \int d\mathcal{E}\ \sum_n \frac{m_{rj}}{\pi\hbar^2} H[\mathcal{E} - E_g - E_{e,z}(n) - E_{hj,z}(n)] \equiv \int d\mathcal{E}\ \rho_{rj}(\mathcal{E})\ .$$

$\rho_{rj}(\mathcal{E})$ is called reduced density of states. (3.37) and (3.38) can be used to express the Fermi distributions $f_e(E_e)$ and $f_h(E_h)$ as functions of the transition energy $\mathcal{E}$ instead of the electron energy or the hole energy. The polarization modification factor δ can be also expressed by the transition energy $\mathcal{E}$ by noticing

$$\cos^2\theta = \frac{E_{e,z}(n) + E_{hj,z}(n)}{\mathcal{E} - E_g}\ . \tag{3.40}$$

Using these results the gain coefficients or the susceptibilities can be calculated by the integration over the transition energy $\mathcal{E}$.

3.2 Rate Equations, Statics and Dynamics

In this section, we will first introduce a set of rate equations which can be used to study the statics and dynamics of a QW laser. As we will show later, with proper change of the terminology in these rate equations, we can obtain the rate equations of the same form for other laser structures. Based on these rate equations, some basic results on the statics and the dynamics of a semiconductor laser are generally discussed. These discussions are applicable to semiconductor lasers of various structures. Thus, the predicted performance in various semiconductor lasers can be compared.

In the case of a separate confinement heterostructure (SCH) QW structure as

schematically shown in Figure 3.4, based on (2.58) and (2.60), a set of rate equations can be obtained to describe the static and dynamic behavior:

$$\frac{dP}{dt} = \Gamma\, G_0\, v_g\, P - \Gamma\, G_1\, v_g\, \frac{P^2}{P_s} - \frac{P}{\tau_p} + \xi\, \Gamma\, \frac{N}{\tau_n} \tag{3.41}$$

$$\frac{dN}{dt} = \frac{N'}{\tau_r} - G_0\, v_g\, P + G_1\, v_g\, \frac{P^2}{P_s} - \frac{N}{\tau_n} \tag{3.42}$$

$$\frac{dN'}{dt} = \frac{J}{e} - \frac{N'}{\tau_r} - \frac{N'}{\tau_n} \tag{3.43}$$

where P is the photon density at the quantum well active region, N and N' are, respectively, the two-dimensional (2D) quasi equilibrium carrier density and non-equilibrium carrier density in the SCH QW structure as schematically shown in Figure 3.4, τ_n is the carrier lifetime, $\tau_p = (v_g \alpha_t)^{-1}$ is the photon life time and $\alpha_t = \alpha_i + \frac{1}{2L} \ln \frac{1}{R_1 R_2}$) is the total loss constant, L, R_1 and R_2 are the cavity length and mirror reflectivity, respectively, τ_r is the equilibrium transport or relaxation time of the carriers, J is the injection current density, ξ is the spontaneous emission coupling factor defined as the ratio of the rate of spontaneous emission into the lasing mode to the total spontaneous emission rate.

From the analysis above, the linear and nonlinear gain coefficients G_0 and G_1 can be written as

$$G_0(E) = \frac{\mu^2}{\hbar c \epsilon_o n_r} \frac{E}{E_{T_2}} \sum_{j=l,h} \int \delta_j\, \rho_{rj}\, (f_e + f_h - 1)\, \mathcal{L}\, d\mathcal{E} \tag{3.44}$$

$$G_1(E) = \frac{\mu^2}{\hbar c \epsilon_o n_r} \frac{E}{E_{T_2}} \sum_{j=l,h} \int \delta_j^2\, \rho_{rj}\, (f_e + f_h - 1)\, \mathcal{L}^2\, d\mathcal{E} \tag{3.45}$$

ρ_{rj} is the step-like 2D reduced density of states for the carriers in the SCH QW structure, j designates either light holes ($j = l$) or heavy holes ($j = h$), δ_j is the

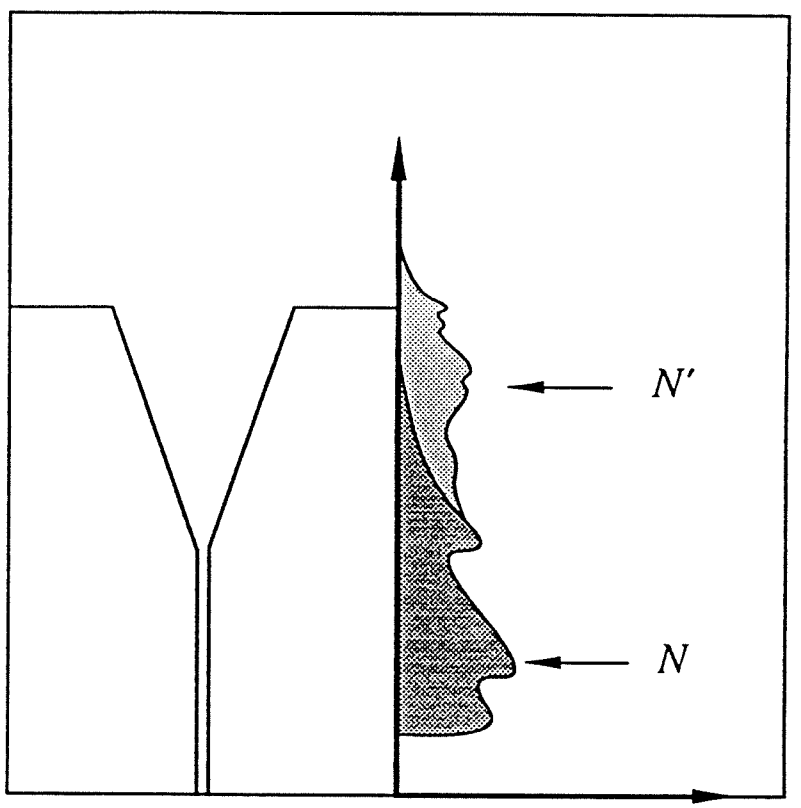

Figure 3.4: The schematic SCH QW structure and the carrier densities. N and N' are, respectively, the two-dimensional (2D) quasi equilibrium carrier density in the SCH QW region and the non-equilibrium carrier density in and out the SCH QW region.

polarization modification factor of the transition matrix elements for light and heavy holes, P_s is the saturation photon density

$$P_s = \hbar^2 \epsilon_o n_r^2 / [\mu^2 E(\tau_e + \tau_h) T_2] \ . \tag{3.46}$$

From (2.53) and Table 2.2, the coupling factor Γ for a QW structure is $\Gamma = 1/t_z$, where t_z is the effective optical mode width along the z direction. Assume that the photon has a normalized distribution function $\Theta_z(z)$ along the z-direction

$$\int_{-\infty}^{\infty} \Theta_z(z)\, dz \ = 1 \tag{3.47}$$

and $\Theta_z(z)$ has its maximum value at the QW active region ($z = 0$). Then we have $t_z = 1/\Theta_z(0)$. The 2D treatment of the carrier density N is justified by noticing that the thickness of the equilibrium carrier population region of the SCH QW structure is usually much smaller than the carrier diffusion length.

The photon density at steady state can be obtained as [15]

$$P = \frac{(\Gamma G_0 - \alpha_t) + \sqrt{(\Gamma G_0 - \alpha_t)^2 + \xi \frac{N}{\tau_n} \frac{4\Gamma^2 G_1}{v_g P_s}}}{2\Gamma G_1} P_s \ . \tag{3.48}$$

If the spontaneous emission coupling is omitted, *i.e.*, $\xi \to 0$, we have

$$P = \frac{(\Gamma G_0 - \alpha_t) + |\, \Gamma G_0 - \alpha_t \,|}{2\Gamma G_1} P_s = \begin{cases} 0 & (\Gamma G_0 < \alpha_t) \\ \frac{\Gamma G_0 - \alpha_t}{\Gamma G_1} P_s & (\Gamma G_0 > \alpha_t) \end{cases} \ . \tag{3.49}$$

From (3.49) it follows that $g \equiv \Gamma G_0 > \alpha_t$ is a necessary condition for coherent output power, i.e., the threshold is determined by the linear gain coefficient. $g_{th} \equiv \alpha_t$ is called threshold modal gain. The gain coefficients only characterize the coherent

optical output power. $\xi \neq 0$ will soften this threshold condition since part of the cavity loss is compensated by the spontaneous emission coupling.

Applying a small-signal analysis to Eqs.(3.41)-(3.43), the modulation response can be obtained as

$$R(f) = \frac{|p/i|^2(f)}{|p/i|^2(f \to 0)} = R_c(f) \cdot R_i(f) \tag{3.50}$$

$$R_c(f) = \frac{1}{1+(f/f_c)^2}, \qquad R_i(f) = \frac{f_r^4}{(f^2-f_r^2)^2+(\frac{\gamma}{2\pi})^2 f^2}, \tag{3.51}$$

where i is the small signal amplitude of the sinusoidal current component and p is the corresponding modulation amplitude in the optical output power, f is the modulation frequency, $R_c(f)$ is a response function like that for an RC low frequency filter. $f_c = 1/(2\pi\tau_r)$ represents the carrier transport or relaxation into the SCH QW active region and the device parasitics as well. Both are associated with the carrier storage outside the carrier equilibrium region of SCH QW structure. In the expression for the intrinsic response $R_i(f)$, f_r is the relaxation resonance frequency

$$f_r^2 = \frac{v_g^2\,\Gamma}{4\pi^2}[(G_0 - G_1\frac{P_0}{P_s})(G_0' - G_1'\frac{P_0}{P_s}) + \frac{G_1}{P_s}\frac{1}{v_g\tau_n}]\,P_0\,, \tag{3.52}$$

the damping rate γ is given by

$$\gamma = \frac{1}{\tau_n} + v_g\,[(G_0' - G_1'\frac{P_0}{P_s}) + \frac{\Gamma G_1}{P_s}]\,P_0\,, \tag{3.53}$$

P_0 is the stationary photon density in the QW active region, $G_0' \equiv dG_0/dN$ and $G_1' \equiv dG_1/dN$ are the differential gain coefficients. Note that if we neglect gain suppression, *i.e.*, $G_1 = 0$, the conventional result $f_r = \frac{1}{2\pi}\sqrt{v_g G_0' P_0/\tau_p}$ can be obtained.

The intrinsic response $R_i(f)$ is more fundamental in the sense that it is determined by the interaction between the quasi equilibrium carriers and the photons at the active region. The 3dB modulation bandwidth of $R_i(f)$ is obtained as

$$f_{3dB} = \sqrt{f_r^2 - \frac{\gamma^2}{8\pi^2} + \sqrt{(f_r^2 - \frac{\gamma^2}{8\pi^2})^2 + f_r^4}} \,. \tag{3.54}$$

(3.52)-(3.54) indicate that the intrinsic 3dB modulation bandwidth f_{3dB} depends on the stationary photon density P_0.

In the limit of low optical output power (low P_0) or low bias current, the damping term γ is negligible so that

$$\begin{aligned} f_{3dB} \approx \sqrt{1+\sqrt{2}}\, f_r &\approx \frac{1.55 v_g}{2\pi} \sqrt{\Gamma G_0 G_0' P_0} \\ &= \frac{1.55}{2\pi} \sqrt{\frac{v_g G_0' P_0}{\tau_p}} \,. \end{aligned} \tag{3.55}$$

As P_0 increases, f_r increases, which leads to an increase in f_{3dB}.

As P_0 increases further, the damping term γ can not be omitted. From (3.54) one can see that the presence of damping leads to a reduction in f_{3dB}. Notice that because $f_r^2 \propto P_0$ and $\gamma^2 \propto P_0^2$, there exists a value of P_0 that maximizes f_{3dB}. For P_0 larger than this value, an increase in P_0 leads to a decrease in f_{3dB}. For a better understanding of the modulation bandwidth limit, we consider the 0dB modulation bandwidth which can be written as

$$f_{0dB} = \sqrt{2(f_r^2 - \frac{\gamma^2}{8\pi^2})} \,. \tag{3.56}$$

It is straightforward to show that f_{0dB} has a maximum value which can be explicitly

written as [14]

$$f_{0dB}^{max} = \frac{v_g}{2\pi} \frac{\Gamma G_0}{G_0' + \Gamma G_1/P_s} G_0' \qquad (3.57)$$
$$\approx \frac{1}{2\pi} v_g P_s \frac{G_0}{G_1} G_0' \qquad (\text{usually } G_0' \ll \Gamma G_1/P_s)$$

at a photon density

$$P_0 = \frac{\Gamma G_0 G_0'}{(G_0' + \Gamma G_1/P_s)^2} \cdot \qquad (3.58)$$

(3.55) and (3.57) indicate that the differential gain directly influence the modulation bandwidth. Higher differential gain will lead to larger modulation bandwidth.

Bibliography

[1] D. Ahn, S. L. Chuang, and Y.-C. Chang, "Valence-band mixing effects on the gain and the refractive index change of quantum well lasers," *J. Appl. Phys.*, vol.64, p.4056, 1988

[2] M. Altarelli, U. Ekenberg, and A. Fasolino, "Calculations of hole subbands in semiconductor quantum wells and superlattices," *Phys. Rev. B*, vol.32, p.5138, 1985

[3] M. Asada, A. Kameyama, and Y. Suematsu, "Gain and intervalence band absorption in quantum-well lasers," *IEEE J. Quantum Electron.*, vol.QE-20, p.745, 1984

[4] A. Baldereschi and N. O. Lipari, "Spherical model of shallow acceptor states in semiconductors," *Phys. Rev. B*, vol.8, p.2697, 1973

[5] D. A. Broido and L. J. Sham, "Effective masses of holes at GaAs-AlGaAs heterojunctions," *Phys. Rev. B*, vol.31, p.888, 1985

[6] G. Dresselhaus, "Spin-orbit coupling effects in zinc blende structures," *Phys.*

Rev., vol.100, p.580, 1955

[7] E. O. Kane, "Band structure of indium antimonide," *J. Phys. Chem. Solids*, vol.100, p.580, 1957

[8] J. M. Luttinger and W. Kohn, "Motion of electrons and holes in perturbed periodic fields," *Phys. Rev.*, vol.97, p.869, 1955

[9] J. M. Luttinger, "Quantum theory of cyclotron resonance in semiconductors: general theory," *Phys. Rev.*, vol.102, p.1030, 1956

[10] A. Twardowski and C. Hermann, "Variational calculation of polarization of quantum-well photoluminescence," *Phys. Rev. B*, vol.35, p.8144, 1987

[11] M. Yamada, S. Ogita, M. Yamagishi, K. Tabata, and N. Nakaya, M. Asada, and Y. Suematue, "Polarization-dependent gain in GaAs/AlGaAs multi-quantum-well lasers: theory and experiment," *Appl. Phys. Lett.*, vol.45, p.324, 1984

[12] M. Yamada, S. Ogita, M. Yamagishi, and K. Tabata, "Anisotropy and broadening of optical gain in a GaAs/AlGaAs multiquantum-well laser," *IEEE J. Quantum Electron.*, vol.QE-21, p.640, 1985

[13] M. Yamanishi and I. Suemune, "Comment on polarization dependent momentum matrix elements in quantum well lasers," *Japan. J. Appl. Phys.*, vol.23, p.L35, 1984

[14] B. Zhao, T. R. Chen, and A. Yariv, "On the high speed modulation bandwidth of quantum well lasers," *Appl. Phys. Lett.*, vol.60, p.313, 1992

[15] B. Zhao, T. R. Chen, and A. Yariv, "The gain and carrier density in semiconductor lasers under steady-state and transient conditions," *IEEE J. Quantum Electron.*, vol.QE-28, p.1479, 1992

Chapter 4

State Filling Effects on Threshold and Modulation Dynamics of Quantum Well Lasers

4.1 Introduction

Because of the confinement and quantization of the injected electrons and holes in the extremely thin active region, the QW semiconductor lasers has been predicted to be superior to the conventional bulk double heterostructure (DH) lasers in nearly all of the important device characteristics [9,18,6,3,4,5,56,15,61]. Chief among these are the threshold current density reduction and the enhancement of the differential gain in the QW lasers due to the reduction of active layer thickness and the step-like density of states for the two-dimensional carriers in the QW, respectively. The reduction

of threshold current density and the enhancement of differential gain should lead to reduction in threshold current and improvement in high-speed modulation bandwidth, respectively.

Very low threshold current density and threshold current have been demonstrated in QW lasers [52,11,17,9,19,7,16,2,58,63,11,4]. It has been theoretically predicted that the differential gain should be enhanced by a factor of at least 2~4 in the QW lasers and this differential gain enhancement would be independent on the number of quantum wells [9,1,5]. However, high-speed modulation experiments to date indicate no significant improvement in QW laser modulation bandwidth compared to DH lasers (see Figure 1.4) [26,17,59,40,41,32,33,29,36,30,13].

Many theoretical models have been proposed to explain the anomalous behavior in the high-speed modulation bandwidth of QW lasers. These models include the carrier well-barrier hole burning [42,55], the carrier diffusion limited transport mechanism [37,38,39,46], the quantum capture [23,24] and bottleneck [47,48,49] of injected carriers, and the state-filling mechanism [64,16,67,68]. Although these models have different names and different approaches, they have one thing in common; *i.e.*, they all consider the carrier population outside the quantum well which can not be simply neglected.

The separate confinement heterostructure (SCH) QW structure is commonly used in QW lasers to achieve low threshold current and high quantum efficiency. In the SCH QW structure, the quantum well active region is sandwiched between optical confining layers (CL). The larger thickness of the confining layer structure compared

to that of the QW results in a large density of states in the CL region. Obviously, at finite temperatures the injected carriers populate not only the energy subbands of the QW but also those of the CL structure. This is the state/band filling effect, *i.e.*, the carrier population of upper subband states of quantum well laser structures.

The state-filling effects directly affect the threshold current and modulation dynamics due to their influence on the quasi Fermi energies of injected carriers. The transparency carrier density and the differential gain depends on the increase rate of the quasi Fermi energies with respect to the increase of injected carriers. The presence of upper subbands with large density of states tends to clamp the Fermi energies and leads to a degradation in the gain increase thus leading to a larger transparency carrier density and lower differential gain. The state-filling effects have been shown to have significant influence on the threshold current [34,35,67] and modulation dynamics [64,16,67,68] of the QW lasers. Specifically, this theory can explain the two experimental facts in modulation dynamics: (i) the unstrained SQW lasers do not show improvement in the modulation bandwidth in comparison to the bulk counterpart; (ii) the use of MQW as active region leads to improvement in the modulation bandwidth over the SQW counterparts.

4.2 Simple Quantitative Arguments

First, we present a simple model which leads to a simple accounting of the state/band filling effects. A simple two-level model is shown in Figure 4.1. The energy level E_0

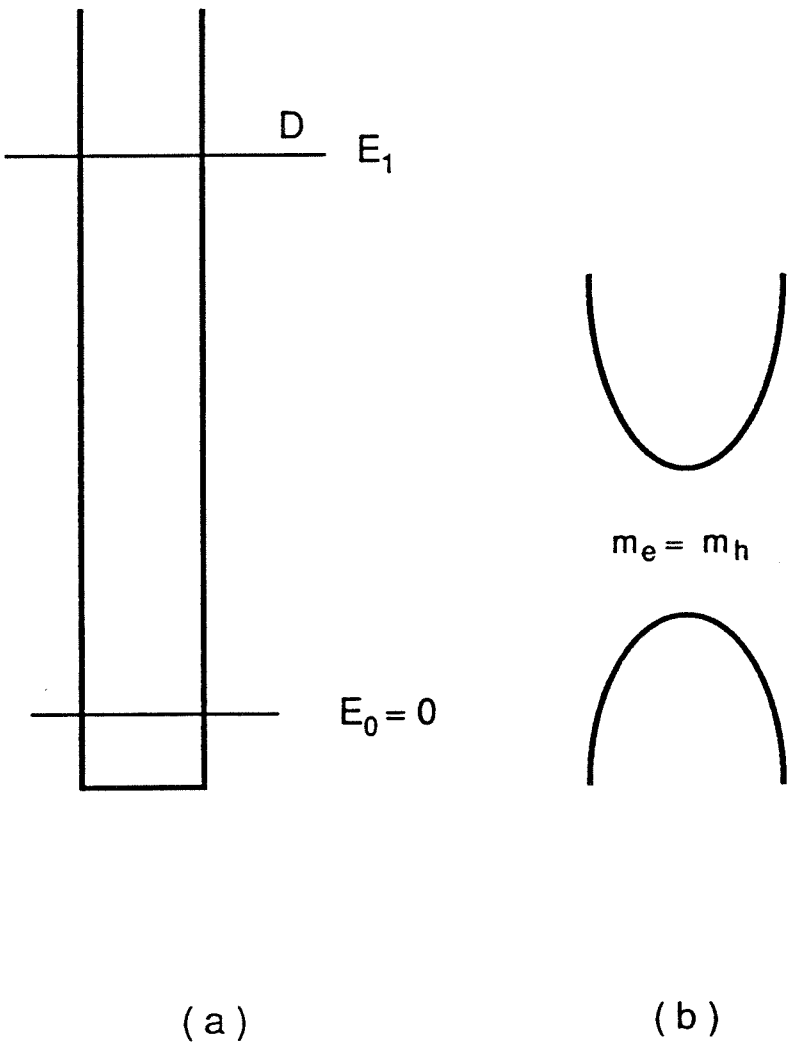

Figure 4.1: The schematic diagram for the simple two-level model accounting of the state filling effects: (a) the QW structure; (b) the electronic band structure for electrons and holes.

represents the first quantized state (band) n=1 of the carrier in the QW. The optical transition is assumed to occur between the first quantized states of electrons and holes in the QW. The energy level E_1 represents the subbands of the CL structure. D is the effective number of these subbands. Typically, at room temperature the effective number of states, *i.e.*, within one kT from the top of the QW in the CL structure is on the order of 20 for a typical SCH QW structure, where T is the temperature and k is the Boltzmann constant. And these states are on the order of 80 meV above the first quantized state of the QW. We also assume for the sake of simplicity that the electrons and holes have the same parabolic electronic band structure ($m_e = m_h$).

Neglecting dephasing collision (T_2) broadening, the maximum optical gain (at $E = E_0$) is written as

$$G_0 = A_0 \, \rho_r \, (2f_e - 1) \tag{4.1}$$

where A_0 is a material-dependent parameter, $\rho_r = \frac{1}{2}\frac{m_e}{\pi\hbar^2} = \frac{1}{2}\rho_e$ is the reduced density of states for the first quantized state optical transition, and the Fermi function is given by

$$f_e = \frac{1}{1 + \exp(-\frac{F}{kT})} \, . \tag{4.2}$$

F is the quasi-Fermi energy level of electrons measured from the first quantized band $E_0 = 0$. The 2D carrier density is obtained by integrating the density of states as

$$N = \rho_e \, kT \, [\, \ln(1 + \exp(\frac{F}{kT})) + D \ln(1 + \exp(\frac{F - E_1}{kT})) \,] \, . \tag{4.3}$$

From (4.1)-(4.3), it is straight forward to derive the differential gain

$$\frac{dG}{dN} = \frac{A_0}{kT} \, \frac{1}{1 + \exp(\frac{F}{kT})} \, [1 + D\frac{1 + \exp(F/kT)}{\exp(E_1/kT) + \exp(F/kT)}]^{-1} \, . \tag{4.4}$$

For given value of gain G_0 (*i.e.*, given value of F), (4.3) and (4.4) show clearly that the presence of (D) upper subbands increases the (injected) carrier density and reduces the differential gain. They also indicate that a large separation between the ground state and upper subbands (parameter E_1) diminishes the effect of these CL states resulting in a smaller carrier density and a larger differential gain. The reduction in the number of the upper subbands (D) leads to the same conclusion.

In Figure 4.2, we show the maximum gain G as function of carrier density n, and the differential gain $\frac{dG}{dn}$ as function of G for different values of the separation energy E_1. We have taken a calculated typical value of $D = 20$ for the results shown in Figure 4.2. It is shown that the optical gain is dramatically affected by the presence of a large number (D) of upper subbands. As the separation energy E_1 increases the differential gain is increased and the transparency carrier density is reduced.

Figure 4.3 shows the calculated linear gain and differential gain coefficients for a typical GaAs/AlGaAs SCH single quantum well (SQW) structure with and without inclusion of the injected carrier population in the SCH CL region. The calculations were based on a more accurate model [see (3.44)]. It is shown that the exclusion of injected carrier population in SCH CL region leads to an overestimation on differential gain and an underestimation on the transparency carrier density. The differential gain is overestimated by about a factor of 2, if the injected carrier population in the CL region is omitted.

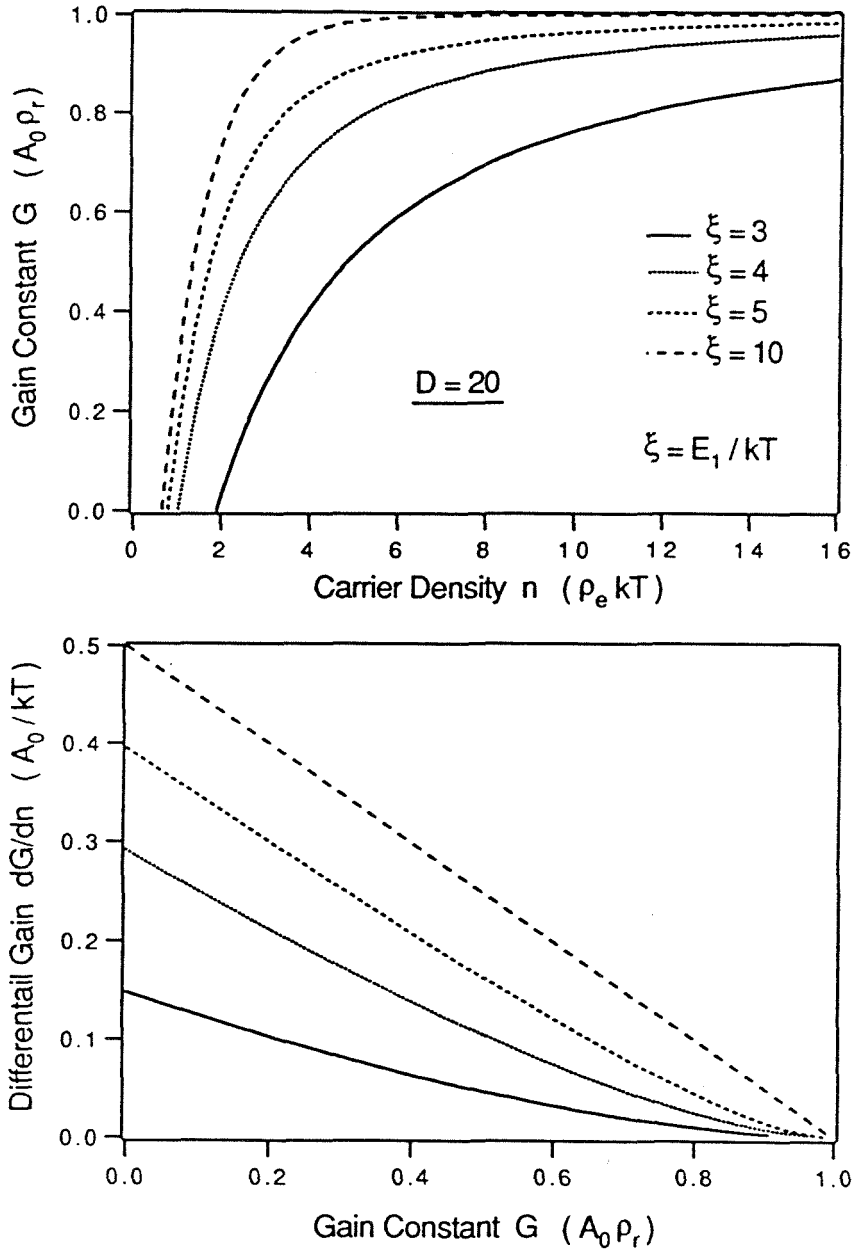

Figure 4.2: The computed gain *vs* carrier density (a) and differential gain *vs* gain (b) by the simple model for $D = 20$ and various E_1 values.

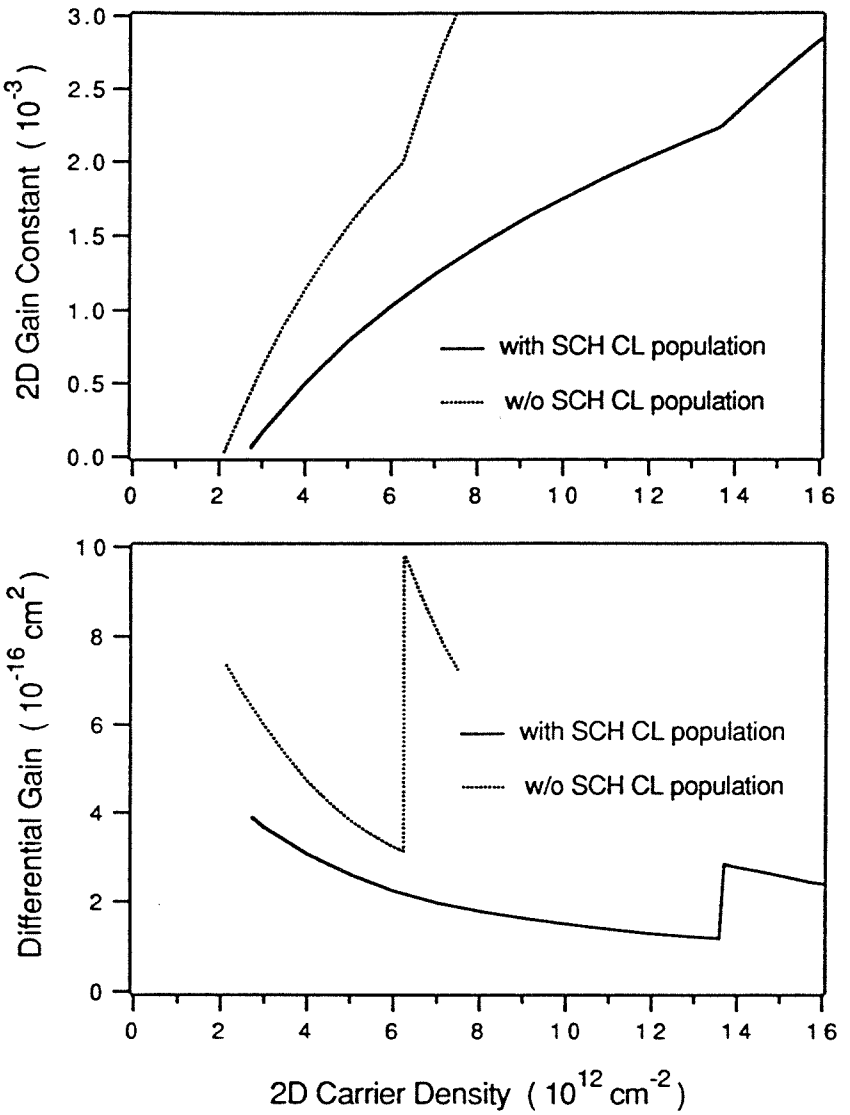

Figure 4.3: Computed maximum two-dimensional (2D) gain constant (a) and corresponding differential gain (b) as a function of carrier density in a typical GaAs/AlGaAs SCH 100 Å single QW laser by a more accurate model. The 2D gain constant divided by the transverse effective optical mode width is the modal gain. The results are obtained with and without the inclusion of carrier population in the SCH confining layer (CL) region, respectively.

4.3 Comparison Between Quantum Well and Bulk Structures

QW lasers have been previously predicted to have enhanced differential gain compared to the conventional bulk double heterostructure (DH) lasers [9,3]. This differential gain enhancement was attributed to the abrupt step-like two-dimensional (2D) density of states in QW lasers. As shown above, the differential gain is significantly affected by the carrier population in the optical confining layers in the QW structure. Thus, the conclusion concerning the differential gain enhancement in QW structures might be modified.

For 3D DH bulk structure lasers, their characteristics can be described by the set of rate equations (3.41)-(3.43) with $J \rightarrow J/d$, where d is the active layer thickness. N and N' are the corresponding 3D carrier density. The gain coefficients G_0 and G_1 are given by (3.44) and (3.45) with $\delta_j = 1$ $(j = l, h)$ and ρ_{rj} is the 3D reduced density of states

$$\rho_{rj}(\mathcal{E}) = \frac{1}{2\pi^2} \left(\frac{2m_{rj}}{\hbar^2}\right)^{3/2} \sqrt{\mathcal{E} - E_g} \tag{4.5}$$

where m_{rj} are the reduced effective masses $(j = l, h)$. The coupling factor for the DH structure is obtained from (2.53) and Table 2.2 as

$$\Gamma = \Gamma_{3D} = \frac{1}{wt_z} \cdot \frac{wd_z}{1} = \frac{d_z}{t_z} = \frac{d}{t} \tag{4.6}$$

which is the conventional confinement factor.

The results related to the threshold and the modulation bandwidth in Section 3.2

are also valid to describe the characteristics of the bulk DH lasers [Eqs.(3.48)–(3.58)]. Notice that the modal gain ΓG_0, ΓG_1, and differential gain $G_0' = dG_0/dN$ have the same units, respectively, for the different 2D QW and 3D bulk DH structures, the modulation dynamics can be compared between the QW and DH lasers in the term of differential gain.

Figure 4.4 shows the calculated differential gain G_0' at the peak of $G_0(E)$ as a function of peak modal gain $g = \Gamma G_0$ for typical GaAs/AlGaAs bulk DH and QW structure lasers at room temperature. The calculations were made for the dominant TE modes in these structures. The typical 3D DH laser structure was assumed to be an $GaAs/Al_{0.35}Ga_{0.65}As$ DH structure with GaAs active layer thickness 0.1 μm. The confinement factor (or the coupling factor) for the DH structure was estimated as $\Gamma_{DH} = 0.33$. The typical SCH QW structures under study consist of a pair of 2000 Å $Al_{0.5}Ga_{0.5}As/Al_{0.25}Ga_{0.75}As$ graded index separate confinement (GRIN-SCH) structures and 100 Å quantum well or quantum wells located at or around the center of the GRIN-SCH structure. The differential gain is calculated for the GRIN-SCH QW laser structures with a single quantum well (SQW), three quantum wells (3QW) and five quantum wells (5QW), respectively. The coupling factors for the QW GRIN-SCH structure is evaluated as Γ_{QW}=3.9×10^{4}cm^{-1} from the effective optical mode width. It is assumed that the quantum wells are uncoupled and they are very close to the center of the GRIN-SCH structrue.

In Figure 4.4, it is shown that there is no differential gain enhancement in the SQW structure compared to the DH structure. The differential gain of the SQW

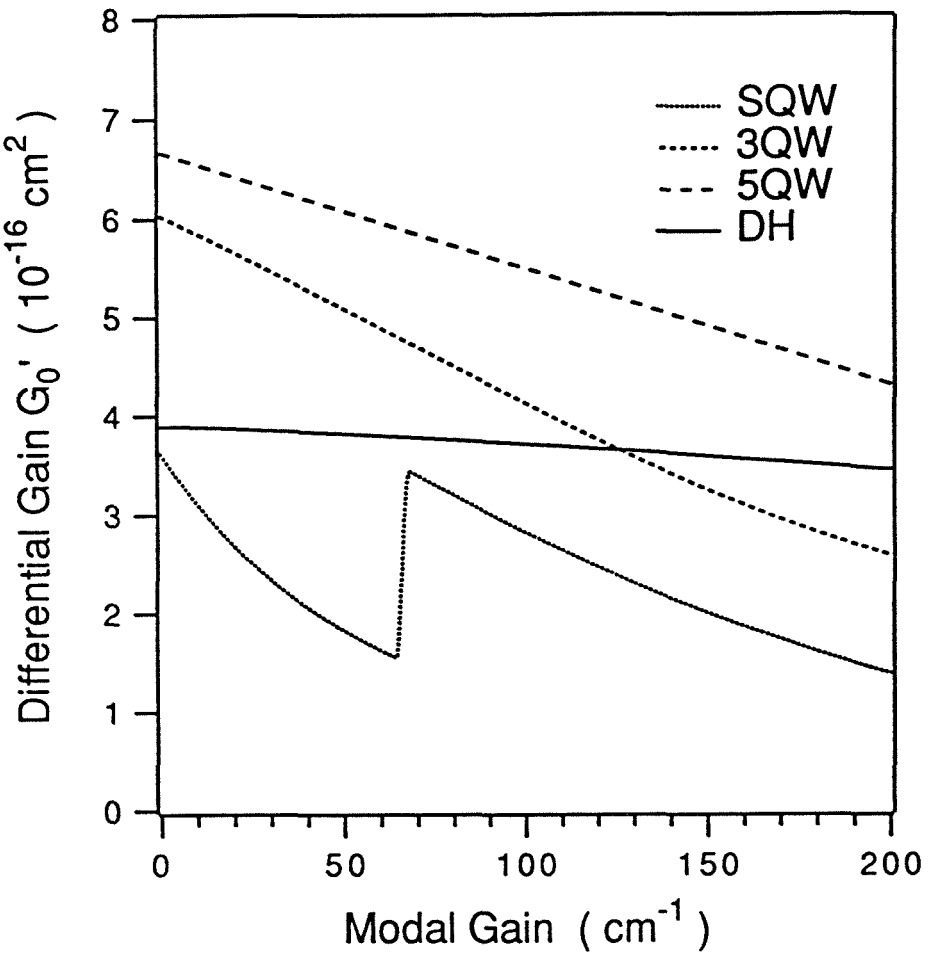

Figure 4.4: The differential gain at gain peak *above transparency* as a function of modal gain for typical bulk DH and QW structures with different number of quantum wells.

structure is comparable with that of the DH structure in the very low modal gain region. In the large modal gain region, the DH structure possesses higher differential gain. The decrease in G_0' with increasing modal gain in the SQW structure results from the finite available gain per quantized state. The abrupt increase in G_0' for the SQW structure is due to the onset of the second quantized state lasing of the QW. The qualitative physical reason for the smaller differential gain of the SQW structure than that of the DH structure is as follows. An increasing fraction of the injected carriers goes into occupation of the large density of states in the GRINSCH optical confining region. These electrons (and holes) contribute very little to the peak gain because of the $(\mathcal{E} - E)^2$ term in the denominator of $\mathcal{L}$ in (3.44). On the other hand, the optical gain is limited due to the flat feature of the 2D step-like density of states for the QW structure. The result is a lowering of differential gain $G_0' = dG_0/dN$ in the SQW structure. It was shown that at low temperatures, there is differential gain enhancement in SQW structure in comparison with DH structure [64]. At lower temperatures, the Fermi-Dirac occupation factor for the states in the GRIN-SCH optical confining region is reduced considerably. The more abrupt cutoff of the Fermi-Dirac occupation functions at low temperatures take advantage of the step-like 2D density of states profile in contributing to relatively large increase in G_0 with increasing N.

In QW structures, above transparency the differential gain decreases as the carrier density (or the modal gain) increases because of the sublinearity in the gain *vs* carrier density dependence. This sublinearity is attributed to the flat feature of the two-

dimensional step-like density of states in the QW structures. For a given value of modal gain, the differential gain increases as the number of quantum wells (N_{qw}) increases because the carrier density (or the modal gain) associated with one single QW decreases with the increase of N_{qw}. This is the conventional differential gain enhancement in MQW structures. Without inclusion of the state-filling effect, it has been predicted that larger differential gain should be achieved at lower carrier density (or at smaller modal gain) and that the maximum attainable differential gain is not affected by the number of quantum wells [1].

Figure 4.4 indicates that the inclusion of confining layer state-filling considerably modifies this picture. The use of multiple quantum wells (MQW) as active region actually leads to an extra differential gain enhancement. More specifically, the maximum attainable differential gain increases as the number of quantum wells increases. A N_{qw}=5 QW laser with a loss of 40 cm^{-1}, for example, will have a differential gain which is appreciably larger than the *maximum* attainable differential gain in a SQW laser and nearly three times as large as a SQW laser with the same loss value. At the loss of 40 cm^{-1}, the differential gain of a MQW laser with N_{qw}=5 is about 60% larger than that in a DH laser.

The physical reason for the extra increase in differential gain in MQW structures is the following. In a SQW laser the need to obtain a sufficient optical gain (to overcome the losses) forces the Fermi energy F to rise toward the top of the quantum well as the pumping level is increased. The confining layer states, say at energy E_{cl}, whose occupation is determined by the factor $\exp[-(E_{cl} - F)/kT]$ are thus more

heavily populated. This increase in the CL carrier density contributes negligibly to the increase in the peak gain because of the nonresonant nature of these carriers' transitions with the transitions at the peak gain. This leads to reduced differential gain since part of the injected carriers are "wasted." The wasted carriers in the CL region must be there due to the fundamental Fermi-Dirac statistics. In a MQW laser, there are several active quantum wells contributing to the gain. The necessary total gain is reached with a much lower population in any one well. This results in a much lower F and consequently the CL states occupation factor $\exp[-(E_{cl} - F)/kT]$ is smaller.

Using the simple two-level model in Section 4.2, we represent the CL states by a fixed number D (equal to the total number of states per unit area within kT from the top of the quantum wells) and take the bottom of the quantum well n=1 state energy as $E = 0$. It is a straightforward task to show that the differential gain is given by [16,67]

$$\frac{dG_0}{dN} = \frac{A_0}{kT} \frac{1}{1 + \exp(\frac{F}{kT})} \{1 + \frac{D}{N_{qw}} \frac{1 + \exp(-F/kT)}{1 + \exp[(E_{cl} - F)/kT]}\}^{-1} . \qquad (4.7)$$

Note that the increase in dG_0/dN with increasing number of wells (N_{qw}) is due to the explicit dependence on N_{qw} as well as to the implicit dependence on F since the latter decreases with increasing N_{qw}. The explicit term $\frac{D}{N_{qw}}$ in Eq.(4.7) shows that the penalty due to CL state-filling is reduced by "distributing" it among the N_{qw} quantum wells in the MQW structures.

These results about the differential gain agree well with experimental observations

of differential gain enhancement in MQW structures [53,54,45] and improved high frequency performance over SQW and DH in MQW lasers as we have mentioned above. For example, a 3dB modulation bandwidth of 11 GHz was demonstrated in GaAs/AlGaAs DH bulk lasers [26] and the best 3dB bandwidth reported in unstrained GaAs/AlGaAs MQW lasers is 16 GHz [41]. However, for the GaAs/AlGaAs SQW structure lasers, the typical bandwidth was just 5 to 6 GHz [17]. Using larger QW barrier, the bandwidth was improved to 9 GHz in an unstrained GaAs/AlGaAs SQW laser due to the reduction of state filling [14]. For other material systems, similar trends exist [32,33,29,36,30,57].

In consideration of the modulation bandwidth, another factor - the operation condition to reach the maximum bandwidth - must be taken into account as well. It was shown that the MQW structure are superior to the SQW structure in the terms of operating injection current density and optical power [65]. Generally the thermal degradation is very severe if the injection current density is beyond 10 kA/cm^2 in a semiconductor laser. The thermal effect will reduce the differential gain and thus the modulation bandwidth. The operating optical power reduction in MQW structures will give reduction in the damage to the laser structures under high optical intensity. The use of MQW as active region makes the QW lasers much easier to approach their optimized high-speed bandwidth limits.

4.4 Some Arguments About the Influence of Strain, Substrate Orientation, and Separate Confinement Structure

The improvement in crystal growth technology has made it possible to grow a semiconductor laser active layer with relatively large built-in strain. This is realized by growing very thin QW layer with its thickness smaller than the critical thickness. The built-in strain in the QW layer significantly modifies the electronic band structures, especially the valence band structures of the QW layer. Since the strained QW layer thickness is smaller than the critical thickness, there are no defects that cause large internal loss and degradation in the optical properties of the QW layer.

Strained QW lasers have shown improved modulation bandwidth and reduced threshold current density compared to their unstrained counterparts [11,19,16,3,58,2, 40,41,50,63,13]. This feature can be first attributed to the reduction of the effective mass of holes in compressive strained QW lasers [60,1,44,28]. The smaller effective mass of holes will cause the Fermi level for holes to increase more quickly with respect to the increase of the injected carriers. This leads to a larger value of differential gain and a smaller value in the injection carrier density to achieve the threshold gain. In addition to the reduction of the hole effective mass, the computed larger energy separation between the ground state subband and the upper subbands of the strained QW compared to the unstrained QW [2,31,43] suggests another possible reason for

the improvement in the strained QW lasers: reduction of state-filling.

It is shown in Figure 4.5 the calculated valence band structures for a 75 Å $In_{0.25}Ga_{0.75}As/Al_{0.2}Ga_{0.8}As$ QW and a 75 Å $GaAs/Al_{0.2}Ga_{0.8}As$ QW, respectively. The valence band structures are obtained by solving the 4×4 Luttinger-Kohn Hamiltonian via the axial approximation (see Chapter 3), *i.e.*, the valence band mixing effect has been taken into account. It is evident that the subbands of the strained QW not only have smaller effective hole masses but also possess larger separation between the subbands of the QW. Most importantly, the energy separation between the ground state and the top of the QW, where there exists a large number of states for the holes, is larger in the strained QW due to the smaller energy band gap of InGaAs compared to GaAs in GaAs/AlGaAs QW laser structures.

In quaternary InGaAsP/InP material system, both compressive and tensile strained QW are available. Recently improved laser performance (modulation response and threshold current) are also observed in *tensile* strained QW (with wide QW width) structures [50,63]. We would like to point out that these improvements in tensile strained QW lasers might be mainly due to the possible larger subband separation induced by tensile strain. In order to show how the gain constant is affected by the separation between the ground state, where the optical transition occurs, and the upper subbands of the QW, we employ the simple model in Section 4.2. But we take $D = 1$ to account for a single upper state in the well. The G-n and $\frac{dG}{dn}$-G relations are shown in Figure 4.6 for different values of E_1 (the energy separation between the lasing ground state and the upper subband) in the simple model. The differential

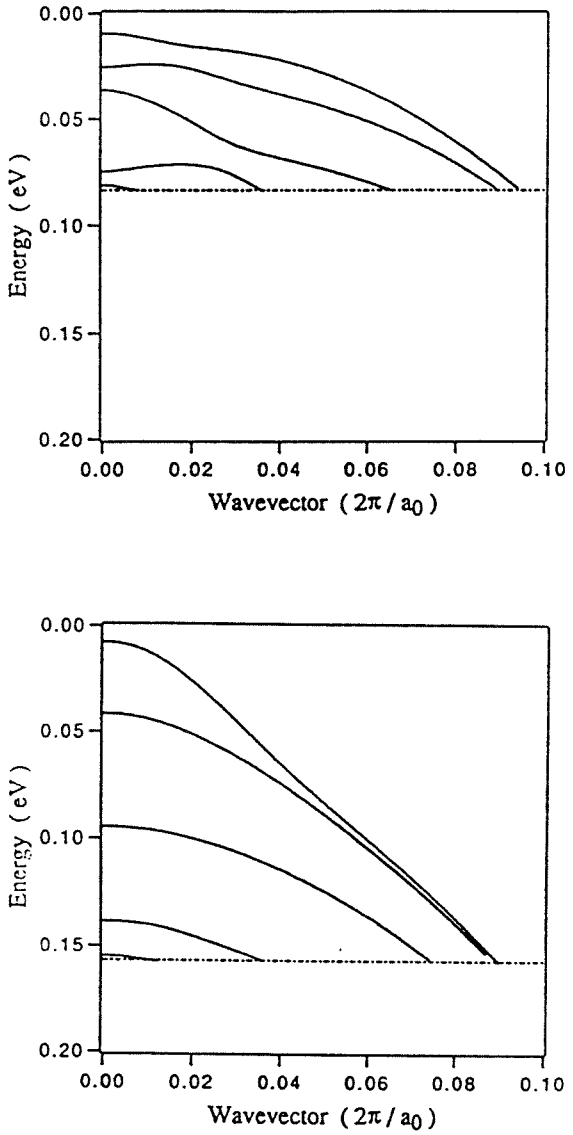

Figure 4.5: the calculated valence band structures for 75 Å $GaAs/Al_{0.2}Ga_{0.8}As$ QW (above) and 75 Å $In_{0.25}Ga_{0.75}As/Al_{0.2}Ga_{0.8}As$ QW (bottom), respectively. The valence band mixing effects have been taken into account under the axial approximation.

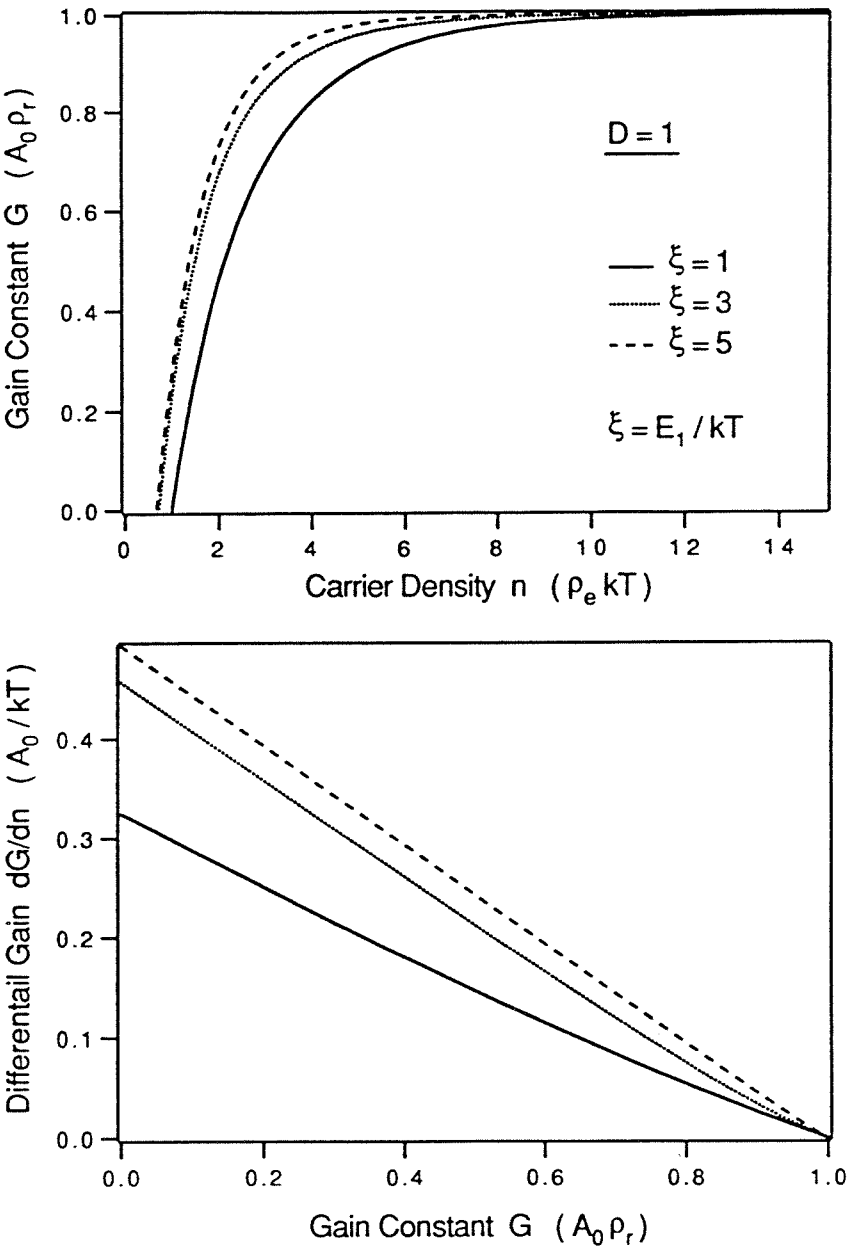

Figure 4.6: The computed gain *vs* carrier density (a) and differential gain *vs* gain (b) by the simple model for $D = 1$ and various E_1 values.

gain is enhanced and the transparency carrier density is reduced when the separation energy E_1 increases. The reduction of hole effective mass and the larger subband separation induced by the tensile strain [43] are both responsible for the performance improvement in the tensile strained QW lasers.

It was shown that, in valence bands, the energy separation between the ground state and first excited state is larger and the ground state is farther away from the top of the QW in (111) GaAs/AlGaAs QW structure than those in (001) GaAs/AlGaAs QW structure if the GaAs QW width is less than 100 Å [7,20]. As the consequence of reduction of the state filling effects, it has been observed in experiments that the (111) GaAs/AlGaAs QW lasers possess consistently lower threshold current densities than the (001) GaAs/AlGaAs QW lasers for QW width less than 100 Å [21,22].

In addition to the QW barrier height or the QW depth, the shape and dimension of the SCH optical confining region also influence the state filling effect. First, the density of states in the SCH optical confining region (most importantly, the number of states within one kT at the top of the QW) is directly influenced by the shape and dimension of the SCH optical confining region. Secondly, the shape and the dimension of the SCH optical confining region will affect the optical confinement or the coupling factor Γ. Tight optical confinement (a large Γ) will cause the threshold gain to be reached at low injection carrier density. The low threshold carrier density, in turn, will result in a large value of differential gain in the QW structure. It was shown experimentally that the smaller density of states in the optical confining region and tight optical confinement resulted in reduction of threshold current and enhancement

in modulation bandwidth [62,8,39].

4.5 Evidence for State Filling Effects on High Speed Modulation Dynamics of Quantum Well Lasers

The above analysis indicates that the increase in the energy separation (E_1) between the ground lasing states of the QW and the large number of states in the optical confining region will result in an increase in the differential gain and a reduction in the carrier population necessary to reach a certain gain value.

Experimental investigations have been carried out to study the influence of the QW barrier height or the QW depth on the performance of the QW lasers by using different composition for the optical confining layers or using different material for the quantum wells. Since the differential gain is not a constant in the QW lasers due to the sublinearity in the gain and carrier density relation caused by the flat feature of the 2D step-like density of states of injected carriers in the QW structures, we need to be cautious when comparing the dynamic properties in the different QW structures.

Two GaAs/AlGaAs graded index (GRIN) SCH single quantum well (SQW) laser structures, we refer to them as A and B, were grown by molecular beam epitaxy (MBE) on (100) n^+-GaAs substrates. As schematically shown in Figure 4.7, the profiles and dimensions of the two GRIN SCH structures are identical. As are the

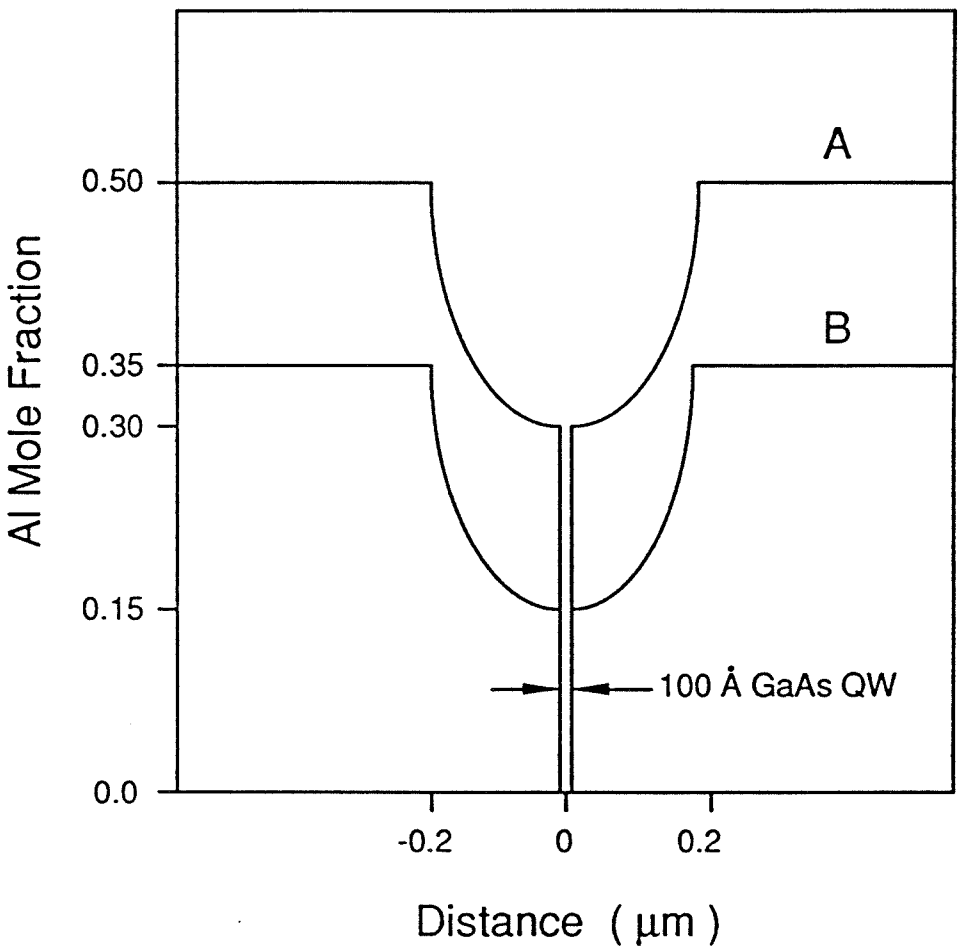

Figure 4.7: The schematic structures of the GaAs/AlGaAs GRIN SCH SQW samples used in experiment.

doping levels and profiles. The only difference between them is the different Al concentration in the GRIN SCH region. The GRIN SCH structures consist of (i) 1 μm n^+-GaAs buffer layer, (ii) a 1.7 μm n-$Al_xGa_{1-x}As$ lower cladding layer (A: $x = 0.50$, B: $x = 0.35$), (iii) a 2000 $\AA$ undoped $Al_xGa_{1-x}As$ composition graded layers (A: $x = 0.50 - 0.30$, B: $x = 0.35 - 0.15$), (iv) an undoped 100 $\AA$ GaAs quantum well, (v) a 2000 $\AA$ undoped $Al_xGa_{1-x}As$ composition graded layers (A: $x = 0.30 - 0.50$, B: $x = 0.15 - 0.35$), (vi) a 1.7 μm p-$Al_xGa_{1-x}As$ upper cladding layer (A: $x = 0.50$, B: $x = 0.35$), and finally (vii) a 2000 $\AA$ p^+-GaAs cap layer. The identical profiles and dimensions of the GRIN SCH structures assure a nearly identical carrier transport effect and optical confinement in these two structures. The different Al concentration in the GRIN SCH structures results in a different energy separation between the quantized states of the QW and the large number of states in the GRIN SCH optical confining region which, in turn, results in very different state filling effects in these two structures. For example, the energy separation between the first quantized state of the QW and the lowest energy state of the GRIN SCH optical confining region are estimated to be 225 meV (structure A) and 102 meV (structure B), respectively, for electrons.

Following the MBE growth, mesas with an active stripe width 4 μm were chemically etched and then a buried heterostructure (BH) was grown by a liquid phase epitaxy (LPE) regrowth. Following the regrowth, the wafers were processed into BH lasers using conventional fabrication techniques. The wafers were then cleaved into lasers and the lasers were mounted in standard microwave packages. The high fre-

quency modulation of the lasers were carried out by a standard experimental arrangement including an S-parameter test set and a network analyzer. We have measured modulation response of 2 sets of lasers of the same cavity length, each of them consists of 5 lasers fabricated from the same wafer of structure A or structure B. The modulation measurement was very consistent in each set of lasers. The variation in the measured differential gain were within 18% for the lasers in each set. Figure 4.8 shows the square of the measured response peak frequency f_p as a function of the optical output power for two typical lasers of the same cavity length of 300 μm. The f_p^2 - P curves do not go through the zero point due to the presence of the constant damping term in the modulation response [65]. Due to the structural and dimensional identity of the two lasers, the carrier relaxation/transport effect and the device parasitics are almost the same, which results in almost the same value of f_c in the two lasers. Thus, the characteristics difference in the two lasers shown in Figure 4.7 is mainly attributed to the different state-filling effects in the two structures. The differential gain values were measured to be 2.8×10^{-16} cm^2 (A) and 0.9×10^{-16} cm^2 (B). The threshold currents of these lasers are 10 mA (A) and 14 mA (B), respectively. The internal loss constants were obtained to be 8 cm^{-1} (A) and 12 cm^{-1} (B) from the measured differential quantum efficiency.

It is well known that the differential gain decreases as the gain increases in QW lasers because of the sublinearity in the gain and carrier density relation caused by the flat feature of the 2D step-like density of states of injected carriers in the QW structure. The mirror loss of these two lasers of cavity length of 300 μm is about 40

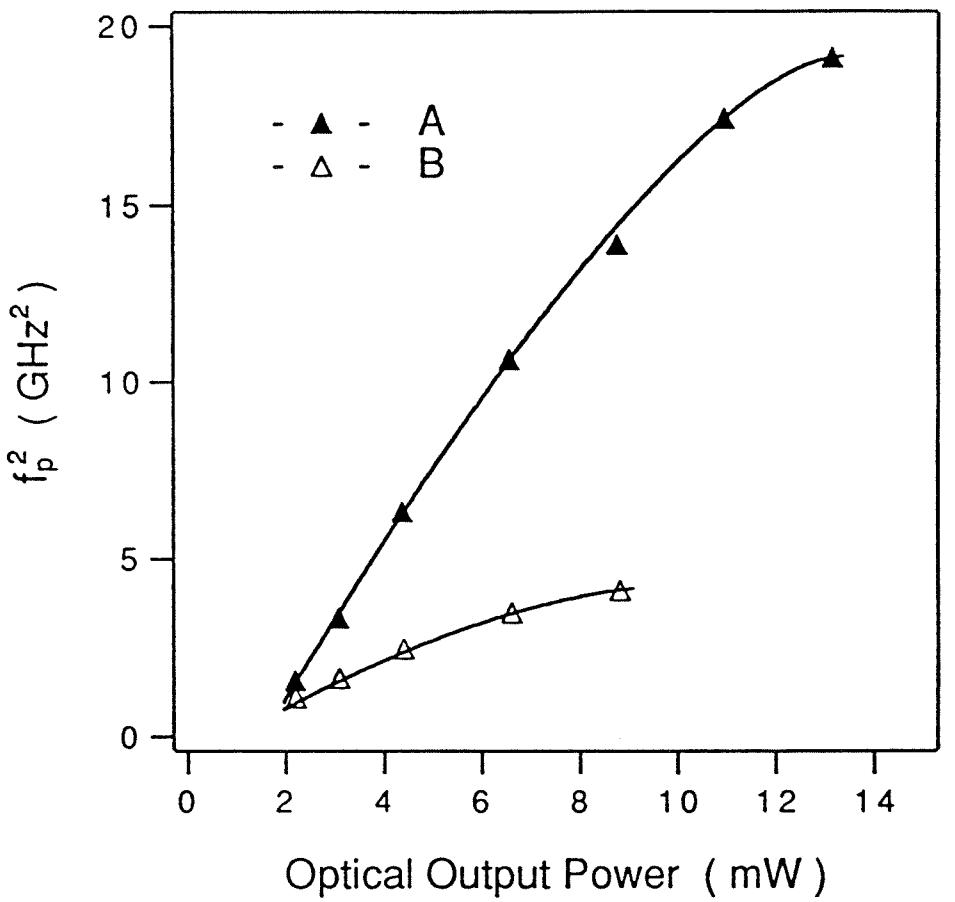

Figure 4.8: The square of measured modulation response peak frequency *vs.* optical output power for lasers of different GRIN SCH structures. The cavity lengths are 300 μm and facets are uncoated.

cm^{-1}. From the measured internal loss constants, we find these two lasers have almost the same value of modal gain. Since the optical confinement in these two structures is almost identical, the two lasers were biased at such a point that the carrier population gave almost the same material gain. However, the carrier population is not the same in the two lasers to reach such a bias point. There is an appreciable carrier population in the SCH optical confining region of the laser structure B due to the smaller energy separation between the quantized states of the QW and the states in the SCH optical confining region. The significant difference in the carrier population of the SCH optical confining region in these two structures gives rise to different impact on the high-speed dynamics. In Figure 4.9 we show the theoretically estimated ratio of differential gain in these two structures as a function of the modal gain, where the state-filling effect has been taken into account. It is shown that the differential gains can differ by as much as a factor of 3.5 at the modal gain of 50 cm^{-1}, which is quite consistent with the experimental results. In addition, this carrier population is also responsible for the threshold current difference and internal loss constant difference (due to free-carrier absorption) in these two lasers.

The difference in differential gain definitely results in different modulation bandwidths in these two structures. In Figure 4.10, we show the measured small signal modulation response for the lasers of cavity length of 300 μm. It is shown that laser A is superior to laser B in the modulation bandwidth. The modulation bandwidth of laser B is severely limited by the state-filling effect. A better high frequency response is expected in the lasers of structure A since this structure possesses a larger

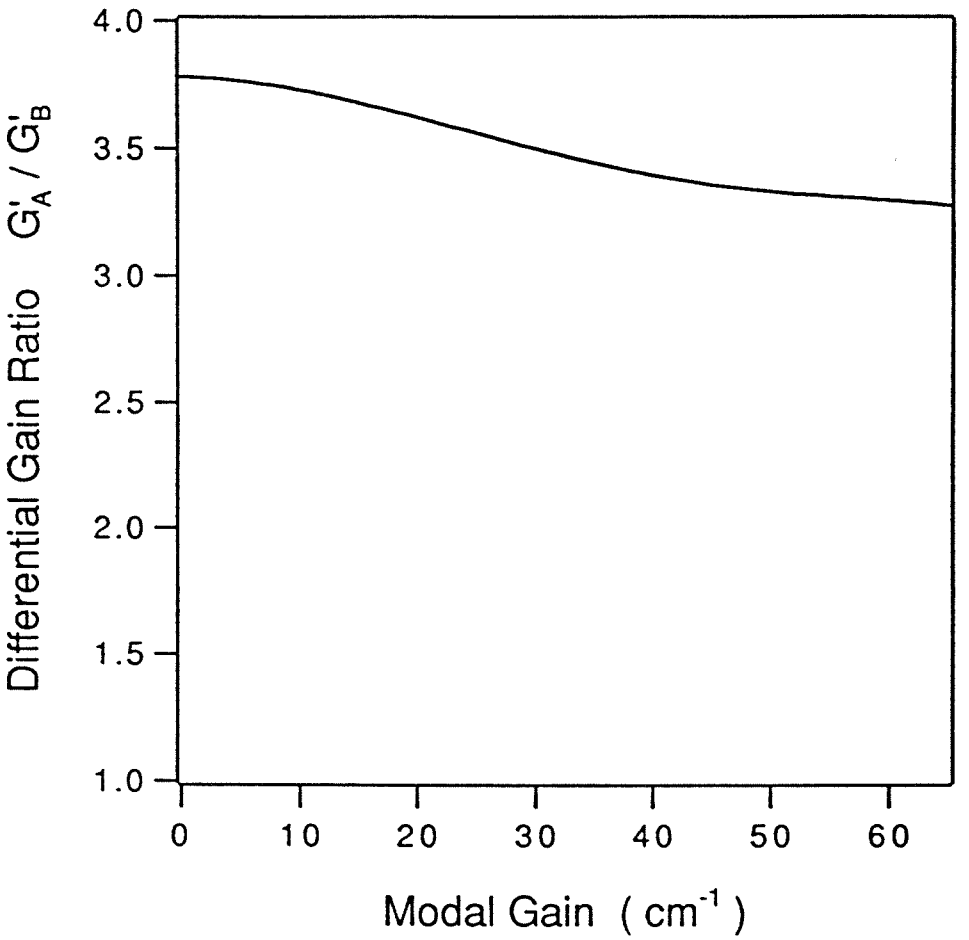

Figure 4.9: The theoretically estimated ratio of differential gain between the two different GRIN SCH structures as a function of modal gain.

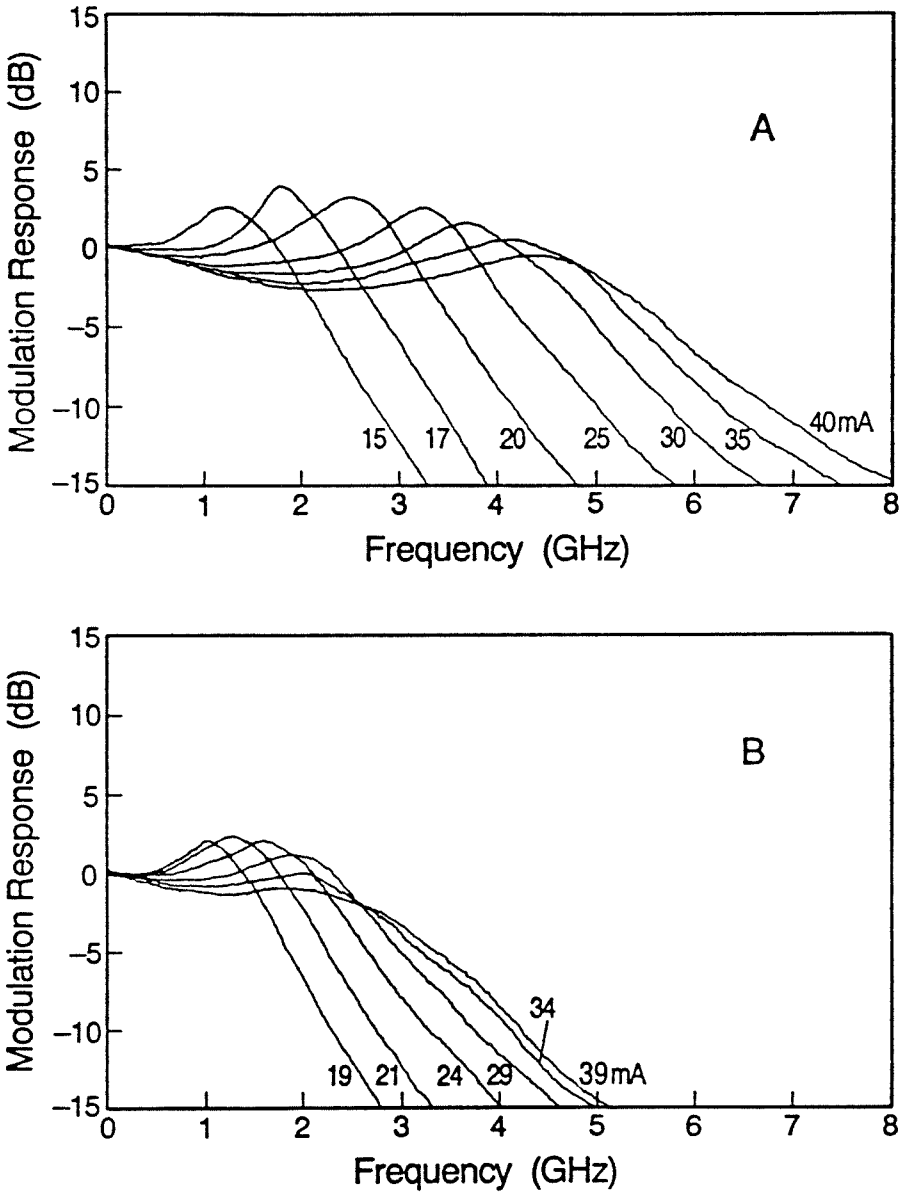

Figure 4.10: The modulation response for the lasers of different GRIN SCH structures. The cavity lengths are 300 μm and facets are uncoated. The threshold current are 10 mA (A) and 14 mA (B), respectively.

differential gain due to the reduction of the state filling.

Due to the presence of the damping we can not increase the modulation bandwidth unlimitedly by only increasing the photon density within the laser cavity. For a laser with given device parameters, there exists a maximum modulation bandwidth at a certain photon density [65]. Both this maximum modulation bandwidth and corresponding photon density depend on the laser device parameters. The higher value of differential gain in the SQW structure A gives the potential of an improved high speed performance. To actually achieve higher speed, a careful tailoring of the laser device parameters such as cavity length and mirror reflectivity is required.

For a laser with cavity length $L = 300\mu$m and cleaved mirrors, *i.e.*, $R_1 = R_1 = 0.3$, a maximum modulation bandwidth of 5.6 GHz is obtained. The threshold current of this laser is 10 mA and the lasing wavelength is about 0.85 m. For an uncoated 150 μm long laser with threshold current of 16 mA, the maximum modulation bandwidth was about 6.2 GHz. However, when the reflectivity of one mirror was increased to 0.7 by a dielectric coating (Si/Al_2O_3 $\lambda/4$ stack), a maximum modulation bandwidth in excess of 9 GHz was demonstrated as shown in Figure 4.11, which is the largest modulation bandwidth ever reported in unstrained GaAs SQW lasers with a uniform current pumping [14].

A further increase of the mirror reflectivity to 0.9 resulted in a decrease of the maximum modulation bandwidth to about 7.5 GHz. It is therefore concluded that for the GaAs SQW laser a cavity length of 150 μm with mirror reflectivities of 0.3 and 0.7 is a good (if not the best) combination for high-speed operation. The maximum

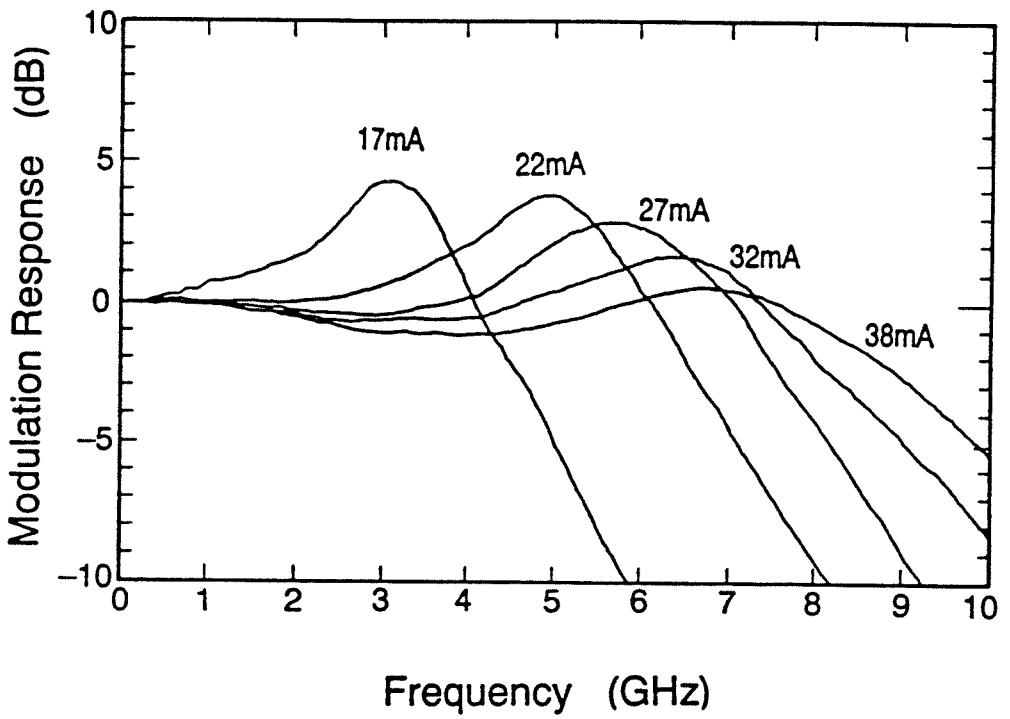

Figure 4.11: The modulation response of GaAs/AlGaAs SQW BH laser of structure A. The laser has a cavity length of 150 μm and facet reflectivities $R_1 = 0.3$, $R_1 = 0.7$.

modulation bandwidth versus threshold current for the SQW lasers is plotted in Figure 4.12 to show the device parameter optimization procedure.

To summarize, in this section we have shown experimentally that the state-filling effect plays a major role in the high-speed modulation dynamics of QW lasers. By using different separate confinement structures for otherwise identical quantum well lasers, we find that the differential gain can vary over a factor of three, which significantly affects the high speed modulation bandwidth in such lasers. These observations are in agreement with the conclusions of the theory which takes the state-filling into account in QW lasers. They bear directly on the design and fabrication of QW lasers of superior high-speed performance.

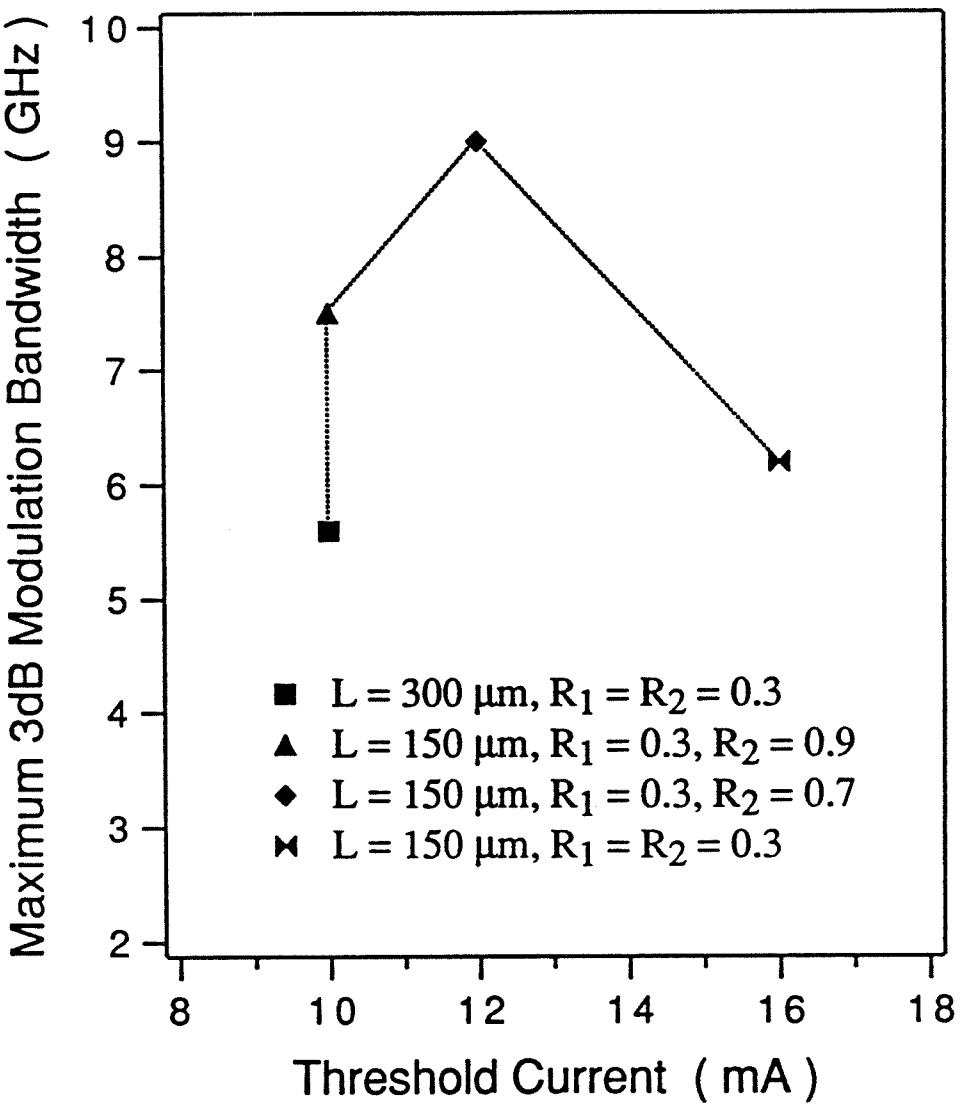

Figure 4.12: The maximum modulation bandwidth and threshold current for different device parameters of GaAs/AlGaAs SQW structure A.

Bibliography

[1] A. R. Adams, "Band-structure engineering for low-threshold high-efficiency semiconductor lasers," *Electron. Lett.*, vol.22, p.249, 1986

[2] D. Ahn and S. L. Chuang, "Optical gain in a strained-layer quantum well laser," *IEEE J. Quantum Electron.*, vol.QE-24, p.2400, 1988

[3] Y. Arakawa, K. Vahala, and A. Yariv, "Quantum noise and dynamics in quantum well and quantum wire lasers," *Appl. Phys. Lett*, vol.45, p.950, 1984

[4] Y. Arakawa and A. Yariv, "Theory of gain, modulation response, and spectral linewidth in AlGaAs quantum well lasers," *IEEE J. Quantum Electron.*, vol.QE-21, p.1666, 1985

[5] Y. Arakawa and A. Yariv, "Quantum well lasers — gain, spectra, dynamics," *IEEE J. Quantum Electron.*, vol.QE-22, p.1887, 1986

[6] M. Asada, A. Kameyama, and Y. Suematsu, "Gain and intervalence band absorption in quantum-well lasers," *IEEE J. Quantum Electron.*, vol.QE-20, p.745, 1984

[7] W. Batty, U. Ekenberg, A. Ghiti, and E. P. O'Reilly, "Valence subband structure and optical gain of GaAs-AlGaAs (111) quantum wells," *Semicond. Sci. Technol.*, vol.4, p.904, 1989

[8] D. P. Bour, R. U. Martinelli, F. Z. Hawrylo, G. A. Evans, N. W. Carlson, and D. B. Gilbert, "Improving the performance of strained InGaAs/AlGaAs single quantum well lasers," *Appl. Phys. Lett.*, vol.56, p.318, 1990

[9] M. G. Burt, "Gain spectra of quantum-well lasers," *Electron. Lett.*, vol.19, p.210, 1983

[10] N. Chand, E. E. Becker, J. P. van der Ziel, S. N. G. Chu, and N. K. Dutta, "Excellent uniformity and very low (< 50 A/cm^2) threshold current density strained InGaAs quantum well diode lasers on GaAs substrate," *Appl. Phys. Lett.*, vol.58, p.1704, 1991

[11] H. Z. Chen, A. Ghaffari, H. Morkoç, and A. Yariv, "Very low threshold current densities (under 100 A/cm^2) in AlGaAs/GaAs single-quantum-well GRINSCH lasers grown by molecular beam epitaxy," *Electron. Lett.*, vol.23, p.1334, 1987

[12] T. R. Chen, L. E. Eng, B. Zhao, Y. H. Zhuang, S. Sanders, H. Morkoç, and A. Yariv, "Submilliamp threshold current strained layer InGaAs/GaAs quantum well lasers," *IEEE J. Quantum Electron.*, vol.QE-26, p.1183, 1990

[13] T. R. Chen, B. Zhao, Y. H. Zhuang, A. Yariv, J. E. Ungar, and S. Oh, "Ultralow threshold strained layer InGaAs multi-quantum well lasers," *Appl. Phys. Lett.*,

vol.60, p.1782, 1992

[14] T. R. Chen, B. Zhao, Y. Yamada, Y. H. Zhuang, and A. Yariv, "Modulation bandwidth enhancement in single quantum well GaAs/AlGaAs lasers," *Electron. Lett.* vol.28, p.1989, 1992

[15] S. R. Chinn, P. S. Zory, and A. R. Reisinger "A model for GRIN-SCH-SQW diode lasers," *IEEE J. Quantum Electron.*, vol.QE-24, p.2191, 1988

[16] H. K. Choi and C. A. Wang, "InGaAs/AlGaAs strained single quantum well diode lasers with extremely low threshold current density and high efficiency," *Appl. Phys. Lett.*, vol.57, p.321, 1990

[17] P. L. Derry, T. R. Chen, Y. H. Zhuang, J. Paslaski, M. Mittelstein, K. Vahala, A. Yariv, K. Lau, and N. Bar-Chaim, "Properties of ultra low threshold single quantum well (Al,Ga)As lasers for computer interconnects," *Optoelectronics – Devices and Technologies*, vol.3, p.117, 1988

[18] N. K. Dutta, "Calculated threshold current of GaAs quantum well lasers," *J. Appl. Phys.*, vol.53, p.7211, 1982

[19] L. E. Eng, T. R. Chen, S. Sanders, Y. H. Zhuang, B. Zhao, A. Yariv, and H. Morkoç, "Submilliamp threshold current pseudomorphic InGaAs/AlGaAs buried-heterostructure quantum well lasers grown by molecular beam epitaxy," *Appl. Phys. Lett.*, vol.55, p.1378, 1989

[20] A. Ghiti, W. Batty, and E. P. O'Reilly, "Theory of reduced threshold current density in GaAs-AlGaAs quantum well lasers," *Superlatt. Microstruct.*, vol.7, p.353, 1990

[21] T. Hayakawa, M. Kondo, T. Suyama, K. Takahashi, S. Yamamoto, and T. Hijikata, "Reduction in threshold current density of quantum well lasers grown by molecular beam epitaxy on 0.5 ^{o} misoriented (111)B substrates," *Japan. J. Appl. Phys.*, vol.26, p.L302, 1987

[22] T. Hayakawa, T. Suyama, K. Takahashi, M. Kondo, S. Yamamoto, and T. Hijikata, "Near-ideal low threshold behavior in (111) oriented GaAs/AlGaAs quantum well lasers," *Appl. Phys. Lett.*, vol.52, p.339, 1988

[23] S. C. Kan, D. Vassilovski, T. C. Wu, and K. Y. Lau, "Quantum capture and escape in quantum-well lasers – implications on direct modulation bandwidth limitations," *IEEE Photon. Technol. Lett.*, vol.4, p.428, 1992

[24] S. C. Kan, D. Vassilovski, T. C. Wu, and K. Y. Lau, "On the effects of carrier diffusion and quantum capture in high speed modulation of quantum well lasers," *Appl. Phys. Lett.*, vol.61, p.752, 1992

[25] E. Kapon, S. Simhony, J. P. Harbison, and L. T. Florez, "Threshold current reduction in patterned quantum well semiconductor lasers grown by molecular beam epitaxy," *Appl. Phys. Lett.*, vol.56, p.1825, 1990

[26] K. Y. Lau, N. Bar-Chaim, I. Ury, and A. Yariv, "11-GHz direct modulation

bandwidth GaAlAs window laser on semi-insulating substrate operating at room temperature," *Appl. Phys. Lett.*, vol.45, p.316, 1984

[27] K. Y. Lau, P. L. Derry, and A. Yariv, "Ultimate limit in low threshold quantum well GaAlAs semiconductor lasers," *Appl. Phys. Lett.*, vol.52, p.88, 1988

[28] K. Y. Lau, S. Xin, W. I. Wang, N. Bar-Chaim, and M. Mittelstein, "Enhancement of modulation bandwidth in InGaAs strained-layer single quantum well lasers," *Appl. Phys. Lett.*, vol.55, p.1173, 1989

[29] I. F. Lealman, M. Bagley, D. M. Cooper, N. Fletcher, M. Harlow, S. D. Perrin, R. H. Walling, and L. D. Westbrook, "Wide bandwidth multiple quantum well 1.55 μm lasers," *Electro. Lett.*, vol.27, p.1191, 1991

[30] L. F. Lester, S. S. O'Keefe, W. J. Schaff, and L. F. Eastman, "Multiquantum well strained-layer lasers with improved low frequency response and very low damping," *Electro. Lett.*, vol.28, p.383, 1992

[31] J. P. Loehr and J. Singh, "Theoretical studies of the effect of strain on the performance of strained quantum well lasers based on GaAs and InP technology," *IEEE J. Quantum Electron.*, vol.QE-27, p.708, 1991

[32] E. Meland, R. Holmstrom, J. Schlafer, R. B. Lauer, and W. Powazinik, "Extremely high-frequency (24 GHz) InGaAsP diode lasers with excellent modulation efficiency," *Electro. Lett.*, vol.26, p.1827, 1990

[33] P. A. Morton, R. A. Logan, T. Tanbun-Ek, P. F. Sciortino Jr., A. M. Sergent, R. K. Montgomery, and B. T. Lee, "25 GHz bandwidth 1.55 μm GaInAsP p-doped strained multiquantum-well lasers," *Electro. Lett.*, vol.28, p.2156, 1992

[34] J. Nagle, S. Hersee, M. Krakowski, and C. Weisbuch, "Threshold current of single quantum well lasers: the role of the confining layers," *Appl. Phys. Lett.*, vol.49, p.1325, 1986

[35] R. Nagarajan, T. Kamiya, and A. Kurobe, "Band filling in GaAs/AlGaAs multiquantum well lasers and its effect on the threshold current," *IEEE J. Quantum Electron.*, vol.QE-25, p.1161, 1989

[36] R. Nagarajan, T. Fukushima, J. E. Bowers, R. S. Geels, and L. A. Coldren, "Single quantum well strained InGaAs/GaAs lasers with large modulation bandwidth and low damping," *Electro. Lett.*, vol.27, p.1058, 1991

[37] R. Nagarajan, T. Fukushima, S. W. Corzine, and J. E. Bowers, "Effects of carrier transport on high-speed quantum well lasers," *Appl. Phys. Lett.*, vol.59, p.1835, 1991

[38] R. Nagarajan, M. Ishikawa, T. Fukushima, R. S. Geels, and J. E. Bowers, "High speed quantum-well lasers and carrier transport effects," *IEEE J. Quantum Electrn.*, vol.QE-28, p.1990, 1992

[39] R. Nagarajan, T. Fukushima, M. Ishikawa, J. E. Bowers, R. S. Geels, and L. A. Coldren, "Transport limits in high-speed quantum-well lasers: experiment and

theory," *IEEE Photon. Technol. Lett.*, vol.4, p.121, 1992

[40] J. D. Ralston, D. F. G. Gallagher, P. J. Tasker, H. P. Zappe, I. Esquivias, and J. Fleissner, "Vertical compact 15 GHz GaAs/AlGaAs multiple quantum well laser grown by molecular beam epitaxy," *Electro. Lett.*, vol.27, p.1720, 1991

[41] J. D. Ralston, I. Esquivias, S. Weisser, D. F. G. Gallagher, P. J. Tasker, E. C. Larkins, J. Rosenzweig, H. P. Zappe, J. Fleissner, and D. J. As, "16 GHz GaAs/AlGaAs multiple quantum well laser with vertical compact structure," *High-Speed Electronics and Optoelectronics*, Proc. SPIE vol.1680, p.127, 1992

[42] W. Rideout, W. F. Sharfin, E. S. Koteles, M. O. Vassell, and B. Elman, "Well-barrier hole burning in quantum well lasers," *IEEE Photon. Technol. Lett.*, vol.3, p.784, 1991

[43] S. Seki, T. Yamanaka, W. Liu, Y. Yoshikuni, and K. Yokoyama, "Pure strain effect on differential gain of strained InGaAsP/InP quantum-well lasers," *IEEE Photon. Technol. Lett.*, vol.5, p.500, 1993

[44] I. Suemune, L. A. Coldren, M. Yamanishi, and Y. Kan, "Extremely wide modulation bandwidth in a low threshold current strained quantum well laser," *Appl. Phys. Lett.*, vol.53, p.1378, 1988

[45] T. Takahashi, M. Nishioka, and Y. Arakawa, "Differential gain of GaAs/AlGaAs quantum well and modulation-doped quantum well lasers," *Appl. Phys. Lett.*, vol.58, p.4, 1991

[46] G. W. Taylor and P. R. Claisse, "Effects of drift and diffusion current flow on the high-speed performance of quantum well lasers," *Appl. Phys. Lett.*, vol.62, p.723, 1993

[47] N. Tessler, R. Nagar, D. Abraham, G. Eisenstein, U. Koren, and G. Raybon, "Coupling between barrier and quantum well energy states in a multiple quantum well optical amplifier," *Appl. Phys. Lett.*, vol.60, p.665, 1992

[48] N. Tessler, R. Nagar, and G. Eisenstein, "Structure dependent modulation responses in quantum-well lasers," *IEEE J. Quantum Electrn.*, vol.QE-28, p.2242, 1992

[49] N. Tessler and G. Eisenstein, "Distributed nature of quantum-well lasers," *Appl. Phys. Lett.*, vol.62, p.10, 1993

[50] P. J. A. Thijs, L. F. Tiemeijer, P. I. Kuindersma, J. J. M. Binsma, and T. van Dongen, "High-performance 1.5 μm wavelength InGaAs-InGaAsP strained quantum well lasers and amplifiers," *IEEE J. Quantum Electron.*, vol.QE-27, p.1426, 1991

[51] P. J. A. Thijs, J. J. M. Binsma, L. F. Tiemeijer, R. W. M. Slootweg, R. van Roijen, and T. van Dongen, "Sub-mA threshold operation of *lambda* = 1.5μm strained InGaAs multiple quantum well lasers grown on (311)B InP substrates," *Appl. Phys. Lett.*, vol.60, p.3217, 1992

[52] W. T. Tsang, "Extremely low threshold (AlGa)As graded-index waveguide

separate-confinement heterostructure lasers grown by molecular-beam epitaxy," *Appl. Phys. Lett.*, vol.40, p.217, 1982

[53] K. Uomi, N. Chinone, T. Ohtoshi, and T. Kajimura, "High relaxation oscillation frequency (beyond 10 GHz) of GaAlAs multiquantum well lasers," *Japan. J. Appl. Phys.*, vol.24, p.L539, 1985

[54] K. Uomi, T. Mishima, and N. Chinone, "Ultrahigh relaxation oscillation frequency (up to 30 GHz) of highly p-doped GaAs/GaAlAs multiple quantum well lasers," *Appl. Phys. Lett.*, vol.51, p.78, 1987

[55] M. O. Vassell, W. F. Sharfin, W. Rideout, and J. Lee, "Small-signal predictions of the well-barrier hole burning model on quantum-well laser dynamics," *Appl. Phys. Lett.*, vol.61, p.1145, 1992

[56] C. Weibbuch and J. Nagle "The physics of the quantum well laser," *Physica Scripta*, vol.T19, p.209,1987

[57] S. Weisser, J. D. Ralston, E. C. Larkins, I. Esquivias, P. J. Tasker, J. Fleissner, and J. Rosenzweig, "Efficient high-speed direct modulation in p-doped $In_{0.35}Ga_{0.65}As$/GaAs multiquantum well lasers," *Electro. Lett.*, vol.28, p.2141, 1992

[58] R. L. Williams, M. Dion, F. Chatenoud, and K. Dzurko, "Extremely low threshold current strained InGaAs/AlGaAs lasers by molecular beam epitaxy," *Appl. Phys. Lett.*, vol.58, p.1816, 1991

[59] H. D. Wolf, H. Lang and L. Korte, "High-speed AlGaAs/GaAs multiple quantum well ridge waveguide lasers," *Electro. Lett.*, vol.25, p.1249, 1989

[60] E. Yablonovitch and E. O. Kane, "Reduction of lasing threshold current density by the lowering of valence band effective mass," *IEEE J. Lightwave Technol.*, vol.LT-4, p.504, 1986

[61] A. Yariv, "Scaling laws and minimum threshold currents for quantum-confined semiconductor lasers," *Appl. Phys. Lett.*, vol.53, p.1033, 1988

[62] P. K. York, S. M. Lansjoen, L. M. Miller, K. J. Beernink, J. J. Alwan, and J. J. Coleman, "Effect of confining layer aluminum composition on AlGaAs-GaAs-InGaAs strained-layer quantum well heterostructure lasers," *Appl. Phys. Lett.*, vol.57, p.843, 1990

[63] C. E. Zah, R. Bhat, B. Pathak, C. Caneau, F. J. Favire, N. C. Andreadakis, D. M. Hwang, M. A. Koza, C. Y. Chen, and T. P. Lee, "Low threshold 1.5 μm tensile-strained single quantum well lasers," *Electron. Lett.*, vol.27, p.1414, 1991

[64] B. Zhao, T. R. Chen, and A. Yariv, "Comparison of differential gain in single quantum well and bulk double heterostructure lasers," *Electron. Lett.*, vol.27, p.2343, 1991

[65] B. Zhao, T. R. Chen, and A. Yariv, "On the high speed modulation bandwidth of quantum well lasers," *Appl. Phys. Lett.*, vol.60, p.313, 1992

[66] B. Zhao, T. R. Chen, and A. Yariv, "The extra differential gain enhancement in multiple quantum well lasers," *IEEE Photon. Tech. Lett.*, vol.4, p.124, 1992

[67] B. Zhao, T. R. Chen, and A. Yariv, "Effect of state filling on the modulation response and the threshold current of quantum well lasers," *Appl. Phys. Lett.*, vol.60, p.1930, 1992

[68] B. Zhao, T. R. Chen, Y. Yamada, Y. H. Zhuang, N. Kuze, and A. Yariv, "Evidence for state filling effect on high speed modulation dynamics of quantum well lasers," *Appl. Phys. Lett.*, vol.61, p.1907, 1992

Chapter 5

Quantum Well Lasers of Low Threshold Current and High Modulation Bandwidth at Low Operation Current

5.1 Design Considerations

Low threshold current semiconductor lasers are key components in high density application, such as optical interconnect in the computer circuits. High packing density and low power consumption are the two critical requirements for this kind of application. Therefore, threshold currents in the submilliampere or microampere region is of importance. In addition, low threshold lasers often exhibit improved reliability

and enhanced modulation bandwidth and also offer the possibility of direct digital modulation under zero bias current condition.

The threshold current density of a semiconductor laser will be reduced if the thickness of the active layer d is reduced. However, once d is reduced to the quantum regime of the injected carriers, any further reduction in d will not lead to significant reduction in the threshold current density since the carriers are quantized in the direction perpendicular to the active layer and are two dimensional in the active layer. In terms of the state filling, there exists an optimal range for the thickness of the QW. If the thickness of the QW is too large, there exist many very closely packed (in the energy domain) subbands for the QW. This will result in a significant carrier population in the upper subbands of the QW at the threshold. If the thickness of the QW is too small, the first quantized states are very close to the top of the QW. This results in a significant carrier population in the optical confining region at the threshold.

For DH bulk semiconductor lasers, the modal gain and injection current density has a linear relation [12,14]

$$g = \Gamma B \, (J - J_{tr}) \tag{5.1}$$

where B is a constant, transparency current density J_{tr} includes the radiative carrier loss due to the spontaneous emission, nonradiative carrier loss such as the carrier leakage in a particular laser device structure used to confine the current injection. At

threshold,

$$g = \alpha_i + \frac{1}{L} \ln \frac{1}{R} \ . \tag{5.2}$$

From (5.1) and (5.2) the threshold current can be obtained as

$$I_{th} = wLJ_{th} = w \ [L(\frac{\alpha_i}{\Gamma B} + J_{tr}) + \frac{1}{\Gamma B} \ln \frac{1}{R}] \ , \tag{5.3}$$

where w and L are the laser strip width and cavity length, respectively. So the strategy to achieve low threshold current in the bulk DH lasers is to reduce the internal loss α_i, to reduce the transparency current density J_{tr}, to reduce the device dimension w and L, to increase the optical mode confinement Γ, to increase the differential gain ($\propto B$), and to use high reflectivity (R) coating.

The lowest threshold current density demonstrated in QW lasers is less than 50 A/cm^2 in a long cavity InGaAs SQW laser [2]. To achieve ultralow threshold current, it is also necessary to consider the device dimensions. As shown in the following, in the QW lasers there exists an optimal cavity length to achieve the lowest threshold current at a given mirror reflectivity R. As the lateral dimension w is reduced to the quantum regime, the lasers become quantum wire lasers.

In QW lasers, the modal gain and injection current density relation is nonlinear due to the flat feature of the step-like density of states for the QW structures [1,10,8,5]. If the quantum well number N_{qw} is not very large, as shown in Figure 5.1, the modal gain g will be roughly scaled by N_{qw}. The nonlinear relation of the modal gain and injection current density relation can be simply written as

$$g = N_{qw} \Gamma B \ \ln \frac{J}{J_{tr}} \ . \tag{5.4}$$

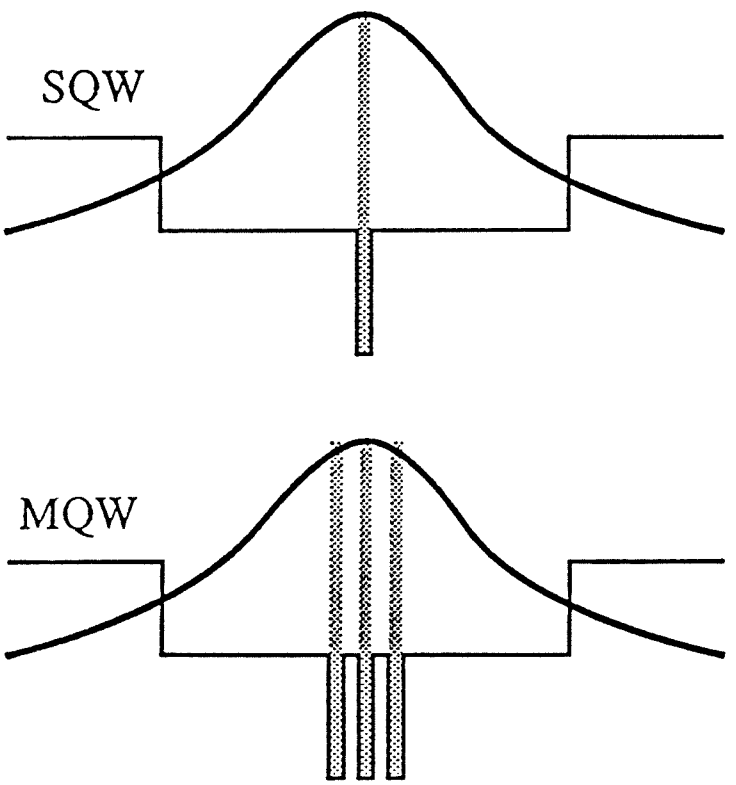

Figure 5.1: The schematic structures of SQW and MQW indicating the modal gain roughly scales as the number of quantum wells N_{qw} in the case that N_{qw} is not too large.

We find that the minimum threshold current

$$I_{th}^{min} = w \frac{J_{tr}}{N_{qw}\Gamma B} \exp(\frac{\alpha_i}{N_{qw}\Gamma B} + 1) \ln\frac{1}{R} \tag{5.5}$$

is achieved at a cavity length

$$L = \frac{1}{N_{qw}\Gamma B} \ln\frac{1}{R} . \tag{5.6}$$

These results indicate that the strategy to achieve low threshold current in the QW lasers is almost the same as that in bulk DH lasers except that there exists an optimal cavity length for the minimum threshold current in the QW lasers.

From (5.5) and (5.6) one can determine how the number of QW will influence the threshold current behavior in the QW lasers. Both J_{tr} and α_i consist of two parts: one part scales as N_{qw} and another is independent of N_{qw}. For J_{tr}, the radiative loss of the carriers within the QW scales as N_{qw}, but the radiative carrier loss of the carriers in the optical confining region and the nonradiative carrier leakage are basically independent of N_{qw}. α_i consists of the free carrier absorption due to the carriers within the QW, the free carrier absorption due to the carriers in the optical confining region, and the waveguide scattering. The first one scales as N_{qw}. The next two are independent of N_{qw}. These features plus the extra differential gain enhancement in the MQW structure ($B \propto$ differential gain) make MQW structure possess advantages in obtaining low threshold current for given mirror reflectivity R. (5.6) shows that the lower threshold current is obtained at shorter cavity length in MQW lasers in comparison with SQW lasers.

It must be borne in mind, however, that the low threshold lasers need to be

modulated at rates up to a few gigabits/sec. and the low power advantage will be lost if the current needed to reach the required modulation bandwidth is excessive. From Eq.(3.55), at low optical power levels, the 3dB modulation bandwidth is proportional to the relaxation resonance frequency

$$f_{3dB} \approx 1.55 f_r = \frac{1.55}{2\pi}\sqrt{\frac{v_g \eta_i}{eV_{opt}}(I - I_{th})G_0'} \,, \tag{5.7}$$

where η_i is the internal quantum efficiency and V_{opt} is the optical mode volume, $V_{opt} = wtL$. From (5.7) it follows that for a given injection current I the achievement of high f_{3dB} requires a low threshold I_{th}, a large differential gain G_0', a small optical mode volume V_{opt}, and a high internal quantum efficiency.

QW lasers become the main contenders for this kind of applications due to the demonstrated submilliampere threshold current [9,7,3]. A lower threshold current can be achieved by increasing the number of quantum wells, using a shorter cavity length and a narrower active strip width. At the same time, shorter cavity length and narrower active strip width lead to smaller optical mode volume, which, in turn, leads to a larger modulation bandwidth. However, shorter cavity length entails operation at higher current (and carrier) densities because of the large threshold modal gain required. This inevitably reduces the differential gain constant G_0' in QW lasers due to the flattening of the gain *vs.* carrier density characteristics of such lasers. High reflectivity coatings on the facets of such lasers with short cavity lengths can dramatically reduce the threshold current and the threshold modal gain, thus retaining a high value of differential gain. On the other hand, the use of MQW as the active

region will lead to a higher differential gain at low threshold modal gain compared to SQW structures due to the reduced effect of confining layer state filling [16]. And the use of strained QW structure leads to further improvement since strained QW lasers have demonstrated lower threshold current density and higher differential gain due to the strain induced valence band modification.

5.2 Laser Device Structures

Using design criteria inspired by the arguments in previous section, a graded index separate confinement heterostructure (GRIN SCH) MQW laser structure was grown by low pressure metalorganic chemical vapor deposition (MOCVD) on (100) n-GaAs substrate. The MQW laser structure is a double quantum well (DQW) laser structure. As shown in Figure 5.2, the GRIN SCH DQW structure consists of a 1.5 μm n-$Al_{0.4}Ga_{0.6}As$ lower cladding layer, a 2000 Å undoped $Al_xGa_{1-x}As$ linearly graded region ($x = 0.4 - 0.05$), a 150 Å undoped GaAs spacer layer, two undoped 75 Å $In_{0.2}Ga_{0.8}As$ quantum wells with undoped 150 Å GaAs barrier layer, a 150 Å undoped GaAs spacer layer, a 2000 Å undoped $Al_xGa_{1-x}As$ linearly graded region ($x = 0.05 - 0.4$), a 1.5 μm p-$Al_{0.4}Ga_{0.6}As$ upper cladding layer, and finally a 3000 Å p^+-GaAs cap layer.

After the MOCVD growth, mesas with an active stripe width $2 \sim 3$ μm were chemically etched in order to fabricate buried heterostructure (BH) lasers. The top GaAs cap layer was removed immediately prior to loading the wafer into a liquid phase

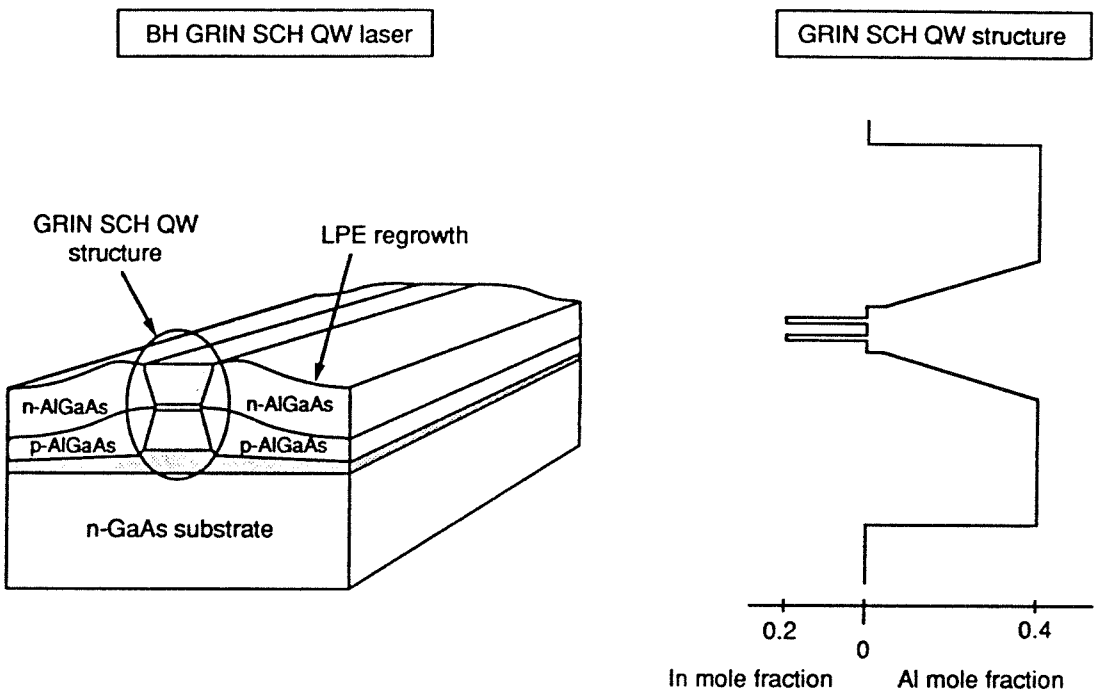

Figure 5.2: The schematic structure of the InGaAs/AlGaAs/GaAs double quantum well laser structure and the schematic structure for the buried heterostructure lasers.

epitaxy (LPE) system for regrowth. A p-$Al_{0.4}Ga_{0.6}As$ layer and an n-$Al_{0.4}Ga_{0.6}As$ were grown successively to form a blocking junction. The schematic structure for the BH lasers is shown in Figure 5.2 After the regrowth, the wafer was processed into BH lasers using conventional fabrication techniques. The wafer was subsequently cleaved into laser bars of various cavity lengths and HR dielectric coatings were applied on some of the laser facets. The device performance will be discussed in the following [4,17].

5.3 Threshold Current

The threshold distribution of the DQW lasers versus the cavity length is plotted in Figure 5.3. For comparison, the results on SQW [3] and triple quantum well (TQW) InGaAs lasers are also presented in the same figure. The SQW lasers are also of ~ 2 μm wide active stripes. It is seen that the optimum cavity length for low threshold current operation in our BH quantum well laser decreases with increasing number of wells. Approximately, the optimum lengths are $300 \sim 400$ μm for SQW, $200 \sim 300$ μm for DQW, $100 \sim 200$ μm for TQW lasers, respectively. From the data of Figure 5.3, we find that the lowest threshold current obtained is 1 mA for an uncoated DQW laser at ~ 200 μm cavity length. The threshold current of TQW lasers are somewhat higher. The lowest threshold current measured is 1.6 mA for a laser of ~ 1.5 μm active width (not shown in Figure 5.3).

To further reduce the threshold current, high reflectivity (HR) coatings were ap-

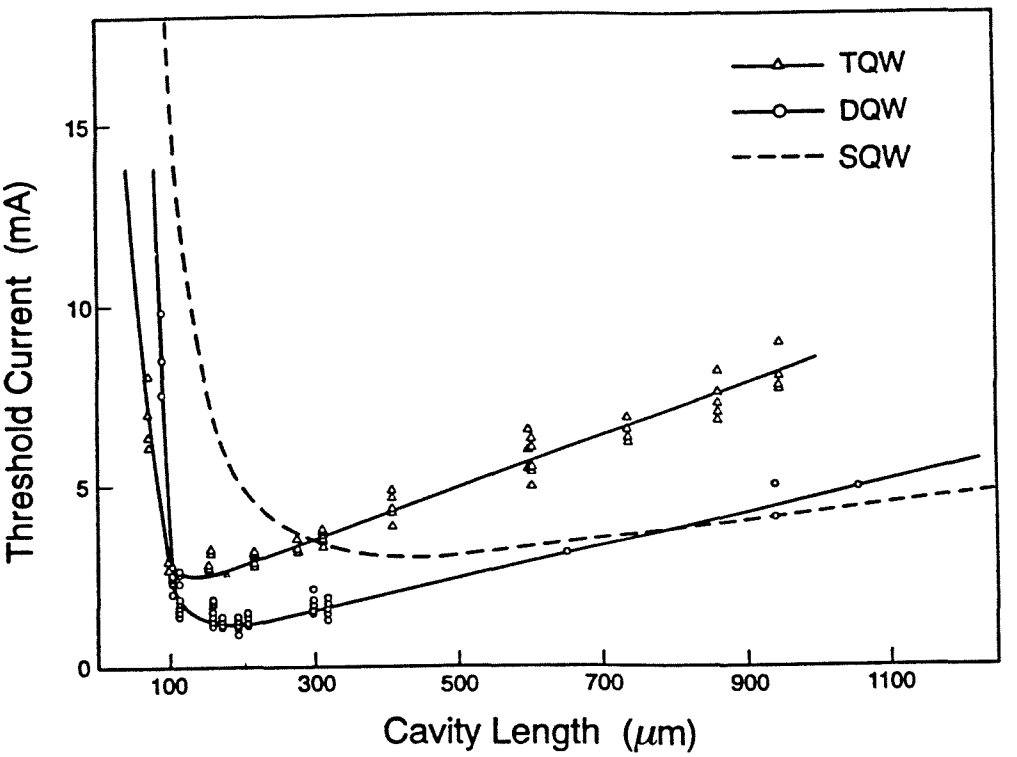

Figure 5.3: The threshold current versus cavity length for SQW, DQW, and TQW lasers. The width of the active stripe is ~ 2 μm.

plied to the facet mirrors of DQW lasers of $\sim$ 110 μm cavity length. Typical results are shown in Figure 5.4. The CW threshold current of the laser was 1.5 mA with cleaved facets, the external quantum efficiency was 0.4 mW/mA and the lasing wavelength was 0.995 μm. When an HR coating of $\sim$ 0.95 was applied to the rear facet, the threshold current dropped to 0.9 mA and the external quantum efficiency from the front facet rose to 0.67 mW/mA. A further application of an HR coating of $\sim$ 0.95 to the front facet of the DQW laser led to a threshold current of 0.35 mA. Under pulsed operation condition, the laser displays a threshold current as low as 0.25 mA. The main performance parameters of the laser with different mirror reflectivities are summarized in Table 5.1.

The lasers operate in a single lateral mode with far field divergence angle of $\sim 25^{o}$. They also operate dominantly in a single longitudinal mode (Figure 5.5). The lasers show very good power performance. The uncoated 150 μm long lasers deliver more than 40 mW CW power per facet at room temperature.

The threshold current value of 0.25 mA is the lowest so far obtained in any materials or any structures. In comparison, a CW threshold current as low as 0.5 mA (pulsed threshold 0.35 mA) has been achieved in a patterned quantum well GaAs/AlGaAs laser [7]. In the InGaAsP long wavelength lasers, submilliampere threshold current (in the vicinity of 0.9 mA) have been demonstrated by using dielectric HR coating [15] and low temperature operation [11]. A threshold current of 0.7 mA was obtained in the vertical cavity surface emitting laser configuration [6].

Theoretically, it appears possible to continuously reduce the threshold by using

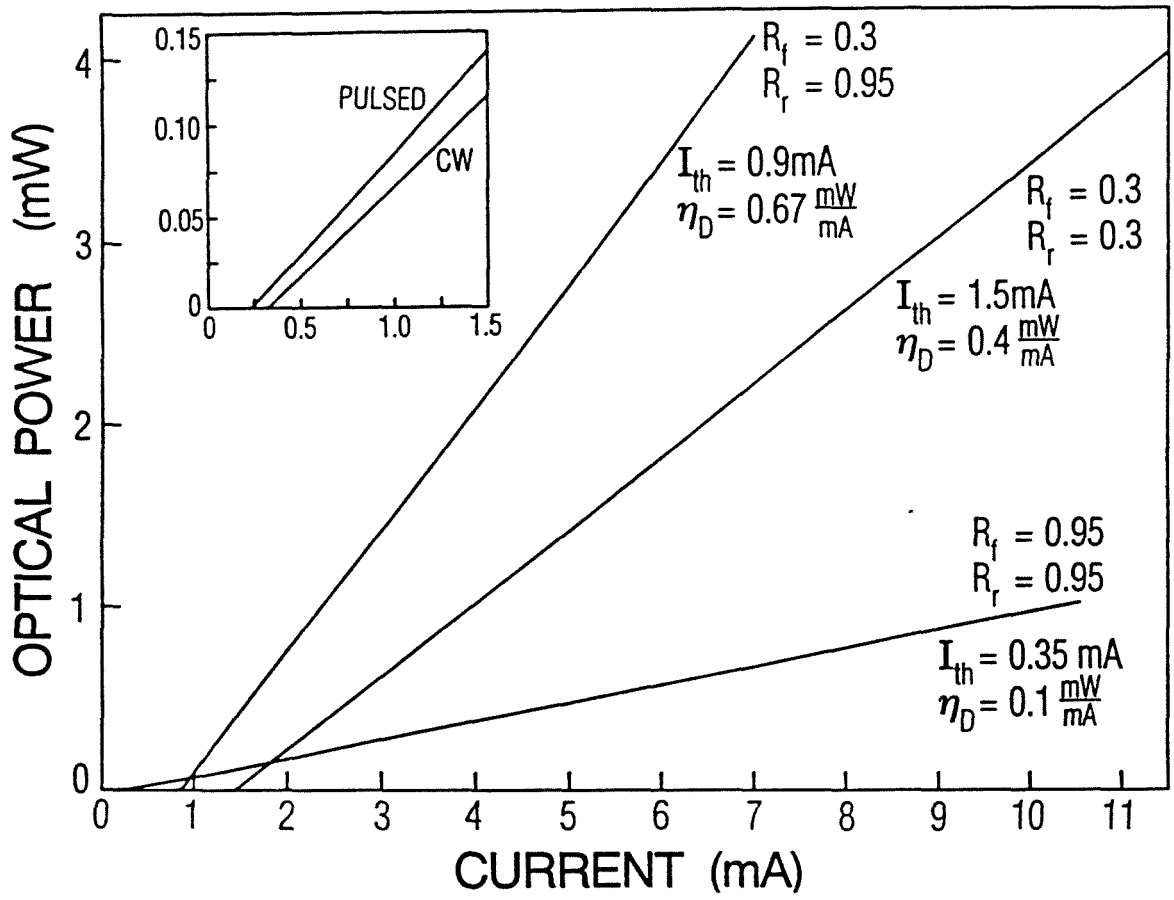

Figure 5.4: The light *vs* current characteristics of a DQW laser with different mirror reflectivities. The cavity length of the laser is 110 μm and active stripe width is 2 μm.

Mirror Reflectivities	CW I_{Th} (mA)	η_D (mW/mA)	λ_L (μm)
R_f = 0.30 , R_r = 0.30	1.50	0.40	0.955
R_f = 0.30 , R_r = 0.95	0.90	0.67	0.961
R_f = 0.95 , R_r = 0.95	0.35	0.10	0.975

Table 5.1: Threshold current, differential quantum efficiency and lasing wavelength for a laser with different facet coatings. The cavity length is 110 μm and active stripe width is 2 μm for this laser.

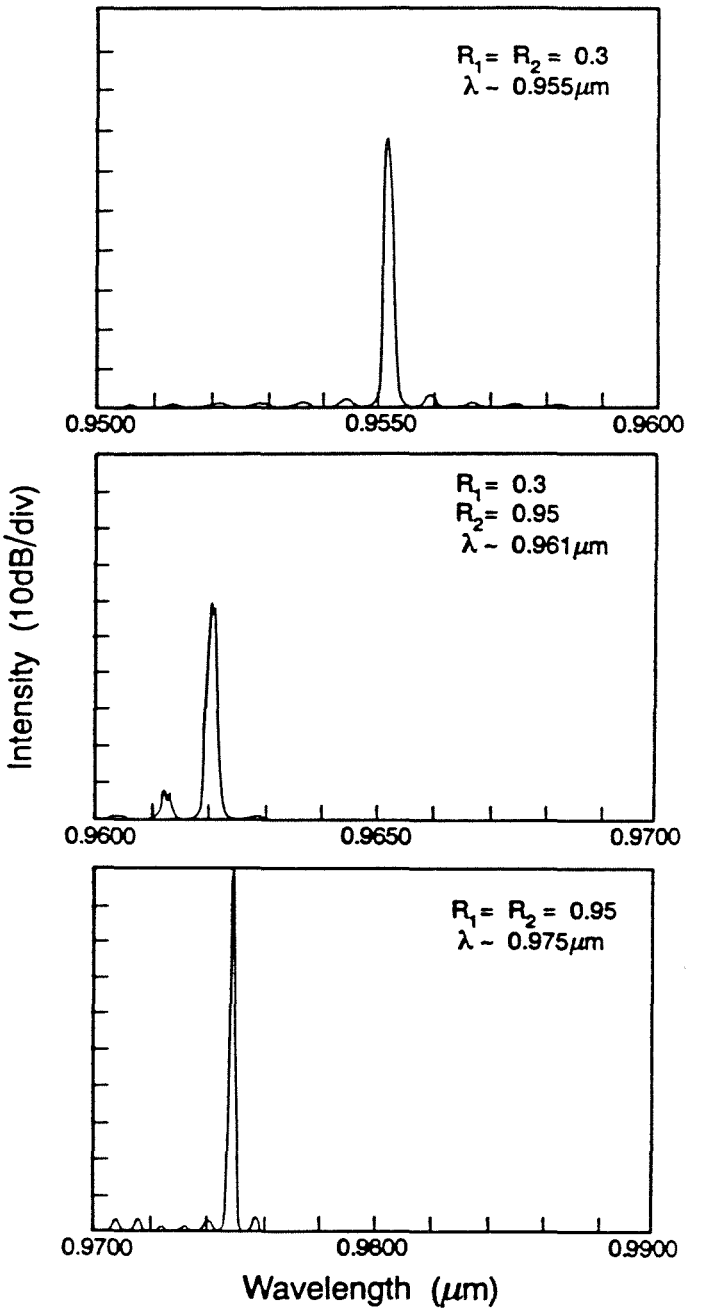

Figure 5.5: Lasing spectra of the device shown in Table 5.1 with different facet coatings. The cavity length is 110 μm and active stripe width is 2 μm for this laser.

shorter SQW cavities and simultaneously increasing the facet reflectivity. However, in practice, very high reflectivity coating (> 95%, *e.g.*) on a short cavity SQW laser are difficult to achieve due mainly to sensitive dependence of lasing wavelengths on the mirror reflectivities [3]. In MQW lasers, the dependence of lasing wavelength on cavity length and mirror reflectivities is reduced, which allows for operation with more easily achieved reflectivities.

5.4 High Modulation Bandwidth at Low Operation Current

The high frequency modulation of the lasers were carried out by a standard experimental arrangement including an S-parameter test set and a network analyzer. Figure 5.6 shows the 3dB modulation bandwidth as a function of the operating current for several lasers with different active strip widths, cavity lengths and HR coatings. The measurements were made on the optical output from front facet (R_1). The corresponding values of active strip width, cavity length, mirror reflectivities, threshold current and differential quantum efficiency (η_D) for each laser are listed in Table 5.2. The corresponding values of K factor are also shown in Table 5.2, which were evaluated from the modulation response by a curve fitting method.

A comparison of the K values among the lasers suggests that the K is a function of threshold modal gain $g_{th} = \alpha + \frac{1}{2L} \ln \frac{1}{R_1 R_2}$. Although the 3dB modulation bandwidth strongly saturates as the operating current increases in laser IV and it has a large

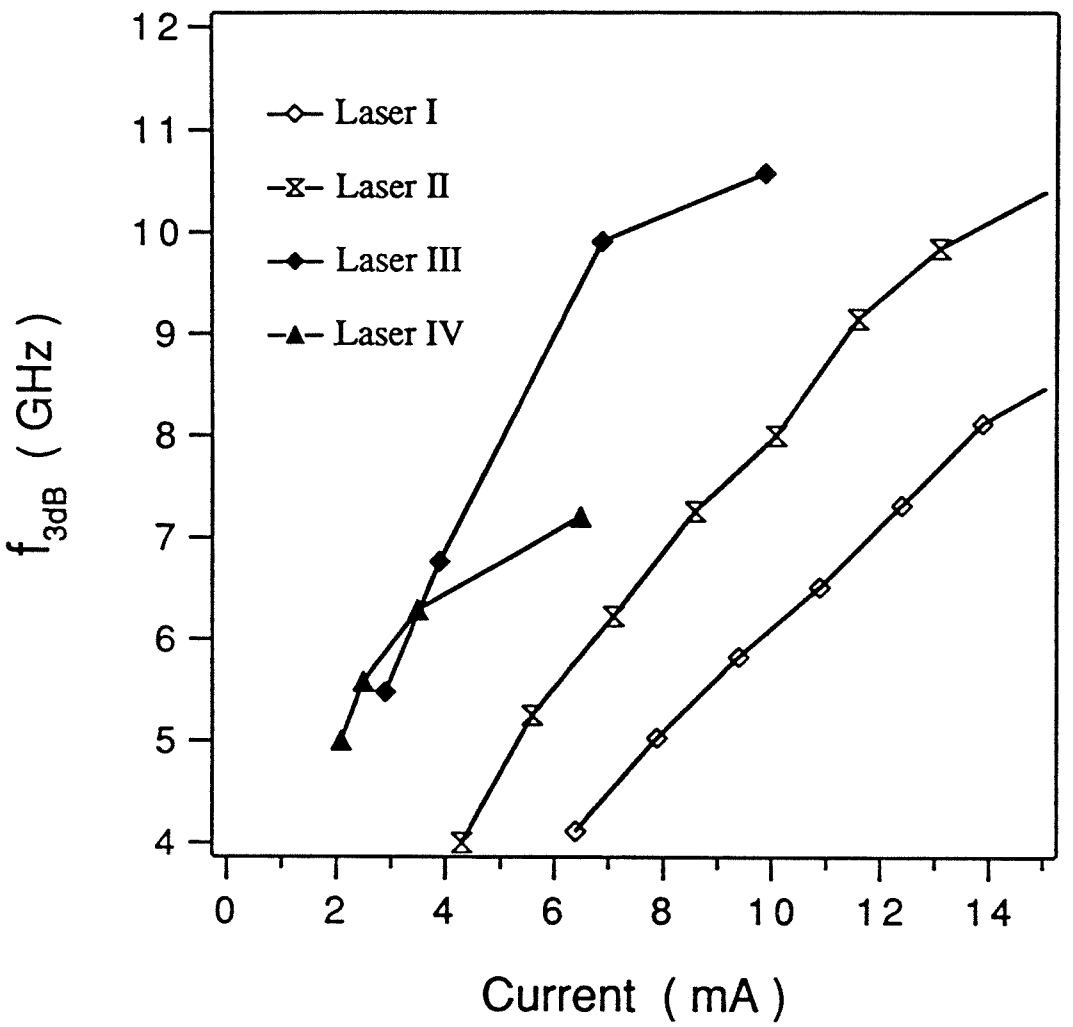

Figure 5.6: 3dB modulation bandwidth *vs* operating current for lasers with different active strip widths, cavity lengths and facet mirror coatings. See Table 5.2 for detailed description about the lasers.

Laser number	Active strip width w (μm)	Cavity length L (μm)	Front facet reflectivity R_1	Back facet reflectivity R_2	Threshold current I_{th} (mA)	Differential quantum efficiency η_D (mW/mA)	K factor (ns)
I	3 μm	300 μm	0.3	0.3	3.4	0.40	0.23
II	3 μm	150 μm	0.3	0.95	2.6	0.72	0.24
III	2 μm	150 μm	0.3	0.95	0.9	0.63	0.23
IV	2 μm	150 μm	0.95	0.95	0.5	0.095	0.44

Table 5.2: A list of laser structures and corresponding obtained results in InGaAs strained DQW BH lasers.

value of K, a 5 GHz 3dB modulation bandwidth has been achieved at an operating current 2.1 mA in this laser as shown in Figure 5.7. This is attributed to the lower threshold current (0.5mA), smaller optical mode volume (short cavity and narrow active strip width) and high differential gain at low modal gain in this laser. The 0.95 HR coatings on both facets of this laser lead to very small threshold modal gain.

These lasers are attractive for the applications of optical interconnects and short distance local area communication systems. Due to the damping effect on the modulation response, at high operation current levels, the operation current increase does not efficiently increase the modulation bandwidth as schematically shown in Figure 5.8. For example, the highest modulation bandwidth of 30 GHz was obtained at an operation current of 114 mA [13]. To obtain 30 GHz communication bandwidth, we can use a system consisting of 6 lasers of 5 GHz at 2 mA. As shown in Figure 5.8, the power consumption of this system is about three orders of magnitude less than that of using one single 30 GHz laser. In the meantime, the requirements for high speed (30 GHz) photo-detectors and other supporting electronics can be relaxed to 5 GHz.

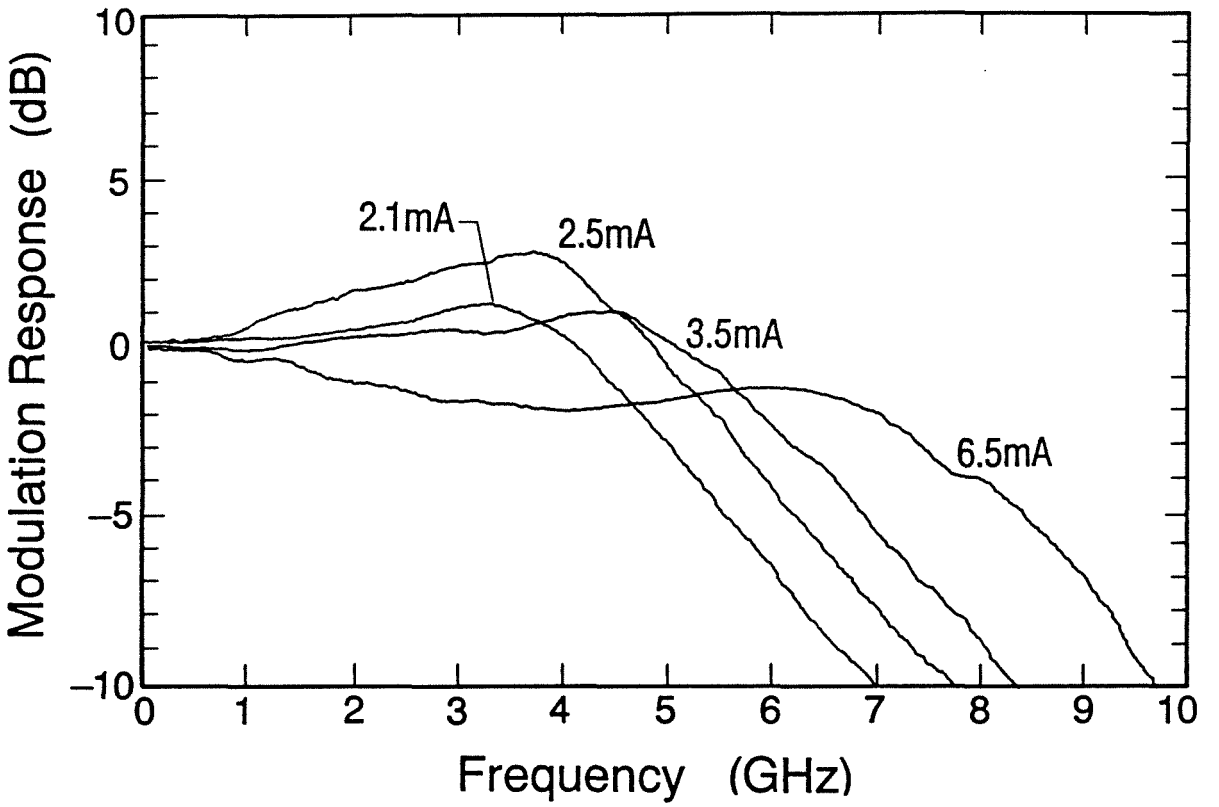

Figure 5.7: The modulation response of a DQW laser. A 5 GHz 3dB modulation bandwidth has been achieved at an operating current 2.1 mA. The threshold current of this laser is 0.5 mA.

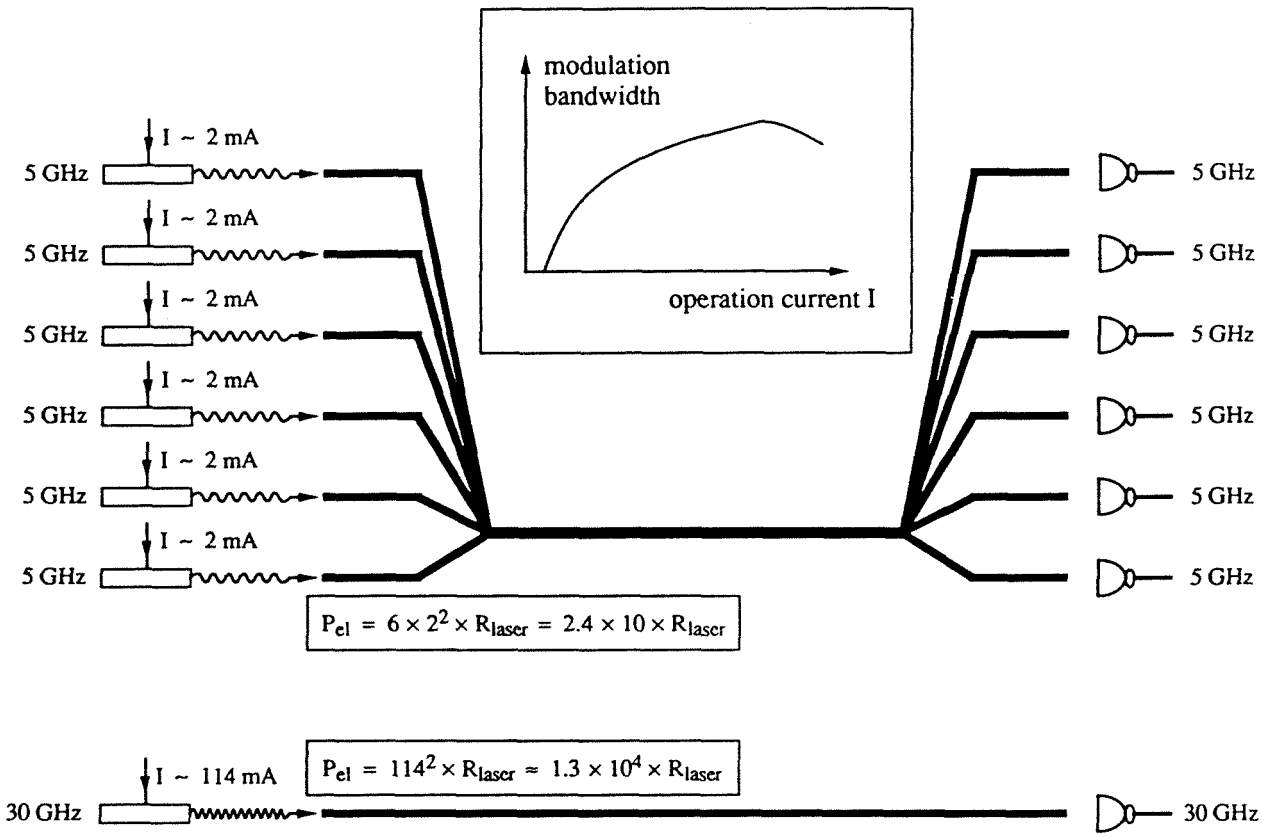

Figure 5.8: The advantages of using lasers of moderate high speed at very low operation current to construct optical interconnect and local area networks.

Bibliography

[1] Y. Arakawa and A. Yariv, "Theory of gain, modulation response, and spectral linewidth in AlGaAs quantum well lasers," *IEEE J. Quantum Electron.*, vol.QE-21, p.1666, 1985

[2] N. Chand, E. E. Becker, J. P. van der Ziel, S. N. G. Chu, and N. K. Dutta, "Excellent uniformity and very low (< 50 A/cm^2) threshold current density strained InGaAs quantum well diode lasers on GaAs substrate," *Appl. Phys. Lett.*, vol.58, p.1704, 1991

[3] T. R. Chen, L. E. Eng, B. Zhao, Y. H. Zhuang, S. Sanders, H. Morkoç, and A. Yariv, "Submilliamp threshold current strained layer InGaAs/GaAs quantum well lasers," *IEEE J. Quantum Electron.*, vol.QE-26, p.1183, 1990

[4] T. R. Chen, B. Zhao, Y. H. Zhuang, A. Yariv, J. E. Ungar, and S. Oh, "Ultralow threshold strained layer InGaAs multi-quantum well lasers," *Appl. Phys. Lett.*, vol.60, p.1782, 1992

[5] S. P. Cheng, F. Brillouet, and P. Correc, "Design of quantum well AlGaAs-

GaAs stripe lasers for minimization of threshold current – application to ridge structures," *IEEE J. Quantum Electron.*, vol.QE-24, p.2433, 1988

[6] R. S. Geels and L. A. Coldren, "Submilliamp threshold vertical-cavity laser diodes," *Appl. Phys. Lett.*, vol.57, p.1605, 1990

[7] E. Kapon, S. Simhony, J. P. Harbison, and L. T. Florez, "Threshold current reduction in patterned quantum well semiconductor lasers grown by molecular beam epitaxy," *Appl. Phys. Lett.*, vol.56, p.1825, 1990

[8] A. Kurobe, H. Furuyama, S. Naritsuka, N. Sugiyama, Y. Kokubun, and M. Nakamura, "Effects of well number, cavity length, and facet reflectivity on the reduction of threshold current of GaAs/AlGaAs multiquantum well lasers," *IEEE J. Quantum Electron.*, vol.QE-24, p.635, 1988

[9] K. Y. Lau, P. L. Derry, and A. Yariv, "Ultimate limit in low threshold quantum well GaAlAs semiconductor lasers," *Appl. Phys. Lett.*, vol.52, p.88, 1988

[10] P. W. A. McIlroy, A. Kurobe, and Y. Uematsu, "Analysis and application of threshold gain curves to the design of multi-quantum-well lasers," *IEEE J. Quantum Electron.*, vol.QE-21, p.1958, 1985

[11] P. J. A. Thijs, J. J. M. Binsma, L. F. Tiemeijer, R. W. M. Slootweg, R. van Roijen, and T. van Dongen, "Sub-mA threshold operation of *lambda* = 1.5μm strained InGaAs multiple quantum well lasers grown on (311)B InP substrates," *Appl. Phys. Lett.*, vol.60, p.3217, 1992

[12] G. H. B. Thompson, *Physics of Semiconductor Laser Devices*, John Wiley & Sons, 1980

[13] S. Weisser, J. D. Ralston, E. C. Larkins, I. Esquivias, P. J. Tasker, J. Fleissner, and J. Rosenzweig, "Efficient high-speed direct modulation in p-doped $In_{0.35}Ga_{0.65}As/GaAs$ multiquantum well lasers," *Electro. Lett.*, vol.28, p.2141, 1992

[14] A. Yariv, *Quantum Electronics*, 3rd Ed., John Wiley & Sons, 1989

[15] C. E. Zah, F. J. Favire, R. Bhat, S. G. Menocal, N. C. Andreadakis, D. M. Hwang, M. Koza, and T. P. Lee, "Submilliampere-threshold 1.5-μm strained-layer multiple quantum well lasers," *IEEE Photon. Technol. Lett.*, vol.2, p.852, 1990

[16] B. Zhao, T. R. Chen, and A. Yariv, "The extra differential gain enhancement in multiple quantum well lasers," *IEEE Photon. Tech. Lett.*, vol.4, p.124, 1992

[17] B. Zhao, T. R. Chen, Y. H. Zhuang, A. Yariv, J. E. Ungar, and S. Oh, "High-speed operation of very low threshold strained InGaAs/GaAs double quantum well lasers," *Appl. Phys. Lett.*, vol.60, p.1295, 1992